PNNL-14437

Pacific Northwest
National Laboratory
Operated by Battelle for the
U.S. Department of Energy

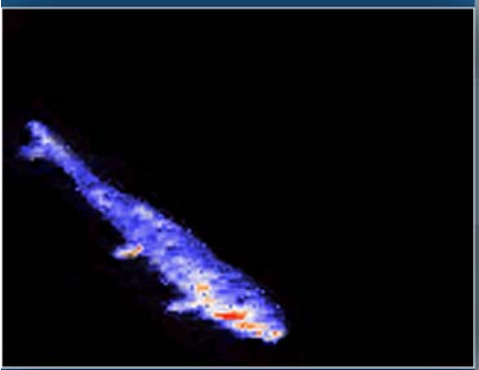

Technologies for Evaluating Fish Passage Through Turbines

Mark A. Weiland
Thomas J. Carlson
Pacific Nothwest National Laboratory

October 2003

U.S. Department of Energy
Energy Efficiency and Renewable Energy

Wind and Hydropower Technologies

Bringing you a prosperous future where energy is clean, abundant, reliable, and affordable

DISCLAIMER

PACIFIC NORTHWEST NATIONAL LABORATORY
operated by
BATTELLE
for the
UNITED STATES DEPARTMENT OF ENERGY
under Contract DE-AC06-76RL01830

Technologies for Evaluating Fish Passage Through Turbines

M. A. Weiland
T. J. Carlson

October 2003

Prepared for:
Pacific Northwest National Laboratory
Richland, Washington 99352

Summary

This study evaluated the feasibility of two types of technologies to observe fish and near neutrally buoyant drogues as they move through hydropower turbines. Existing or reasonably modified light-emitting and ultrasonic technologies were used to observe flow patterns, the response of fish to flow, and interactions between fish and turbine structures with good spatial and temporal accuracy. This information can be used to assess the biological benefits of turbine design features such as reductions in gaps at the tips and hub of turbine runner blades, reshaping wicket gates and stay vanes, modifications to draft tube splitter piers, and design changes that enhance egress through the powerhouse and tailrace.

The light-emitting technologies evaluated were standard frame rate cameras and high-speed digital cameras capable of sample rates of up to 1000 frames/s; the cameras were used to observe light-emitting diode arrays. The high-speed digital camera provided the best spatial resolution for use in the turbine environment, where flow rates can exceed 9.1 m/s. A spatial resolution of about 3.8 cm at 250 frames/s was achieved in flow rates of 9.1 m/s, although the range of observation is only about 6.1 m during normal water conditions in the Columbia River, where the evaluations were conducted. There is an inverse relationship between frame rate and range of detection because of the increasing light requirements as the frame rate increases. Compromises need to be made between the detection range and the spatial resolution desired to detect strikes on structure and the influence of hydraulic conditions.

Two ultrasonic tracking arrays and an acoustic camera were evaluated. One tracking array, a line-of-sight short-baseline system, used the phase of received transmissions from a transmitter to estimate the direction of the incoming transmission. The second tracking array, typically used in situations where the baseline array extends over a larger volume, used a variation of hyperbolic tracking based on differences in the time-of-arrival of a transmitted signal at a minimum of four omnidirectional hydrophones. In this second tracking array, an acoustic camera is used. The camera uses acoustic technology, but it is quite different from standard hydroacoustics in that, while still based on active acoustic principles, the echoes from ensonified fish and other objects in the water column are received on a large number of elements and processed to produce an image of the ensonified objects. Sequences of such images are similar to black-and-white video where the shape and motion of the ensonified fish can be observed during its residence in the ensonified volume.

The advantages of the two acoustic technologies are their range of detection. The line-of-sight array and the acoustic camera have a range of over 30.5 m, and the detection range of the time-of-arrival array is limited only by the number of hydrophones used and the design of the receiving array. Spatial resolution of these technologies is low, and resolution is affected by noise within the turbine environment. Acoustic tags used with tracking arrays have duty cycles of 15 ping/s or less. With improvements in technology, the duty cycle of the tags can be increased but is constrained by tag size and multi-path of the signal within the confines of the turbine environment. The acoustic camera though not constrained by the ping rate of an acoustic tag is limited by its frame rate that is currently less than 21 image/s at very short ranges and is typically limited to 8 to 10 image/s at ranges likely to be necessary in turbine environments.

Acknowledgments

The authors are grateful for the contributions and input of many people on this project. George Keilman and Alan Wirtz provided technical help with obtaining sound measurement and data analysis. Brian Cunitz provided computer programming assistance. Charlie Escher, Derrek Faber, Bob Mueller, Carl Schilt, and Shon Zimmerman provided field assistance and input. Kristin Manke was the technical editor for this document. Finally, thanks to the U.S. Department of Energy's Advanced Hydropower Turbine System Program and Peggy Brookshire at the Idaho Falls Operations Office for funding these studies.

Contents

Figures

Tables

Acronyms

CCD	charge coupled device
CLE	chemical light emitter
DIDSON	Dual Frequency Identification Sonar
LED	light-emitting diode
LET	light-emitting tag
PNNL	Pacific Northwest National Laboratory
USACE	U.S. Army Corps of Engineers

List of Units

µPa	micro-Pascal
C	Celsius
cm	centimeter
dB	decibel
g	gram
Hz	hertz
kHz	kilohertz
m	meter
mcd	millicandella
MHz	Megahertz
min	minute
mm	millimeter
mps	meters per second
MW	Megawatt
m^3/s	cubic meters per second
pps	pings per second
s	second

1.0 Introduction

Conditions that fish experience during passage through a turbine at a hydroelectric dam vary depending upon the design of the turbine and the way the turbine is operated. Characterization of these conditions and, in particular, the exposure to deleterious conditions fish experience during turbine passage has been difficult because of the challenges in placing instruments within a turbine. Light-emitting and ultrasonic technologies offer opportunities to directly observe features of the hydraulic environment and the response of fish to this environment. These technologies are in common use for similar data acquisition applications external to the turbine environment. Therefore, evaluating these technologies involves identifying the additional demands created by the turbine environment and assessing the capability of each technology, or reasonable modifications of that technology, to meet those demands.

In addition to observations of flow patterns, the response of fish to flow, and interaction between fish and turbine structures, information is needed to assess the biological benefits of turbine design features such as reductions in gaps at the tips and hub of turbine runner blades, reshaping of wicket gates and stay vanes, modifications to draft tube splitter piers, and design changes that enhance egress through the powerhouse and tailrace. Before this additional information can be acquired, several aspects of the deployment and performance of monitoring and measurement technologies need to be understood. Of particular interest are (1) the achievable spatial and temporal resolution in position estimates of fish and other objects, (2) the basic challenge of deploying instruments in the turbine environment, and (3) sufficiently large volume coverage to ensure adequate sample size for experiments requiring a high detection probability of fish and drogues passing through a monitored volume. For example, higher levels of resolution are needed to acquire data for assessing the likelihood of a fish strike on stay vane / wicket gate surfaces and exposure to runner blade tip and hub gaps. Information on fish movement and interactions is necessary to evaluate the biological benefits of turbine design changes and to assess the performance compromises and construction costs of such changes.

To address this need for information, researchers at Pacific Northwest National Laboratory (PNNL)[1] conducted studies to resolve some of the uncertainties related to use of light-emitting and ultrasonic technologies within the turbine environment.

[1] Pacific Northwest National Laboratory is operated for the U.S. Department of Energy by Battelle.

2.0 Background

2.1 Light-Emitting Devices

Light emitters that meet the needs of this study, including the need to attach them to small fish, are of two types: (1) chemical light emitters (Cyalume Lightsticks™) and (2) light-emitting diodes.

Chemical light emitters (CLEs) require no outside energy source and produce light through a chemical reaction called chemiluminescence. The light emitter is a hollow plastic tube filled with a solution of phenyl oxalate ester and a fluorescent dye. Also inside the plastic tube is a glass capsule filled with hydrogen peroxide. Flexing the plastic tube breaks the glass capsule, a chemical reaction between the phenyl oxalate ester and hydrogen peroxide occurs. The energy released from this reaction is in the form of light. The illumination level of light emitters varies from several lux up to over 2000 lux. Today, CLEs are in common use as emergency lighting, party favors, and other applications, including fishing, and vary from 3.8 to 30.5 cm long.

Light-emitting diodes (LEDs) are solid-state semiconductors that convert electrical energy directly into light and are common in automobiles and aviation where they are used because of their resistance to damage from vibration, low heat production, and long service life, typically on the order of 100,000 hours of continuous operation with low electrical power consumption. Depending on the application, LEDs come in a variety of shapes and sizes. Power requirements vary from less than 2 volts to about 3.5 volts for LEDs with the highest light intensity varying from less than 1 mcd to over 20,000 mcd.

Because of the wide range of uses, which has resulted in high quantity manufacture and competition, the per unit cost of both types of light emitters is low, ranging from a few cents to approximately one dollar. Each of these light sources comes in a variety of colors, sizes, and light intensities. Though, only a small range of colors and the higher light intensities are useful for most underwater studies. Both types produce cold light and do not generate significant amounts of heat, and important feature in their use with fish. Both types of emitters also are near the density of water and require little alteration to attain neutral buoyancy (Table 1).

Table 1. Characteristics of chemical light emitters and light-emitting diodes.

Device type	Size	Volume (cm^3)	Mass (g)	Buoyancy (g)*
LED	5 mm	0.18	0.25	-0.07
CLE	3.8 cm	0.65	0.6	+0.05
CLE	5.1 cm	1.40	1.35	+0.05
CLE	10.2 cm	10.5	9.1	+1.4
*Buoyancy was calculated relative to fresh water at 14°C. CLE = chemical light emitter. LED = light-emitting diode.				

In previous studies (1999) performed by PNNL for the Portland District U.S. Army Corps of Engineers (USACE), CLEs were used at Bonneville Dam, the first dam on the Columbia River, with engineering tests to evaluate the performance of an injection system designed to introduce test fish and sensor fish devices directly into the runner section of a Kaplan turbine. The injection system (Lindgren 2000) consisted of a system of head tanks, valves, pumps, pipes, and supports leading from the dam intake deck to the test turbine stay vanes. The injection system was designed so that the velocity of water from the injection system terminus matched ambient water velocity at the test turbine stay vanes. Large (10.2 cm) CLEs, weighted to neutral buoyancy, were released into the injection system and their trajectories observed as they exited the injection pipe and moved toward the test turbine runner blades. In addition, smaller (3.8 and 5.1 cm) CLEs were attached to fish using a specially designed socket. The socket was attached to the fish with a stainless steel pin through the musculature of the upper back anterior to the fish's dorsal fin. The trajectories of the CLEs, both those attached to test fish as well as those not attached to fish, were observed using standard video frame rate (30 Hz) black-and-white video cameras. All of the CLEs deployed, except the 3.8 cm, were detected, and the images obtained used to assess the operation of the injection system. For this application, the maximum distance of the video cameras from the most distant injection pipe terminus (blade tip release pipe) was approximately 3.05 m. These tests were conducted during the winter when water clarity in the Columbia River was excellent (Carlson and Weiland 2001).

In a similar injection system performance evaluation conducted by PNNL for the Walla Walla District USACE, a LED array was incorporated into self-righting drogues designed to be near neutrally buoyant in fresh water at ambient temperatures. The drogues were released into the intake of a test turbine at McNary Dam, last dam on the Columbia River before the confluence with the Snake River, in the plane of the emergency gate slot. The drogues were tracked after exiting the injection system using a linear array of four standard analog black-and-white video cameras. These tests were conducted in July when water clarity was low. In spite of poor water clarity, it was possible to track the drogues in three dimensions for approximately 6.1 m following injection. This tracking distance was sufficient to characterize the performance of the injection system and the behavior of acoustic drogues (which were the same design as the LED drogues) following injection. In particular, it was critical to the experiment being conducted to ensure that the drogues' self-righting feature was functioning as expected (Carlson et al. 2001). Large (10.2 cm) CLEs released during the same test were viewed for only 1.5 m because of water conditions.

For this study, the extensions of light-emitting technologies considered beyond those already applied were as follows:

1. Design of high-intensity LED arrays with mass and buoyancy typical of that of subyearling and yearling salmonid smolts.

2. Design of high-intensity LED arrays that can be attached to juvenile and adult test fish.

3. The light intensity requirements for LED arrays and chemical emitters necessary for production of useful tracking images using high-speed digital camera arrays at ranges of 4.6 m and further.

2.2 Ultrasonic Micro-Transmitters and Short-Baseline Receiving Arrays

Small ultrasonic transmitters have been commercially available for many years. Current technology provides micro-transmitters less than 1 g in dry weight capable of encoded transmit pulses for unique identification of individual fish. With these devices, it is possible to implant ultrasonic transmitters, either surgically or gastrically, in fish as small as 90 mm in length, the size of subyearling Chinook salmon.

The primary challenges in applying this technology within a turbine are as follows: (1) the placement of receiving array elements and corruption of transmitted signals by multi-path, (2) the short "lines-of-sight" typical of many portions of the turbine environment, (3) acoustic noise generated by turbine machinery and other sources, and (4) source levels and duty cycles of micro-transmitters.

In recent years, two types of ultrasonic three-dimensional tracking systems have been developed and deployed to track juvenile fish implanted with ultrasonic transmitters. These systems use different methods for estimating the position of transmitters. One, a short-baseline system, uses the phase of received transmissions to estimate the direction of the incoming transmission. The location of the transmitter is estimated by the intersection of two or more lines of sight based on phase angle of the receiver pulse from the transmitter by two or more receivers in the baseline array. The second method, typically utilized in situations where the baseline array extends over a larger volume, uses a variation of hyperbolic tracking based on differences in the time of arrival of a transmitted signal at a minimum of four omnidirectional hydrophones.

At PNNL for the Walla Walla District USACE, we developed and utilized a line-of-sight system to track neutrally buoyant drogues and fish through a turbine intake at McNary Dam. In addition to the receiving array, we developed a high output, high duty cycle micro-transmitter that was gastrically implanted in juvenile salmonids and also potted into near neutrally buoyant acoustic drogues. Using this receiving system and micro-transmitters, drogues and fish were tracked from a point immediately downstream of the turbine emergency gate slot to the turbine wicket gates in the A intake of a test turbine. This was the slot with the longest direct path to the wicket gates. This experiment was designed to determine if fish were carried passively by flow or if they were active during passage through the intake. We tested our hypothesis that fish were passively transported by comparing the trajectories of drogues and fish. Our results showed that the fish were not passively transported, showing both temporal and spatial differences in their trajectories compared to the trajectories of the passive drogues (Carlson et al. 2002).

We have also tracked fish through much larger areas. At Bonneville Dam in the spring of 2000, we implemented a modified hyperbolic tracking system (time-of-arrival) to track juvenile salmonids as they moved through the forebay of Bonneville Dam's first powerhouse (PNNL for Portland District USACE). The baseline array for this system consisted of 16 hydrophones

positioned in a grid pattern in the dam's forebay. Observations of fish behavior obtained using this tracking system were compared with flow field estimates obtained using three-dimensional computation fluid dynamics models. The results clarified the approach patterns of the fish to the dam, showed holding areas, differences in behavior during day and night, and aspects of the response of the migrating juveniles to water flow dynamics (Faber et al. 2001).

Experience with the time-of-arrival tracking system clearly showed the dependence of transmitter location estimation error on the relative geometry of receiving array nodes and transmitter location. To better understand the characteristics of position estimation error and to optimize the design of receiving arrays, we developed a software tool to estimate the error structure for a receiving array (PNNL for Portland District USACE). This software tool, FishTrack3D™, was also configured to be used to design receiving arrays (Faber et al. 2002). We used this tool in this study to estimate the error for baseline configurations within the turbine environment and in the immediate tailrace region.

In this study we evaluated the application of both line-of-sight and time-of-arrival within the turbine environment downstream of the turbine runner to the exit of the draft tube plus a short distance downstream in the tailrace to the downstream edge of the turbine discharge backroll. We focused on the following: (1) the noise level in the region of the frequencies most commonly used for micro-transmitters, (2) the source level and duty cycle (pulse repetition rate) of micro-transmitters, (3) the achievable location of receiving array elements, and (4) the expected error in transmitter location estimates given the geometry of the receiving array.

2.3 Ultrasonic Imaging

Fixed location and mobile active acoustic methods (typically called "hydroacoustics") have been used for many years to assess the timing and abundance, and to observe aspects of the behavior of fish as they approach and pass hydropower dams. In some cases, hydroacoustic system transducers have been deployed in turbine intakes. These typical acoustic instruments rely on the detection and correct classification of echoes from individual fish. Up to this time, hydroacoustic systems have not been deployed in the turbine environment downstream of the turbine wicket gates. This is due to the difficulty of mounting transducers in these locations and routing their cables through the turbine environment back to system transmitting and receiving electronics.

Ultrasonic imaging is quite different from standard hydroacoustics in that while still based on active acoustic principles, echoes from ensonified fish and other objects in the water column are received on a large number of elements and processed to produce an image of the ensonified objects. Sequences of such images can be obtained at rates approaching 21 image/s so that the result is similar to black-and-white video where the shape and motion of the ensonified fish can be observed during its residence in the ensonified volume. These ultrasonic imaging devices are called acoustic video cameras.

In this study, we evaluated aspects of the performance of a commercially available acoustic video system. This was the Dual Frequency Identification Sonar (DIDSON) developed by the Applied Physics Laboratory at the University of Washington for the Space and Naval Warfare Systems

Center harbor surveillance program. It can detect objects out to 42 m and provide video-quality images out to ranges of 12 m. The DIDSON bridges the gap between existing hydroacoustic systems and optical systems. Hydroacoustic systems can detect targets, such as fish, at long ranges (several hundreds of meters); however, the resulting echoes do not contain enough information to determine the shape or reliably estimate the size or species of the fish. Optical systems, which are implemented using video cameras of varying capabilities, typically produce useful information at reasonable ranges in clear water but are limited at low light levels or when turbidity is high.

The DIDSON has been designed to allow it to substitute for lower resolution optical systems in turbid or dark water. Images within 1 to 12 m of the device are of sufficient resolution that the undulation of fish can be observed as they swim and the head can be distinguished from the tail. The system's highest spatial resolution, which is available at shorter ranges, is achieved using 96 0.3-degree by 10.5-degree beams operating at 1.8 MHz. At longer ranges, the system uses 48 individual 0.6-degree by 10.5-degree beams operating at 1 MHz. The DIDSON is capable of operating at 4 to 21 frames/s at high resolution and short ranges and has a 29-degree by 10-degree field of view.

In a 2001 study (PNNL for Portland District USACE), a DIDSON was successfully applied in the forebay at The Dalles Dam, the second dam on the Columbia River and upstream of Bonneville Dam, to record the complex behavior of juvenile salmonids approaching the sluiceway entrance at powerhouse main unit 1 and to visually assess gap loss between adjacent J-plates at units 1 and 4 (Moursund et al. 2002). Acquired images were of sufficient quality to permit researchers to classify imaged fish as smolts or adults. However, the images were non sufficient to allow researchers to differentiate an adult salmonid from the adults of other species present, such as American shad or northern pikeminnow.

In this study, we conducted additional laboratory tests using the DIDSON to better understand how it might operate in the turbine environment. Essentially all deployments of the DIDSON to date have been in locations where the levels of turbulence, entrained air, and water velocity are lower than typical in many portions of the turbine environment. In particular, we examined DIDSON image quality in confined, acoustically noisy environments where fish and other objects moved rapidly through the systems ensonified volume.

3.0 Goals and Objectives

The goal of this study was to evaluate light- and acoustic-based technologies for observing the hydraulic conditions and trajectories of fish passing through hydropower turbines. The study focused on technologies successfully applied in other studies of fish passage at hydropower dams. In addition, this study considered the opportunities for applying these technologies to the turbine environment, particularly the region from the leading edge of turbine stay vanes to the draft tube exit.

4.0 Methods

4.1 Light-Emitting Technology

Light-emitting tags (LETs) and high-speed digital (60-1000 Hz) as well as standard frame rate (30 Hz) video cameras were evaluated to assess the potential use of light-emitting technologies for tracking fish and near neutrally buoyant objects through draft tubes of hydroelectric projects. The geometry of camera arrays to track LETs was evaluated to estimate the location estimation bias associated with each geometry for the tracking algorithm, which was used to estimate the location of the tracked object. Two types of LETs were tested: high-intensity LEDs and CLEs (Figure 1). High-intensity LEDs and CLEs were compared to determine the detection range of each technology using current video camera technology. Of particular interest was the relationship between frame rate and image quality for high-speed digital cameras. It is well known that as the frame rate for high-speed digital video cameras increases, the intensity of light from the image source must also increase to achieve adequate image quality to resolve objects and to estimate their position in space. Very high frame rates are required to achieve good spatial resolution for trajectories of fish and drogues at the high water velocities present at many locations in the turbine environment. For example, a spatial resolution of 7.6 cm requires a frame rate of 120 frames/s at a water velocity of 30 frames/s. Significantly higher frame rates than this would be required for adequate temporal and spatial resolution in the trajectories of fish or drogues to observe their interaction with runner blades or the dynamics of shear at the trailing edges of wicket gates.

4.1.1 LET Development

We searched the commercial market for available LEDs that were bright but small enough to be mounted on a fish or built into small clusters to create a bright sphere having mass and buoyancy

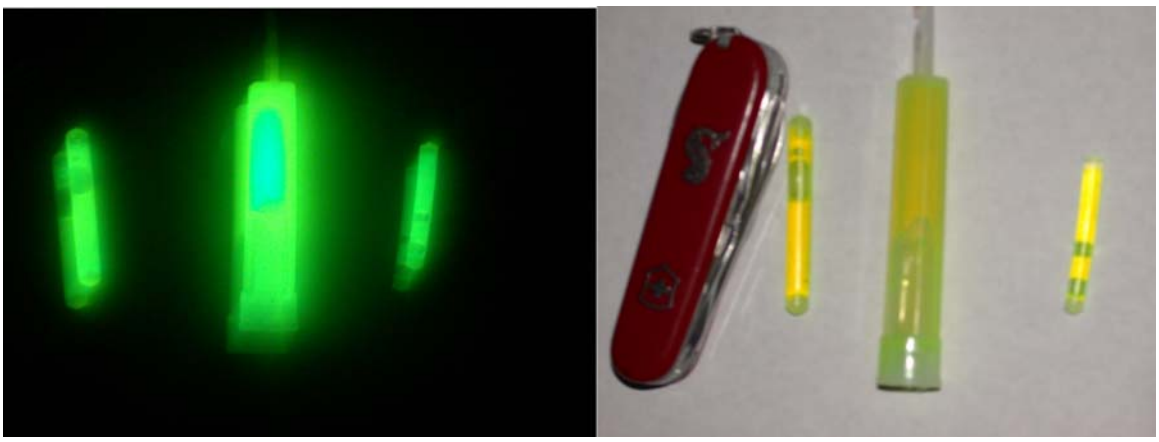

Figure 1. Green (Cyalume Lightsticks™) chemical lightsticks (5.1 cm, 10.2 cm, and 3.8 cm from left to right) used in feasibility testing at Bonneville and McNary Dams and in evaluation of camera tracking arrays. (Studies conducted by PNNL for Portland and Walla Walla District USACE, respectively.)

similar to that of juvenile salmonids. In addition, we searched for batteries powerful enough to drive the LEDs but low enough in weight so that the total weight of a micro-LED array could be mounted on a juvenile fish. Several small batteries with different chemistry are available on the market: lithium, zinc air, alkaline, manganese dioxide, and silver oxide batteries. Finally, we searched for the basic electronic circuits to drive the LEDs. As in the case of the batteries and LEDs, circuits were selected that minimized the total weight of the assembly. For the smallest fish of interest, subyearling Chinook salmon, the total assembly dry weight was limited to 1 g. For larger smolt and adult fish, weighing more than 100 g, assemblies weighing several grams are acceptable.

We obtained detailed specifications for most commercially available ultrabright LEDs. The term ultrabright is used loosely in the industry, with an LED intensity as low as 150 mcd being advertised as ultrabright. Based on our previous experience with underwater use of LEDs for imaging applications, we chose 400 mcd as a lower threshold of LED intensity; however, we didn't test any LEDs with intensities below 3500 mcd. We chose LEDs across the full visible color spectrum to determine the best color combination of LEDs that would provide good contrast in a video image. The LEDs shaded in Appendix A were selected for additional testing. Our selection included LEDs with a range of illumination intensities and angles of illumination. Angle of illumination and light intensity are related in that as the angle of illumination increases, light intensity is reduced.

We researched battery technologies to determine the sizes of batteries available to power LEDs. The criteria for the batteries was that they were small enough to be attached to fish and the weight of all components would not exceed 1 g in total weight and be able to power an array for at least 30 min.

4.1.2 Image Quality Evaluation

To see if the response of the black-and-white video cameras could be used to identify individual colors, LEDs of varying colors were potted in polyurethane to produce near neutrally buoyant drogues. These distinctions could then be used, during image analysis, to estimate the attitude of the fish or drogue in an image. Color combinations tested were blue/yellow, blue/orange, blue/red, green/yellow, green/orange, and green/red (Figure 2). A drogue with all green LEDs was used as a control.

Two Red Lake Motion Scope high-speed digital cameras were positioned in viewing windows alongside a high-velocity flume (see Neitzel et al. 2001) perpendicular to the flow. Near neutrally buoyant drogues with various color combinations of ultrabright LEDs were released through an induction pipe (Figure 3) and were transported into the receiving pool past the camera array in discharge jets of known centerline velocity. The discharge velocities used for testing were 1.5, 3.0, and 4.6 mps.

Video images were recorded at frame rates of 125, 250, and 500 frames/s as the drogues passed in front of the camera array. Acquired images were recorded directly to a computer hard drive as avi files. Acquired videos were viewed using Adobe Premiere version 5.1, and single frames

Figure 2. Near neutrally buoyant drogues lighted with different colors of ultrabright light-emitting diodes.

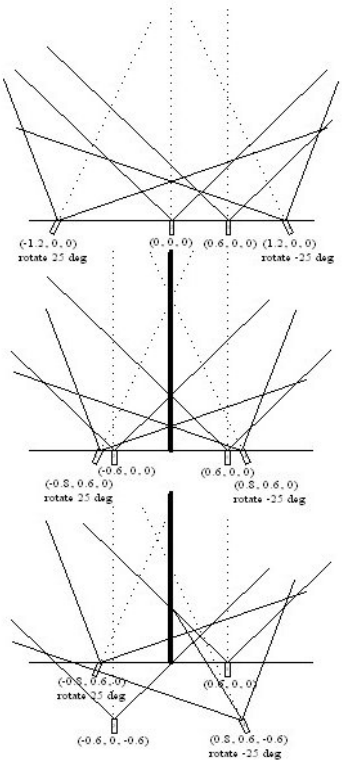

Figure 3. Configuration of (a) linear planar, (b) rectangular planar, and (c) three-dimensional arrays used in modeling the bias of tracking objects through a camera array as a result of camera orientation.

were clipped and saved in jpg format. Image clarity and contrast data were analyzed to determine the relationship between camera frame rate and ambiguity in the position of the LEDs caused by "smearing" and "blooming." Blooming occurs when the dynamic range of the image is greater than the dynamic range of the charge coupled device (CCD). This may cause more electrons to be generated than can be stored in an individual pixel and spill into adjacent pixels. Blooming is usually localized and can arise in scenes containing strong local illuminations. The spread of photocharges appears as a white blot or streak on a TV monitor (Jähne and HauBecker 2000). Smearing appears as a streak; it is caused by the image source moving faster than the frame rate of the camera. Images were also examined to determine if the contrast in the different color pairs of LEDs was detectable.

4.1.3 Evaluation of Camera Tracking Array Geometry

To evaluate the bias in location estimates associated with camera array geometry, LETs were passed through three different camera array geometries (linear planar, rectangular planar, three dimensional). Four different types of LETs were tracked using each array geometry. Three sizes of CLEs (3.8, 5.1, and 10.2 cm) (Figure 1) and a LED drogue (Figure 2) were passed through each array. The self-righting LED drogues were 25.4-cm long and 4.6 cm in diameter and were composed of a polyurethane material that encapsulated the rest of the components. The components consisted of a plastic ball for floatation, battery, ballast, and a LED array.

Four black-and-white Sony SSC-M370 CCD cameras with 0.3-lux low-light capability were used to track the LEDs. Each camera was equipped with a 3.6-mm lens. The output from each camera was recorded to an individual Sony EV-C200 Hi-8 format videocassette recorder. Video camera images were continuously monitored using Sony SSM-171 black-and-white monitors.

In each camera array geometry tested, two of the four cameras were oriented perpendicular with the array, and the remaining two were aimed in at a 25-degree angle (Figure 3). The cameras were mounted on a rigid frame in a 7.3- by 3.7- by 2.0-m tank for testing. The cameras were oriented so that each of the LETs would be viewed by all of the cameras as the LET moved past the camera array.

A trolley system was used to pull the LETs away from the camera array at offsets incremented in 0.3-m intervals from 0.6 m in front of the camera array to a distance of 5.5 m. At each 0.3-m offset, 30 s of video was collected. Camera images were synchronized to the clock on each of the videocassette recorders. Because the LETs were stationary at each interval, an exact synchronization of images was not necessary.

4.1.4 Data Analysis

Segments from the videotapes were processed using a Matrox RT2400 video acquisition and editing system and Adobe Premiere software and saved as avi files to computer hard drive. The video segments were then reduced to sequences of single frame, 320 by 240 pixel, bitmap images in Adobe Premiere. These bitmap images were then viewed in Paint Shop Pro and the X-Y pixel coordinate at the center of the LET image was recorded.

Pixel coordinate data were converted to angle data for both the X and Y coordinates where 0 degrees was the center pixel of the frame (X=160 and Y=120). To convert from pixels to angular coordinates, a camera attached to a monitor was positioned at a known distance from a blank wall. A high-contrast target was moved laterally starting at the coordinate system origin (the middle of the image) until it was no longer in view in the camera image frame, a mark was then put at this position on the blank wall. The object was then moved in the opposite direction and a mark was made where it was lost from view. The distance between these two marks was then measured. Using the distance between the marks and the distance the camera was positioned from the wall, the angular view of the camera for that particular offset relative to the pixels in the images was determined. This measurement was repeated for the vertical dimension. The conversion equations derived using this procedure were as follows:

- Angle X=0.2884*(X pixel)-46
- Angle Y=-0.2837*(Y pixel)+33.9

For each set of overlapping video images from the array, a three-dimensional estimate of LET location was computed. Image overlap from two or more cameras results in a stereoscope view of the LET. Using the equations above, the angles to the LET from each camera were estimated. The angular estimates obtained for each camera (for camera j=1..n) consisted of one angle θ_j, the estimate of the vertical angle to the LET from the camera, and another angle Φ_j, the estimate of the horizontal angle to the LET from the camera. Because each camera in the array has a unique aiming direction, it was necessary to transform the original angles to a common coordinate geometry. This adjustment was made using the aiming angles of the cameras measured relative to the mounting frame. See Appendix D in Carlson et al. (2002) for a more detailed description of the methods used to calculate position.

4.2 Ultrasonic Tracking

Two types of ultrasonic tracking were assessed: line-of-sight and time-of-arrival. The basic data required to perform the analysis were obtained by making laboratory and field measurements. Tracking arrays to evaluate the passage of fish and drogues for both tracking technologies were developed to best assess passage through the draft tubes.

Ultrasonic Micro-Transmitter Source Level Measurement – We measured the acoustic output of a micro-transmitter typical of those used to track the movements of juvenile fish. These measurements were collected in a laboratory test tank, where factors affecting the accuracy of the measurements could be controlled. The source levels (acoustic output) of typical ultrasonic micro-transmitters (Hydroacoustic Technologies Inc. Model 795A and 795E) were measured by suspending them in a 7.3- by 3.7- by 2.0-m tank. The tags were suspended 1 m from a Reson TC4014 omnidirectional hydrophone. This hydrophone is broadband with nearly linear sensitivity from 15 Hz to 480 kHz (Figure 4). Hydrophone output was digitally sampled and stored to a computer hard drive using a National Instruments DAQPad-6070E. Acquired data were processed using the LabVIEW program developed for the Reson hydrophone.

Figure 4. Reson hydrophone used to measure noise.

Background Noise Level Measurement – In the field, we measured the sound field at the exit to draft tubes of Bonneville Dam powerhouse 2 and Lower Granite Dam when turbines were in use. In addition, we measured the sound field for 200 m downstream of Lower Granite Dam. We used these measurements to estimate the background acoustic noise levels over the ultrasonic frequency range that would affect detection of ultrasonic micro-transmitters.

Micro-Transmitter Detection Range Estimation – The level of background noise relative to the level of a micro-transmitter signal was measured at several distances. This was done in the tailraces of Bonneville Dam powerhouse 2 and Lower Granite DamThe hydrophone was placed at a depth of 3.0 m at one end of the powerhouse, about 7.6 m downstream of the face of the dam. A micro-transmitter of known source level was lowered off the face of the dam to a depth of 3.0 m and moved along the downstream face of the dam away from the hydrophone. The output of the hydrophone was recorded at 15.2 m increments from a range of 7.6 m to a maximum range of 107 m.

The signal-to-noise ratio in decibels of the acoustic tag relative to background noise levels at draft tube exits and in the tailrace was estimated by the ratio of power of the micro-transmitter signal to that in an equivalent bandwidth adjacent to that for the micro-transmitter using the following formula:

$$\text{Signal-to-noise ratio} = 10*\log_{10}(P1/P2)$$

where: P1 = power of the transmitted signal (volts)

P2 = background noise level (volts).

Acoustic Tracking Baseline Array – To evaluate draft tube passage, time-of-arrival baselines were developed for tracking fish and neutrally buoyant objects through draft tubes. This was done in the tailraces immediately downstream of McNary Dam's powerhouse and Bonneville Dam's powerhouse 1. A line-of-sight baseline was also developed for within the draft tubes at McNary Dam.

Previous work has shown estimates of transmitter location to be sensitive to baseline geometry for both tracking baselines. Estimates of error caused by array geometry were calculated for the time-of-arrival array and estimates of error due to transducer position and distance of the transmitter from the receiver. Velocity data from the 1/25-scale model at Waterways Experiment Station were also taken into account in the development of the estimation of error.

4.3 Ultrasonic Imaging

The DIDSON operates at three frequencies: 1.0, 1.8, and 2.0 MHz. At the 1.0 MHz operating frequency (detection mode), the operating range of the DIDSON is 0.75 m to 42 m. At 1.8 and 2.0 MHz operating frequencies (identification mode), the operating range is 0.4 m to 12 m. While the operating range is longer at 1.0 MHz, image resolution and quality are markedly lower. At the two higher frequencies, the shape and movement of fish are discernable allowing for better fish identification and orientation determination. The instrument's display can be further limited; this allows the user to obtain a clearer image of objects that are 0.4 to 12 m from the instrument by zooming in on the objects. We concentrated on the two higher frequencies to determine in different flow conditions the resolution at which we were able to identify images and differentiate between fish species.

To estimate the resolution of images in complex fields and under turbulent conditions similar to the flow fields in turbines, the DIDSON was mounted in a laboratory flume and positioned next to the induction pipe aimed with the flow (Figure 5). For a complete description of the flume and

Figure 5. Induction pipe (left) and DIDSON (right) mounted in the test flume.

induction system, see Neitzel et al. (2000). Images were collected of near neutrally buoyant drogues as they passed from the induction pipe at flow rates of 1.5 to 4.6 mps into a low flow environment. The drogues were inducted through a double ball valve assembly (Figure 5) into the jet of water and drogue trajectories were recorded with the DIDSON as they passed into the flume. By leaving the valves open, large amounts of air were entrained in the water jet producing a bubble cloud; this was done to simulate a bubbly turbine environment. Also, to simulate a turbid environment, 10-micron glass spheres were released into the flume and the images of near neutrally buoyant drogues were compared to images of drogues in the clear water.

To determine whether fish species and orientation can be differentiated, the DIDSON was deployed at one end of a 7.3-m-long by 3.7-m-wide by 2.0-m-deep tank of water, at a depth of 0.9 m. Fish were released into the tank and allowed to swim freely. We recorded images of the main species of concern that pass through the dams, juvenile Chinook salmon (*Oncorhynchus tshawytscha*) and steelhead (*O. mykiss*), and the two main predator species, northern pikeminnow (*Ptychocheilus oregonensis*) and smallmouth bass (*Micropterus dolomieui*). Images were collected within 6 m of the DIDSON operated in either high-frequency mode (1.8 or 2.0 MHz) and to a lesser extent at 1.0 MHz.

Image data from the DIDSON were converted into avi video image files. Individual frames were clipped from the video using Adobe Premier. This allowed us to examine individual frames and compare object detectability at different flow and entrained air levels. Images of drogues were compared at three flow levels to determine if the drogues could be detected and resolution of the objects. Images of the fish in the tank were compared to determine if it was possible to differentiate between species and if it is possible to determine the orientation of fish.

5.0 Results and Discussion

The evaluations conducted in this study were at hydroelectric dams on the Snake and Columbia Rivers equipped with Kaplan turbines. A Kaplan turbine is a reaction hydraulic turbine with a propeller-type runner (rotating element). The intake feeds water to a scroll or semi-spiral case, which in turn feeds the circular distributor. The distributor consists of an outer ring of fixed stay vanes, which are structural support elements, and an inner ring of moveable wicket gates which control the volumetric flow rate. The feature that distinguishes a Kaplan turbine is that, unlike a fixed blade propeller turbine, the blades on the runner can be moved to different angles of pitch. The optimum pitch angle to maintain maximum turbine efficiency is a function of both the wicket gate opening and head. As the flow leaves the runner, the pressure has generally been reduced to subatmospheric pressure. It enters the draft tube, which is an expanding conical diffuser. The action of the diffuser is to gradually reduce the velocity of the flow and thereby recover the pressure before discharging from the powerhouse.

The Kaplan turbines in this report are run of the river, vertical-shafted turbines with elbow draft tubes. Run of the river means the powerhouse is integral to the dam, and therefore there are no penstocks. Instead, the intakes consist of three bays each formed by two intermediate piers, in-between the unit's main piers. After the flow has gone through the elbow and turned horizontal, the draft tube is bifurcated into two branches by a single intermediate pier. These intake and draft tube intermediate piers are needed for structural reasons because of the large sizes of these turbines. The draft tubes at Bonneville powerhouse 1 are unique in that there is also a horizontal, curved, splitter pier extending up into the elbow.

The hydraulic conditions within a turbine change as the operating conditions change due to forebay and tailrace elevations (head differential), wicket gate opening, blade angle, and power output of the unit. These factors all affect where the unit is operating relative to its efficiency profile (peak efficiency, full power, etc.). Other related conditions which affect the hydraulic environments within a turbine include whether fish screens were in place and if the trash racks had been raked. All of these operation variables affect the hydraulic conditions and the trajectories and rate at which fish and instrumented objects will pass through the turbine as well as background noise levels. Units were all running within the 1% efficiency range during our testing. Specific data on operating conditions, however, were not used for this report.

5.1 Light-Emitting Technologies

Successful implementation of LETs to better understand the turbine environment and what fish experience during turbine passage is based on acquisition of good quality images of LET drogues or LET devices attached to fish and the geometry of cameras in the imaging array. Acquisition of images is a function of many interrelated factors; the most important for turbine applications being water clarity, distance between the LET and cameras, the intensity of light emitted by the

LET, camera frame rate, and water velocity. The geometry of cameras in the imaging array can be severely constrained by the locations available for cameras in the turbine environment.

5.1.1 LET Development

Of the dome LEDs available, the 5-mm-diameter LED best met our size requirements. The 3-mm LEDs were not as intense as the 5 mm, and the 7.6- and 10-mm LEDs were too large for most of our applications. Maximum intensity of LEDs of a given type varies with color and angle of illumination. We found the green 10,000-mcd LED had the best illumination range underwater followed by the 6000-mcd blue and the 8000-mcd yellow LEDs. A list of LEDs by size, color, angle of illumination, light intensity, company, and part number is provided in Appendix A.

Of the different batteries available, only the silver oxide battery was small enough to be used in a LET assembly that could be attached to a juvenile salmonid. Three of the smallest silver oxide batteries available were tested to determine if they were able to drive the ultrabright LEDs and not drain too fast. We tested the silver oxide type 335, 337, and 379 produced by Eveready (Table 2). For large drogues, 9-volt batteries were used to power the LEDs. Depending on the battery chemistry, 9-volt batteries vary in weight from about 33 to 45 g and are 49 by 26.5 by 17.5 mm.

Table 2. Silver oxide batteries and dimensions used to power LEDs.

Battery type	Volts	Diameter (mm)	Height (mm)	Weight (g)
335	1.55	5.8	1.25	0.14
337	1.55	4.8	1.65	0.12
379	1.55	5.8	2.15	0.25

The forward voltage drop of a LED varied, with LEDs in the same batch having different current draws. However, the normal forward voltage drop of a typical ultrabright LED is 3.6 to 4.0 volts. Therefore, three 1.5-volt silver oxide batteries are required to power an LED array. All of the batteries tested were able to power pairs of ultrabright LEDs for at least 30 min, though LED intensity decreased with time, relative to initial intensity. When four or more LEDs were tested at one time, the batteries were not capable of powering all of the LEDs for 30 min. However, in all cases, two and sometimes three of the LEDs continued to operate beyond 30 min though not as bright as initially. In addition to differences within a batch of LEDs, the color of the LEDs did impact the battery drain. The forward voltage and current requirements vary between colors of LEDs.

In future efforts, to eliminate mismatch in current draw between different colored LEDs in an array and keep all array LEDs operating as long as possible, a step-up converter can be used to regulate current and also reduce the number of batteries necessary to drive the array, thereby reducing the size and weight of the array. There are many different commercially available drivers that are small and inexpensive, originally designed for use in cell phones and other electronics.

It is possible to package an LET using ultrabright LEDs for use on subyearling salmonids that weigh less than 1 g with readily available components, though view of the light would not be omnidirectional due to LEDs' angle of illumination. A tag built with two LEDs (0.25 g each) and three batteries (0.12 g each) would weigh about 1 g with packaging. Reducing the number of batteries and using a step-up converter can further reduce weight of the tag. A tag of this size should cost less than $10 for components. For kelts and adult salmon, a greater number of LEDs can be added to the array to provide a greater likelihood of tag detection with greater angle of illumination and greater range of detection with more LEDs. This will also require extra batteries but will not add much weight relative to the weight of the fish. The size of the LEDs, batteries, and step-up converter are shown in Figure 6.

Near neutrally buoyant drogues of similar mass, buoyancy, and volume similar to subyearling Chinook salmon (≈8 g) and yearling Chinook salmon (≈25 g) can be produced to evaluate the trajectory of the fish relative to a passive particle. For simplicity, the drogues would be a cylindrical composite of polyurethane, similar to the large drogues used in previous studies. For the subyearling drogue between 4 and 8 LEDs can be potted in the drogue and up to 16 could be potted into the 25-g drogue (Figure 7). Plastic balls would be potted in with the LED array and batteries to provide orientation to the drogue and also add buoyancy to counter the negative buoyancy of the LEDs, batteries, and polyurethane.

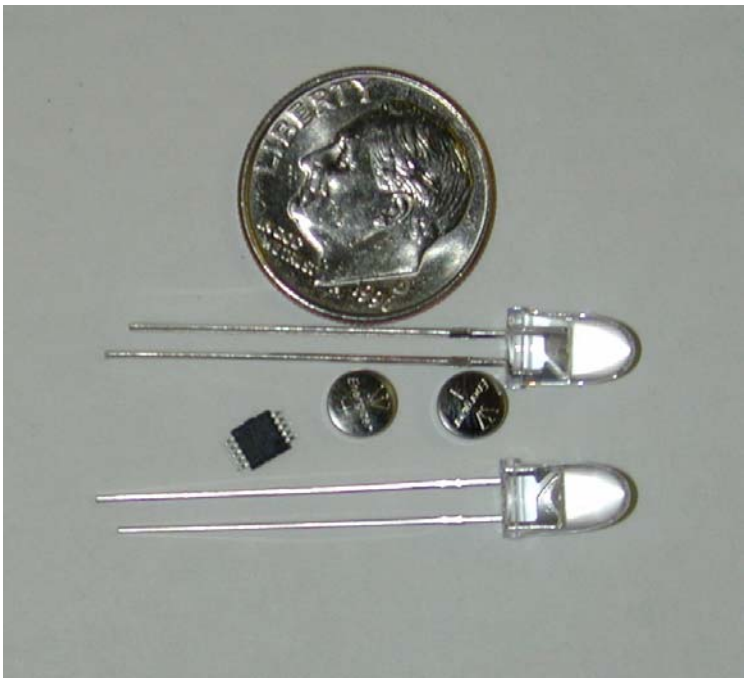

Figure 6. Silver oxide batteries, 5-mm light-emitting diodes, and a step-up converter used in the design of light tags for attachment to juvenile salmonids.

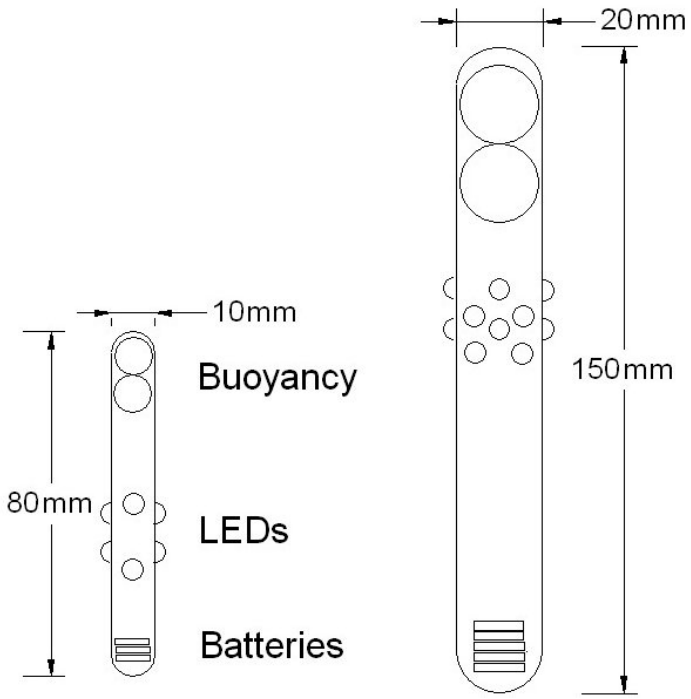

Figure 7. Design of near neutrally buoyant light-emitting diode drogues similar in size and volume to subyearling and yearling Chinook salmon.

5.1.2 Image Quality Evaluation

From the images of near neutrally buoyant drogues released into the flume, we could not discriminate between LEDs of different colors, by contrast, in video images acquired using black-and-white video cameras. While simple above-water testing indicated that distinguishing between colors in black-and-white images might be possible because of the frequency-dependent response of the CCD array, additional transmission losses due to the water reduced the contrast too much. Filters over the camera lens may be used to distinguish between different colors of LEDs. The filters can be used to (1) reduce the intensity of an individual color LED by reducing the intensity of the peak wavelength or (2) reduce the intensity further by reducing intensity over a broad spectral range. Filters to reduce light passage over a range of wavelengths are commercially available and are inexpensive.

The drogue LED array was highly visible in camera images at all flume flow conditions (1.5, 3.0, 4.6 mps) and camera speeds (125, 250, 500 frames/s) tested. The effect of high water velocity on drogue detectability and of high turbulence on change in drogue orientation could be evaluated by looking at images acquired as the drogue exited the injection nozzle and continued until it was fully contained in the turbulence, dissipating the energy in the discharge jet transporting the drogue. At all jet discharge velocities, the drogues were easily detected and tracked for several frames before involvement in the turbulence associated with discharge jet entrainment in the receiving pool. Changes in LED drogue orientation and trajectory were easily distinguished using distinctive features of the drogue's LED arrays. Figure 8 shows individual frames of the

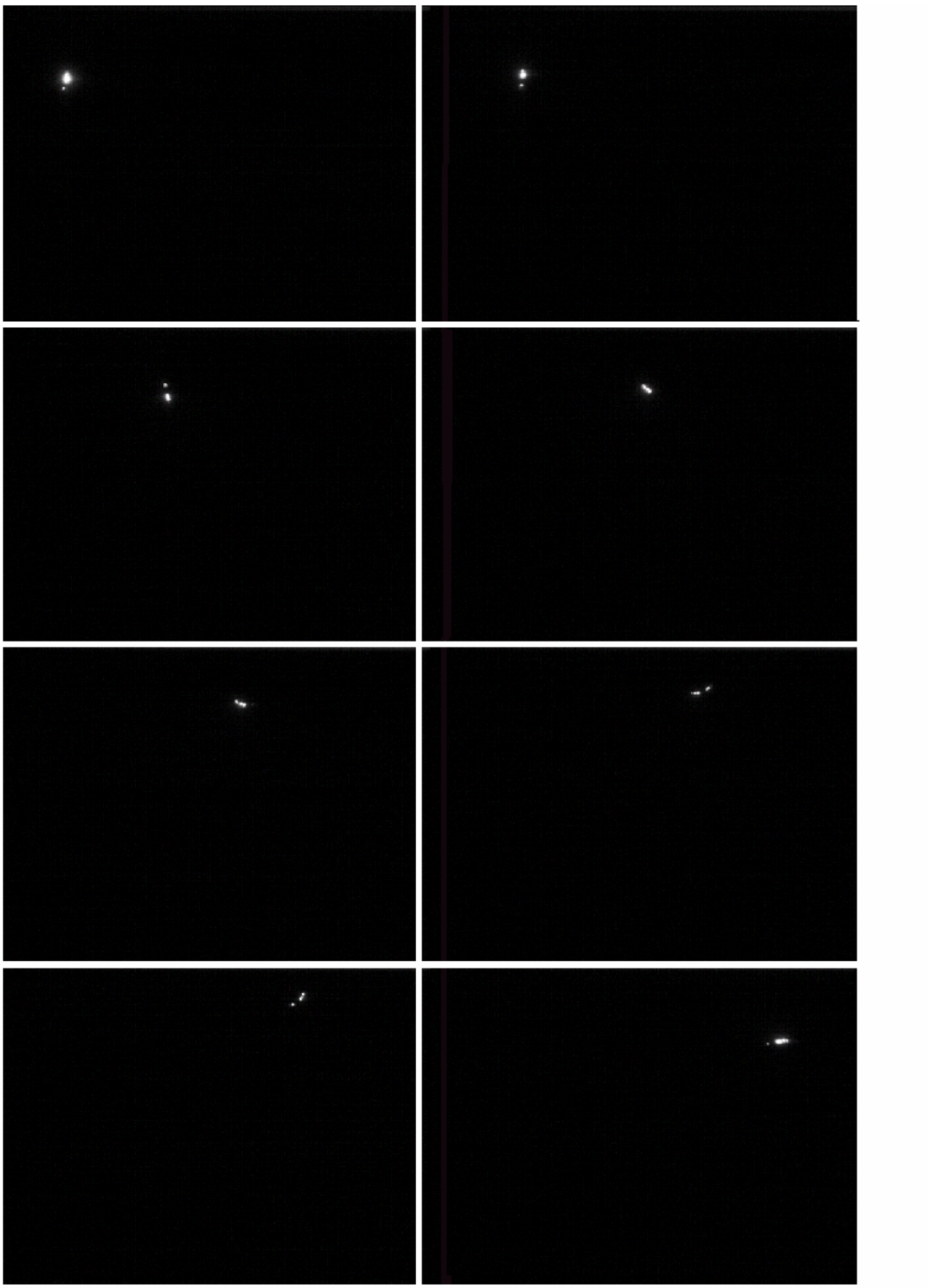

Figure 8. Rotation of light-emitting diode drogue as captured by high-speed video camera.

trajectory of a drogue as it passed through the field of view of a digital camera. The difference in orientation of the LEDs is quite distinct in these single frames and is even more distinct when a video clip showing motion is viewed.

The ability to determine orientation of drogues was reduced as blooming of the LEDs in the image increased. The level of blooming is not affected by water velocity but is correlated with camera frame rate. Significantly greater blooming occurred at 125 frames/s than at either 250 or 500 frames/s (Figure 9). Blooming (saturation of portions of the LED array and charge leakage from saturated CCD elements) from the LEDs was extensive and was the norm more than the exception. Blooming of LEDs was found to varying degrees in all of the digital files collected. This made differentiating between individual LEDs difficult in some instances. The blooming was the result of the bright LEDs used and that 16 LEDs were potted into each drogue. In turbid water, scattering of light by particles resulted in extensive scattering of light from the LEDs, reducing our ability to differentiate between individual LEDs even further. At the frame rates and discharge jet velocities tested, individual frames showed no "smearing" of recorded drogue and LED images, which is caused by significant movement of the drogue while the camera shutter is open.

In the test flume, we were able to detect LED drogues the entire length of the test flume (9.0 m) from the release nozzle (9.0 m) though the image was quite small due to the wide-angle lens on the cameras. The LED drogues were much more visible than 3.8-, 5.1-, and 10.2-cm CLEs in video images obtained during laboratory testing in a tank of water, though the images were collected in clear water. In a study conducted by PNNL for the Portland District USACE, Images of CLEs being released into the turbine intakes at Bonneville Dam showed the 10.2-cm CLE were much more visible than 5.1-cm CLE in turbid water and could be detected for at least 3.0 m. The 3.8-cm CLE could not be seen at all on the videotapes given the water clarity at the time of test (Carlson and Weiland 2001). Observations of LED drogues and 10.2-cm CLE released into the turbine intake at McNary Dam (study conducted by PNNL for Walla Walla District USACE) found that drogues with LEDs could be tracked for about 6.1 m from the point of injection while 10.2-cm CLE were visible and could be tracked for about 1.5 m. The images recorded at

Figure 9. High-speed digital images showing little blooming from the light-emitting diodes (left) and high levels of blooming (right).

Bonneville Dam were in January and February when turbidity was relatively low. Images recorded during releases at McNary Dam were collected during normal turbidity levels in late summer. The LED drogues tracked through the turbine intake at McNary Dam were an array of 16 green LEDs with an intensity of 10,000 mcd each.

Drogues with 16 LEDs during normal summer water conditions in the Columbia River can be viewed for approximately 6.1 m with standard 30 frames/s low light black-and-white video cameras (0.3 lux) or high-speed, low-light black-and-white video cameras at up to 250 frames/s. These viewing distances would increase with the increased clarity of the water as found in the river during winter. The 10.2-cm CLE was viewed for only 3.0 m when the river was at its clearest in winter. Large CLEs such as the 15.2, 20.3 and 30.5 cm will provide greater illumination than the 10.2-cm CLE but still won't produce the illumination necessary during normal summer water conditions. We did discover that by placing the CLE in a warm water bath before induction that the heat stimulated the chemical reaction, noticeably increasing the light intensity but still not near the brightness of the LED.

5.1.3 Evaluation of Bias Associated with Orientation of Camera Tracking Array

Preliminary studies at Bonneville and McNary Dams by PNNL for Portland and Walla Walla District USACE, respectively, showed it is possible to detect LETs (Carlson and Weiland 2001) and also track LETs through portions of a turbine intake (Carlson et al. 2002). These studies also proved the possibility of tracking the path of LETs, but there were some problems with accurately estimating three-dimensional location with time (i.e., their trajectories). In the study, the three-dimensional trajectory of a LED drogue was calculated using each of the six camera combinations, for the X-Z plane (Figure 10a) and the Y-Z plane (Figure 10b). There was variation between the calculated trajectories of the drogue being tracked using different pairs of cameras due to an error in the measured location of the camera. However, we were able to distinguish the trajectories of individual drogues and were also able to describe differences in drogue trajectories that resulted from differences in intake flows as turbine discharge increased when turbine operation level was increased from 40 to 60 MW. At 60 MW turbine operation level, the LED drogues had a narrower dispersion pattern than at 40 MW (Figures 11 and 12).

Errors in the calculated trajectories of LETs can result from errors in the measured location of cameras as well as errors in camera calibration and estimation of the location of the LET in image frames. During initial calibration of the cameras (i.e., when converting pixels to angles), distortion from the camera lens was minimal, but it did increase near the edges of the lens by several pixels. This distortion is minimal but measurement error will increase with increased distance of the object of interest from the camera. Tracking individual pixels accounted for some tracking error due to choosing an adjacent pixel and also due to pixel resolution. However, as a source of error, it was minimal, less than 1%. The major source of systematic error (bias) in LED drogue trajectory was errors in camera position and aiming angle estimates and propagation of those errors in derivation of pixel-to-angle conversion formulae. Of these errors, the aiming angle of the cameras contributed the most to drogue position estimation error.

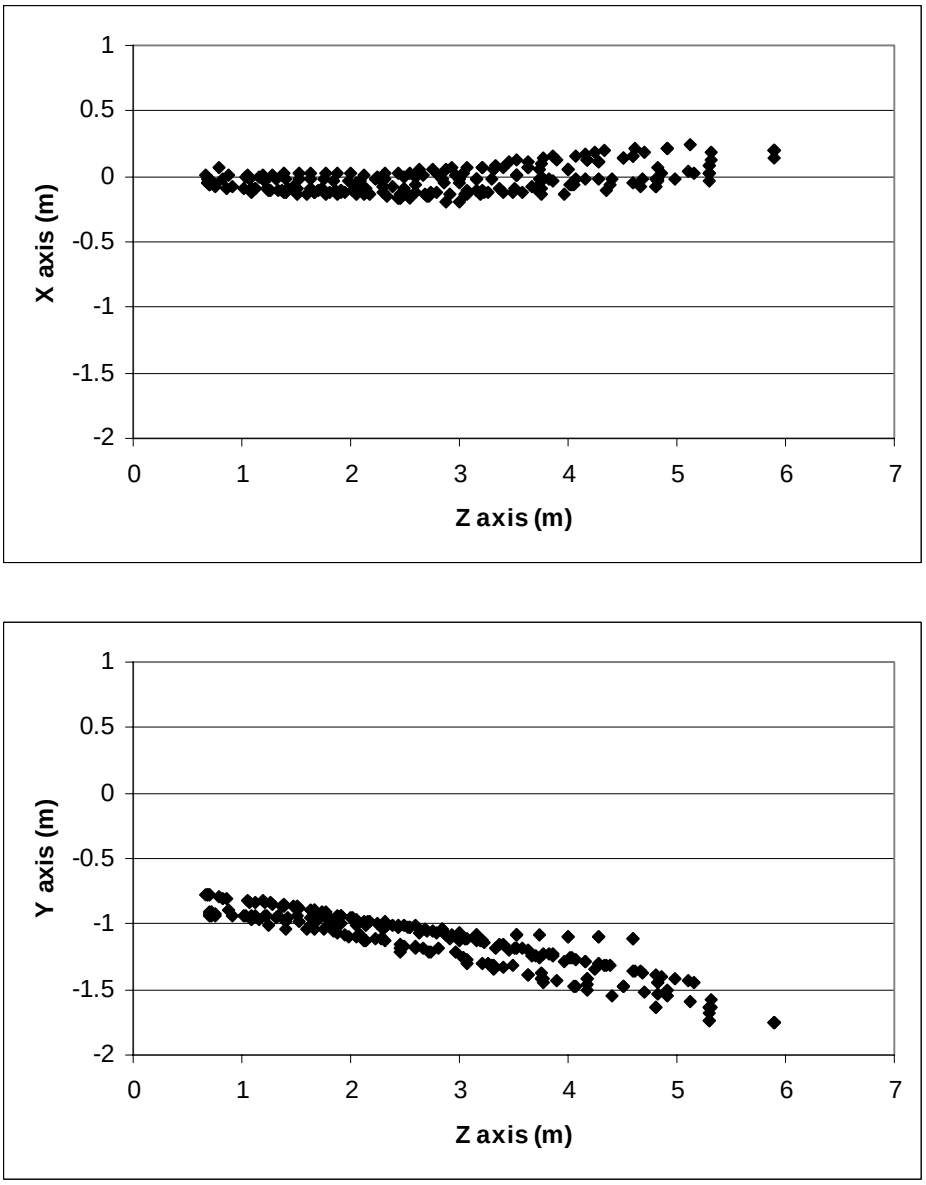

Figure 10. Trajectory of an individual LED drogue as it passed through a turbine intake at McNary Dam in the (a) X-Z plane and (b) Y-Z plane tracked with all six pairs of camera combinations. The different paths of the LED drogue are due to error in orientation of the pairs of cameras used to calculate drogue trajectory. With four cameras used six trajectories were calculated using all combinations of camera pairs. (Study conducted by PNNL for Walla Walla District USACE.)

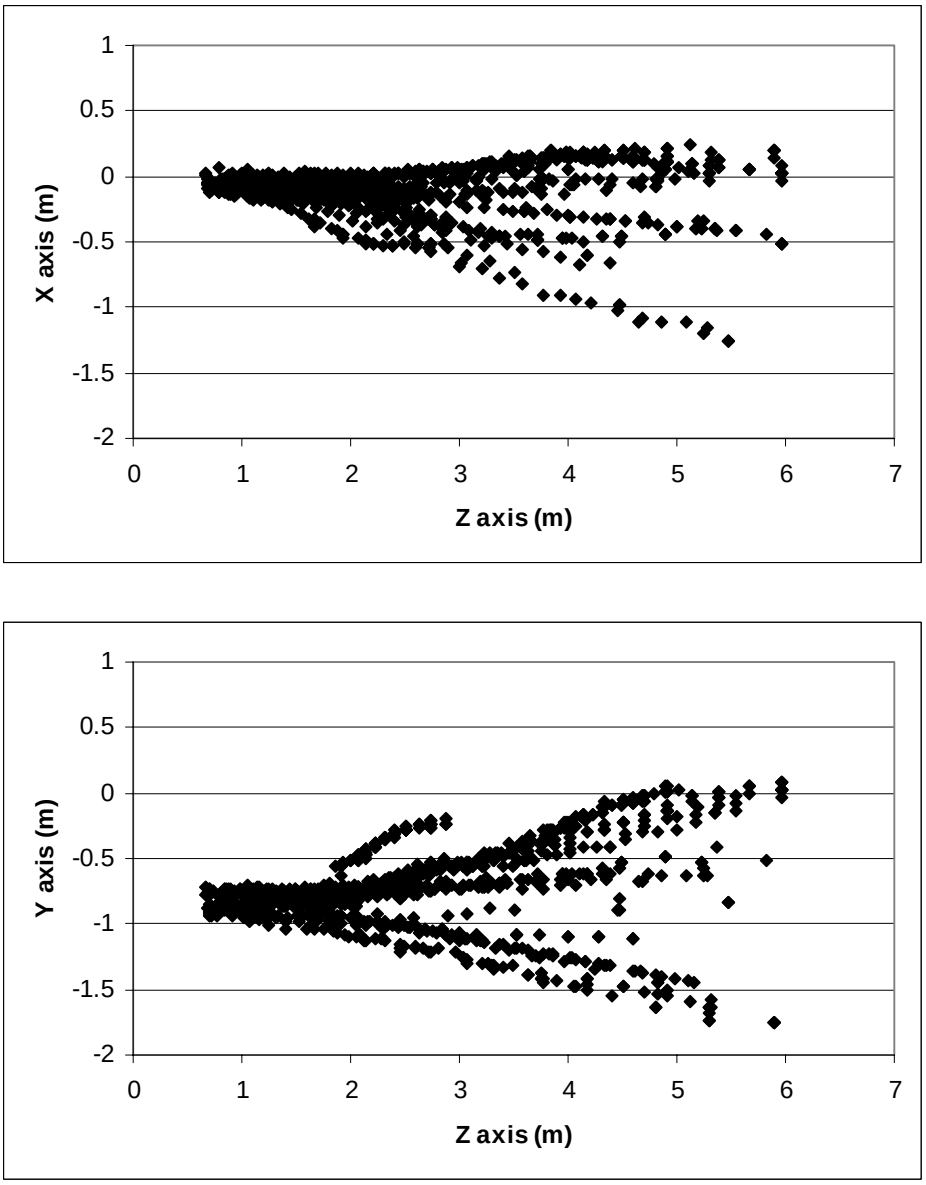

Figure 11. Trajectory of all LED drogues released into a turbine intake at McNary Dam at 40 MW load in the (a) X-Z plane and (b) Y-Z plane tracked with all six pairs of camera combinations. (Study conducted by PNNL for Walla Walla District USACE.)

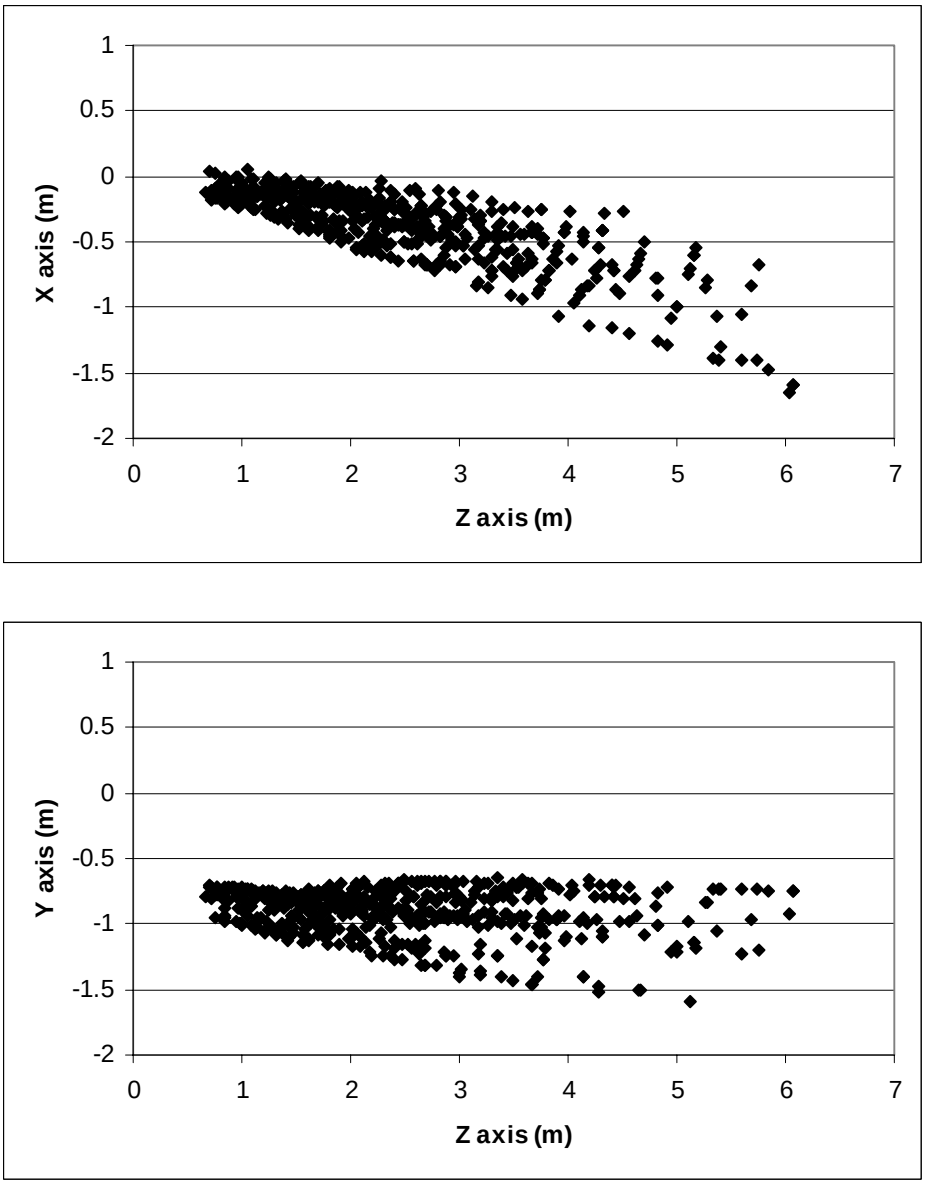

Figure 12. Trajectory of all LED drogues released into a turbine intake at McNary Dam at 60 MW load in the (a) X-Z plane and (b) Y-Z plane tracked with all six pairs of camera combinations. (Study conducted by PNNL for Walla Walla District USACE.)

It is usually not difficult, and relatively error free, to mount the camera in a known location; however, the aiming angle of the camera into the region of interest is much more difficult to measure accurately. To estimate the magnitude of possible LET location estimate error resulting from uncertainty in camera aiming angle, we modeled the trajectory of a LET through a four-camera array. The modeled trajectory was a straight line extending along the Z-axis (see Figure 3 for array orientations). We modeled the trajectory of an object with all cameras where certain cameras had a known error in orientation. Camera positions were as follows:

- On a known axis
- Camera 1 rotated positively 2 degrees along the X plane
- Camera 1 rotated positively 5 degrees along the X plane
- Camera 1 rotated positively 2 degrees along the Y plane
- Camera 1 rotated positively 5 degrees along the Y plane
- Camera 1 rotated positively 5 degrees in both the X and Y planes.

The trajectories modeled with known camera orientations provided correct trajectories for all three arrays (Appendix B). As expected, error in the calculated trajectory relative to the true trajectory of the LET introduced by camera aiming angle estimation error increased with distance along the Z-axis. Error in trajectory ranged from no error when the cameras were oriented correctly to over 4.7 m error when camera 1 was rotated positively 5 degrees in both the X and Y planes. The greatest error in position estimates occurred with cameras that were close together. By increasing the distance between cameras, bias due to error in measurement of camera placement can be reduced. A list of calculated errors for each camera pair and camera array geometry is provided in Appendix C.

5.1.4 Camera Arrays for Tracking LET Through Turbine Units

This section considers the placement of cameras in the draft tube and at the scroll case region of McNary Dam and Bonneville Dam powerhouse 1.

Scroll Case – Flows at the entrance to the scroll case at both Bonneville and McNary Dams can reach upward of 9.1 mps. Of the technologies discussed in this report, the high-speed cameras provide the finest scale spatial resolution (Figure 13), though not the longest range of detection. At flows of 9.1 mps, spatial resolution is about 7.6 cm at 125 frames/s and 3.8 cm at 250 frames/s. Spatial resolution of LET images recorded using a standard video camera (30 frames/s) would be 0.3 m under these conditions.

Though 0.3-m resolution will provide the trajectory of an LET, it will not provide information about fine-scale hydraulic conditions that fish experience during turbine passage. If the LET comes in contact with a structure (i.e., wicket gate or runner) during passage, the strike will most likely be missed because the camera frame rate is too slow, though a direction change after the strike may be recorded. Images of drogues and fish with LED arrays recorded using high-speed digital cameras will be more useful in observing their response to hydraulic conditions during passage through the scroll case but will not provide precise information on fine-scale turbulence and instantaneous shear forces due to the short duration of these events.

There are several points a fish can come in contact with as it enters the scroll case and passes the turbine runner. The stay vanes, wicket gates, and the turbine runner are the main possible points

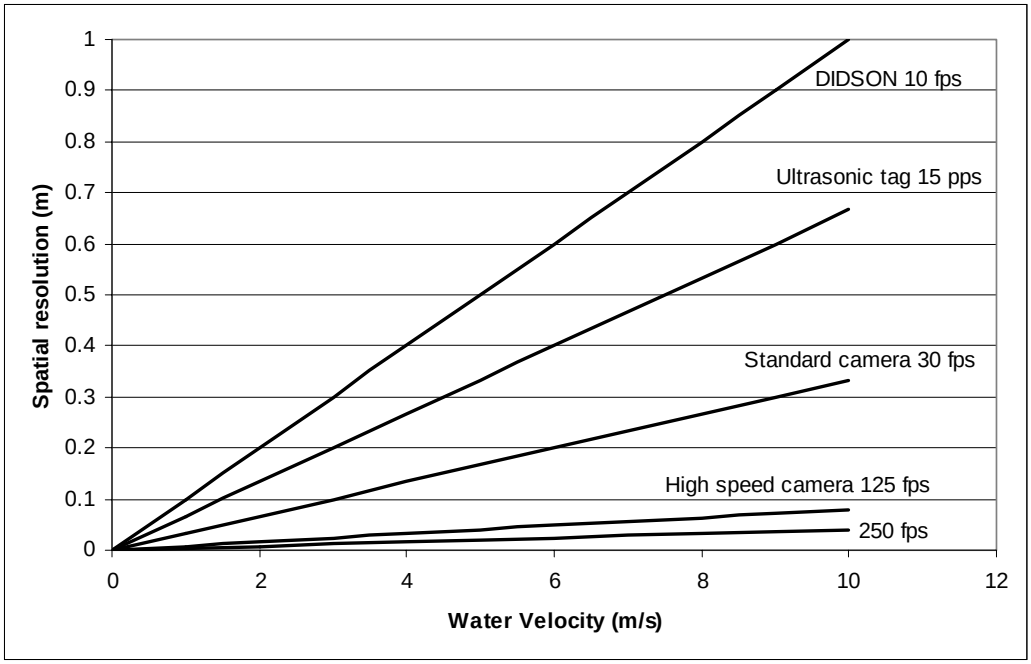

Figure 13. Spatial resolution possible of an object at various water velocities using the DIDSON at 10 frames/s, micro-transmitter at 15 ping/s, standard camera at 30 frames/s, and a high-speed digital camera at 125 and 250 frames/s.

of contact. Mounting a single high-speed camera above a stay vane will either show (1) the approach path and a record of the strike or (2) immediately before and immediately after the strike (Figure 14, camera 1). Images from a single camera can tell if a strike occurred and an X and Y location of the LET relative to the camera. The data will not provide information about the actual three-dimensional location of the lighted object relative to the camera because no distance component can be determined. The velocity that the object was traveling and force of impact if there was a strike cannot be estimated either. To obtain three-dimensional location data and velocity measurements, a second camera of known location relative to the first is necessary. Mounting both cameras above the stay vanes so both have fields of view overlapping the region of interest should provide good coverage. As noted earlier, spacing the cameras at least several feet apart will reduce errors in trajectory calculations caused by errors in the measurement of a camera location. A similar mount design could be used to evaluate strikes on wicket gates and—if cameras are positioned properly—could provide coverage of both the stay vane and wicket gate.

Image trajectory of the LET could be continued from the wicket gates into the scroll case and to the leading edge of the runner by adding four cameras aimed into the scroll case and with the flow (Figure 14, cameras 2-5). No single camera would provide complete coverage of the LET as it entered the scroll case until it exited through the runner. With proper spacing and angling of the cameras, and correctly mapping the location of the cameras relative to each other and the scroll case, a complete trajectory of the LET should be possible to cover a certain section of the scroll case, depending on where the LET enters the scroll case.

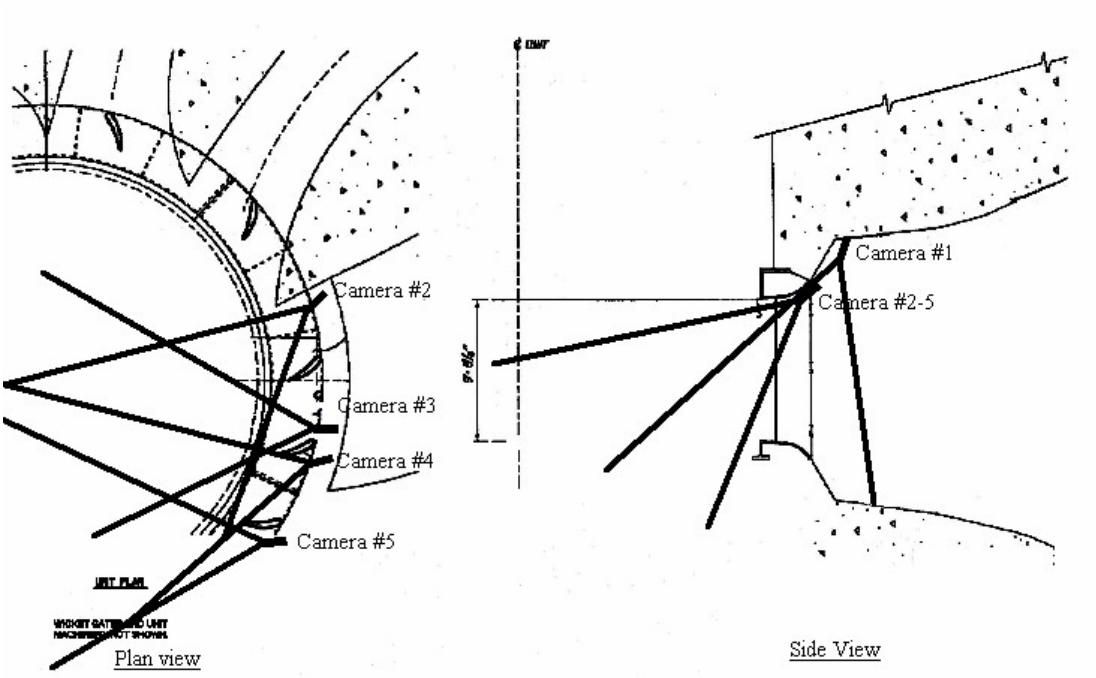

Figure 14. Plan and side view of a turbine scroll case and the deployment of cameras for tracking trajectories of light-emitting technologies from upstream of a stay vane to the tip of the runners.

Cameras were deployed at the scroll cases in the turbines at both Bonneville Dam powerhouse 1 (Figure 15) and McNary Dam (studies conducted by PNNL for Portland and Walla Walla District USACE, respectively). Because of flows and debris, the cameras and cables were well protected. To ensure that fish and drogues with LETs passed through the correct region of the scroll case, a system of pipes was installed to release the fish into the proper location (Figure 15) (Lindgren 2000; Carlson and Weiland 2001).

Draft tubes – In the draft tube, detection of all LETs will be less likely because placement will be more random due to being released above the runner. To ensure detection, a large number of cameras would be necessary to detect all LETs. Locations of interest need to be identified and bead releases in the physical model need to be conducted to determine the best release point for detection at a chosen location.

Looking with the flow could be deployed to view strikes on the vertical splitter at the centerline of the draft tube (Figure 16, camera 1-3). A second potential location for strikes is along the leading edge of the horizontal splitter. Eight cameras would be needed to cover the entire leading edge of the horizontal splitter. Data from the physical model could be used to determine the most likely location of impact, and cameras could be installed to view only a certain section of the horizontal splitter. Another location with an easier deployment is the downstream edge of the splitter with cameras aimed into the flow. Cameras could be attached to a frame and lowered into the stop log slot (Figure 16, cameras 4-8 and 9-13). The trajectory of LETs as they pass through

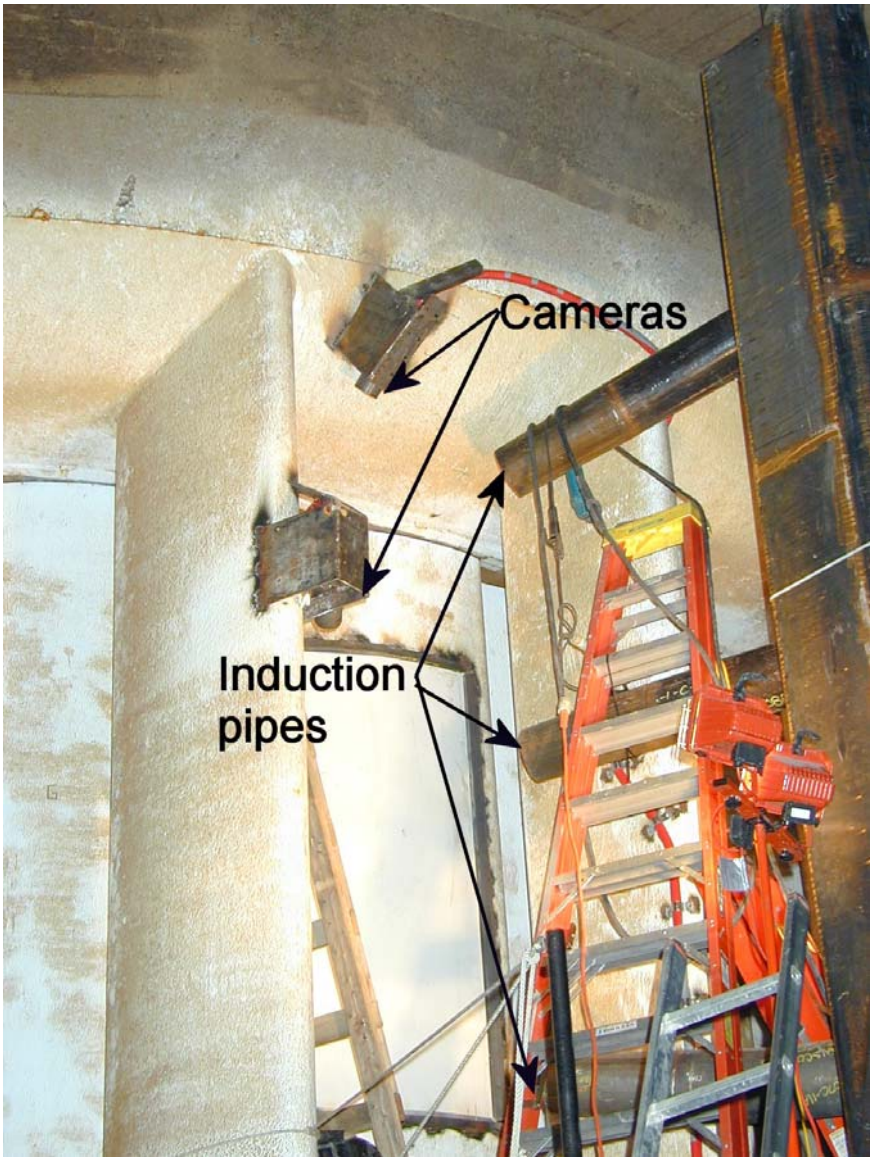

Figure 15. Standard frame rate cameras and protection mounted to a stay vane and the scroll case of a turbine unit at Bonneville Dam powerhouse 1 downstream of induction pipes for release of fish and drogues at specific locations. (Study conducted by PNNL for Portland District USACE.)

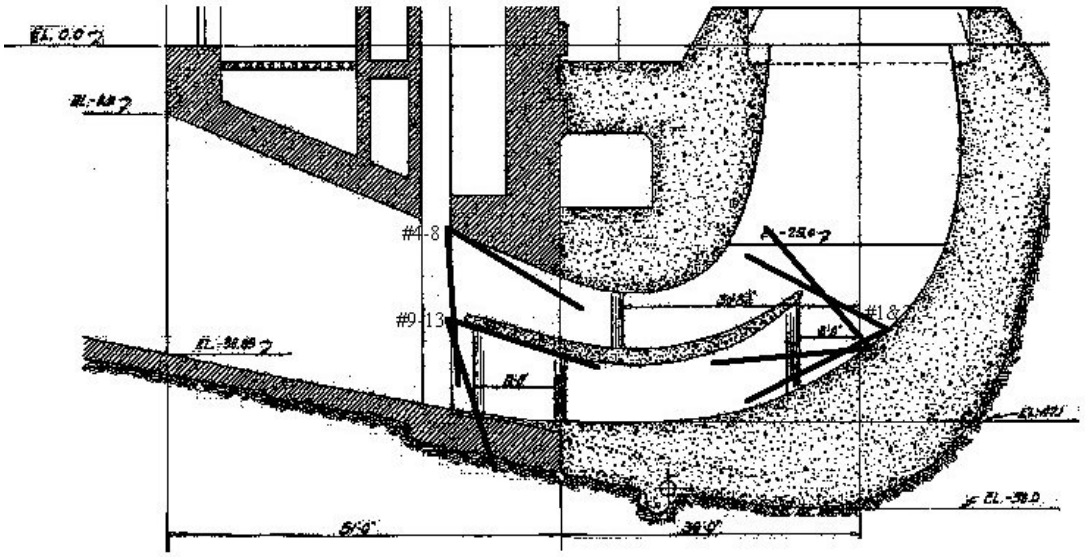

Figure 16. Draft tube at Bonneville Dam powerhouse 1 with the horizontal and vertical splitter and potential locations of cameras for viewing images of light-emitting tags during passage to evaluate strikes and affects of hydraulic conditions on trajectory.

the divided sections of the draft tube could be determined, and movement relative to hydraulic conditions could be described including the affect of the downstream edge of the splitter wall on LET trajectory. To get complete coverage of either the upper or lower section of half the draft tube, five cameras would be needed. Deploying cameras on a frame in this region is useful for initial testing before installing cameras in regions of more difficult deployment and can be useful in determining orientation of fish.

Camera configuration for deployment in the draft tube of McNary Dam would be similar to Bonneville Dam except for McNary Dam draft tubes have only a vertical splitter. Three cameras deployed upstream of the splitter wall would cover most of the splitter wall and trajectory of the LET as it approached the splitter and as it passed by (Figures 17 and 18, cameras 1-3). As at Bonneville Dam, it would require five cameras mounted on a frame lowered into the stop log slot to view across half the width of the draft tube at McNary Dam (Figures 17 and 18, cameras 4-8). Data from the physical model show water velocities as high as 5.8 mps at the center point of the stop log slot. At this velocity if the LET were in view for 6.1 m over 130 frames of data could be collected at 125 frames/s. This would provide a resolution of about 4.6 cm/frame. There are trade-offs between frame rate and the distance an LET can be viewed. As frame rate increases, the amount of light received by the CCD decreases. At higher frame rates, the LET will not be viewed for as great a distance as more light will be necessary to maintain the same viewing distance. Minimum light requirements for the Redlake Motionscope PCI camera at different frame rates and the Sony SSC-M370 camera are provided in Table 3. The infrared filters were left off both cameras, increasing the sensitivity at low light levels.

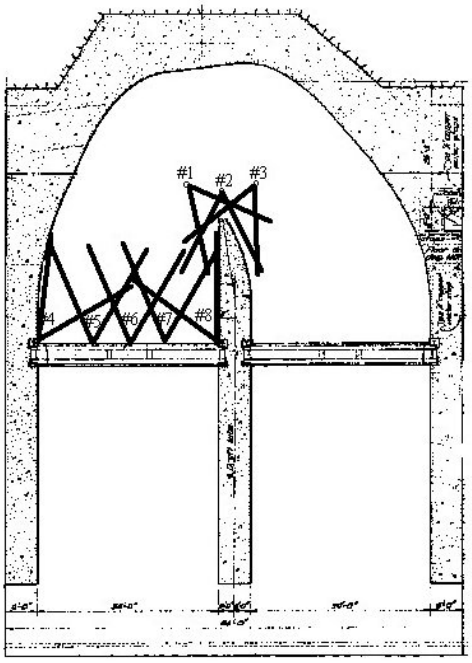

Figure 17. Plan view of a draft tube at McNary Dam and potential locations of cameras for viewing images of light-emitting tags during passage to evaluate strikes and affect of hydraulic conditions on trajectory.

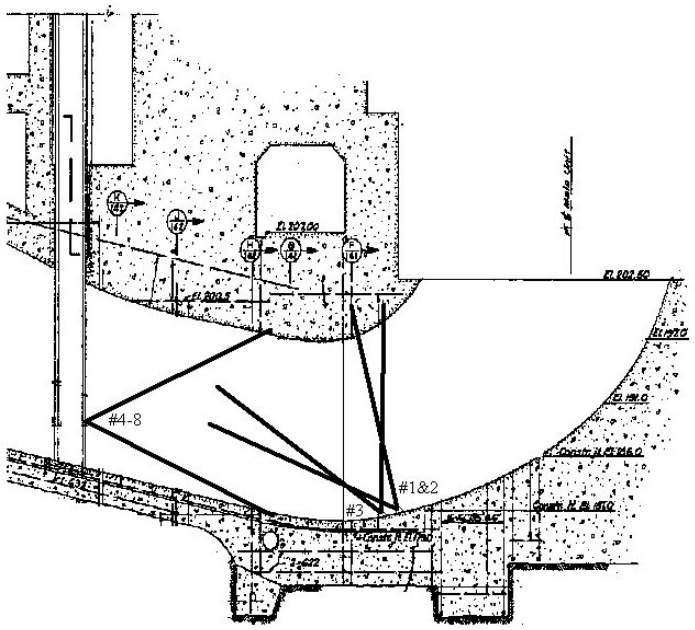

Figure 18. Side view of a draft tube at McNary Dam and potential locations of cameras for viewing images of light-emitting tags during passage to evaluate strikes and affect of hydraulic conditions on trajectory.

Table 3. Camera sensitivity relative to sample rate of cameras tested.

Camera	Sample rate (frames/s)	Illumination sensitivity (lux)
Sony SSC-M370	30	0.3
Redlake Motionscope PCI	60	0.10
Redlake Motionscope PCI	125	0.21
Redlake Motionscope PCI	250	0.43
Redlake Motionscope PCI	500	0.86
Redlake Motionscope PCI	1000	1.72

5.1.5 Summary

As an inexpensive and simple method of testing release pipes and areas of interest over a short distance or in water with low turbidity, CLEs can be used effectively. However, in turbid water and when the area of interest is a greater distance, LED drogues provide a greater distance of illumination for tracking and are bright enough to be viewed through turbid water for a much longer range than CLEs. During normal summer Columbia River conditions, LED drogues were visible for 6.1 m compared to only 1.5 m for CLEs.

Of the LEDs tested, the 5-mm dome LED was most applicable because of its size and intensity. Silver oxide button batteries were capable of powering the LEDs and were small enough for use in a subyearling salmon smolt tag.

We were not able to use differences in brightness to distinguish between LEDs of different color using black-and-white video cameras. The ability to identify individual LEDs within an array could provide useful information about the orientation of the drogue or fish at a point in time and how orientation may change in response to turbulence. Patterns in the location of LEDs in an array might provide orientation information using black-and-white cameras or the use of filters over the camera lens to change intensity of one of the color LEDs. Another possibility is flashing the LEDs in code. If this is done, the flashing of the LEDs can't be at the same rate or a multiple of the frame rate of the camera.

Of the three camera arrays, the linear array with all cameras in the same plane produced the most accurate trajectory estimate even when camera aiming angle errors were introduced into the calculations. Errors in calculated trajectory, however, decreased with an increase in the spread of the cameras for each of the three array geometries, where error was greatest for camera combination 1 and 2 and was smallest for cameras 1 and 4. Calibrating the camera array before deployment can further reduce LET position estimate error. This is accomplished by placing an object at a known location (i.e., its coordinates within the test environment space are known or can be determined) visible to all of the cameras in the array and measuring the angular offset of this point relative to each camera. This can also be accomplished by finding a stationary feature of the test environment visible to all cameras, determining its position, and establishing it as a reference mark. In the turbine environment, this could be accomplished by placing a light source

at a known location, within the field of view of all the cameras in an array. Such a reference would aid in the detection of shifts in camera aiming angle during data collection.

To track LETs through the scroll case of either McNary or Bonneville Dam powerhouse 1, two cameras are needed to detect and describe a strike on a stay vane or wicket gate, and an additional four cameras will be necessary to provide a complete trajectory to the runner blade. It will be necessary to release LETs in defined locations for maximum detectability by the camera array. Flows at the scroll case reach about 9.1 mps, and depending on the camera frame rate, spatial resolution will vary from 0.3 m at 30 frames/s to 3.8 cm at 250 frames/s.

In the draft tubes, the splitter walls are primary locations of interest for strike and injury to fish. To cover the vertical splitter at Bonneville Dam powerhouse 1 and McNary Dam, three cameras are needed to cover the entire vertical splitter. At Bonneville Dam powerhouse 1, there is also a horizontal splitter where eight cameras would be needed to provide complete coverage of the leading edge of the horizontal splitter.

Deployment of five cameras on a frame lowered in the stop log slot at either dam would provide cross-section coverage of half the draft tube width and provide trajectory and orientation data of LETs as they pass through a region of the draft tube. This is of most interest at Bonneville Dam with the horizontal splitter because ultrasonic tag technologies cannot be applied in this environment. Deployment on the frame is also ideal for feasibility testing before mounting cameras within the draft tube.

Drogues with sixteen 10,000-mcd LEDs can be tracked to a distance of up to 6.1 m under normal summer water conditions in the Columbia River. Greater distances can be tracked in winter when the water is less turbid using standard low-light cameras or high-speed, low-light cameras at frame rates up to 250 frames/s. There will be a trade-off between frame rate and the distance that targets will be detected. There is an inverse linear correlation between camera frame rate and camera sensitivity to light. Frame rate can be reduced to increase range of detection, though this reduces the spatial resolution of the trajectory. There is also a trade-off between the total range of detectability of the LET and the decreased precision in LET position estimates at short ranges because of the blooming of very intense light sources.

The frame rate used will also depend on the section of the draft tubes to be evaluated. Water velocity in the draft tube varies depending on the turbine load and the area of the draft tube being evaluated. Velocities calculated in the 1/25-scale McNary Dam turbine model at Waterways Experiment Station in Vicksburg, Mississippi, showed flows varying from less than 0.7 mps near the ceiling of the intake to 7.3 mps at a discharge of 466 m^3/s. These variables all factor into the range of detection and the number of images of the target of interest recorded. When the frame rate is doubled, the effective range of operation will be cut in half. Increasing LED intensity is the best means to improve detection and maintain a high frame rate.

5.2 Ultrasonic Tracking

5.2.1 Ultrasonic Micro-Transmitter Tests

Ultrasonic Micro-Transmitter Source Level Measurement – The source levels of a sample of 6 ultrasonic micro-transmitters operating at 307 kHz were measured in a test tank. For this sample, the source level of the micro-transmitters was about 147 dB re//1µPa at 1 hr. The measured source levels were consistent with specifications provided by the micro-transmitter manufacturer. For the rest of this report, an average source level of 147 dB re//1µPa at 1 m will be used. The bandwidth of the micro-transmitter pulse was 3 kHz, from 306 kHz to 308 kHz.

Background Noise Level Measurement – Sound pressure measurements downstream of the draft tube outlets at Bonneville Dam powerhouse 2 looking across the tailrace showed average sound pressure levels in the tailrace at about 99 dB re//1µPa, above 10 kHz, and maximum noise levels were below 5 kHz (Figure 19). Six of the eight turbines were operating at this time. At Lower Granite Dam, sound pressure measurements were collected in spring when five of the powerhouse's six turbines were operating. Measurements were taken again in late summer when only one unit was operating. In spring when five turbines were operating sound pressure levels above 10 kHz averaged 109 dB re//1µPa and in summer averaged 15 dB lower than spring at 94 dB re//1µPa (Figure 19).

To evaluate if sound pressure levels varied at different draft tube outlets in the tailrace, the hydrophone was lowered in front of four units at Lower Granite Dam during the spring generation. Sound pressure measurements were lowest at units 1 and 6, at opposite ends of the powerhouse, and were highest at units 4 and 5. According to this data, sound pressure levels are highest near the center of the powerhouse and are not dependent on the generation of a single unit, as unit 5 was not operating during our testing. In a similar study, a directional hydrophone was deployed from shore in the tailrace at Bonneville Dam powerhouse 1 and sound pressure measurements collected with the directional hydrophone aimed toward the dam, across the tailrace and downstream. The sound spectrum for the three different directions of measurements is almost identical (Figure 20). These data show (1) higher noise levels over a wider range at lower frequencies and (2) lower noise levels at higher frequencies in the measured spectrum, as we found in our data. However, the previous data also show a small peak in noise at about 300 kHz.

Micro-Transmitter Detection Range Estimation – The detection range of an acoustic tag depends on the source level of the tag and the ambient noise in the study environment. If the micro-transmitter signal when it reaches the receiver is not higher than the noise level at the receiver, the signal will not be detected. The amplitude of an acoustic signal decreases as it propagates because of spherical spreading and absorption (Urick 1983). Absorption losses in fresh water are minor; therefore for most fresh water applications, the major reason for decrease in the strength of the transmitted signal with distance is spherical spreading. This signal loss, background noise level, and characteristics of the system receiver determine the detectability of micro-transmitter transmissions.

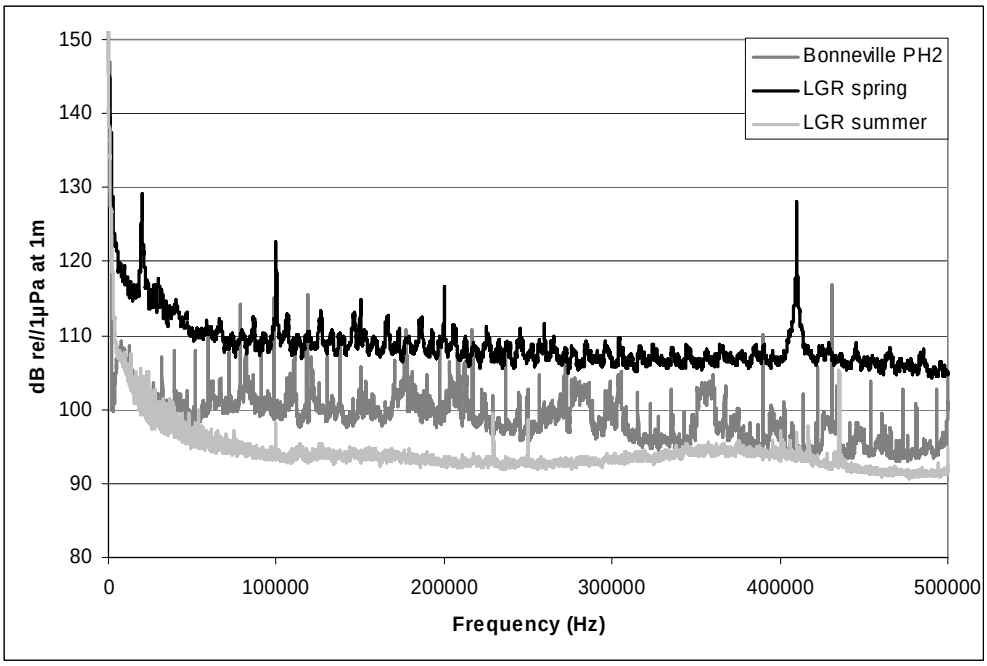

Figure 19. Background sound spectrum frequency measurements collected in the tailrace at Bonneville Dam powerhouse 2 and at Lower Granite Dam during spring and summer generation.

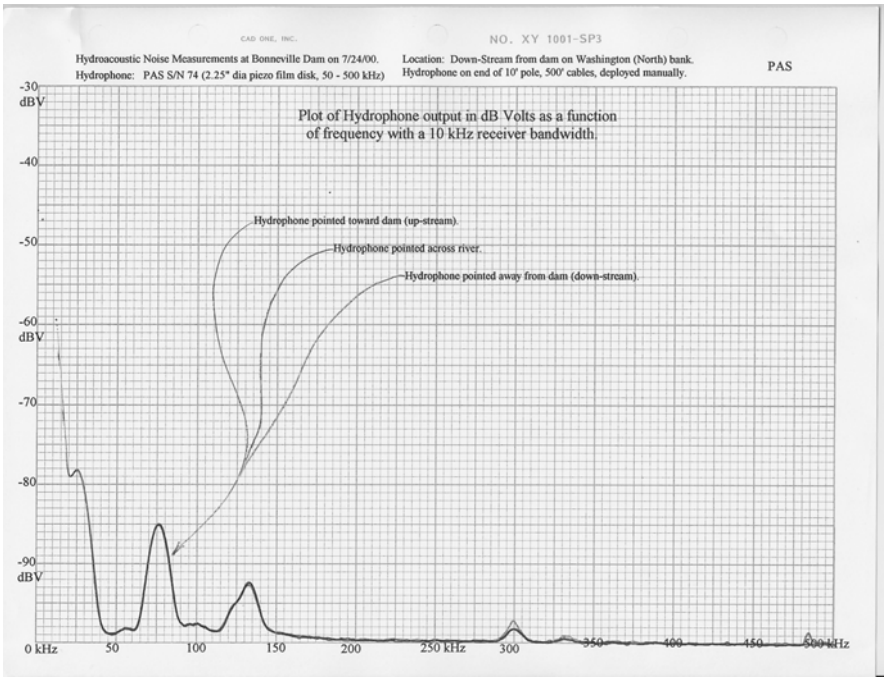

Figure 20. Directional sound measurements collected in the tailrace at Bonneville Dam powerhouse 1 (printed with permission of Robert Johnson, Pacific Northwest National Laboratory).

Using the 147 dB measured source level for the 307-kHz acoustic micro-transmitters and the background noise level presented in Figure 19, we estimated the theoretical micro-transmitter detection distance assuming only spherical spreading. This was done assuming a 3-dB signal-to-noise ratio as our detection threshold. At Bonneville Dam powerhouse 2, assuming only spherical spreading, we should be able to detect the tag at ranges up to 195 m, given the sampling conditions. At Lower Granite Dam, the detection range varied from 70 m when five units were operating in spring to 375 m detection range in summer when only one unit was operating (Figure 21).

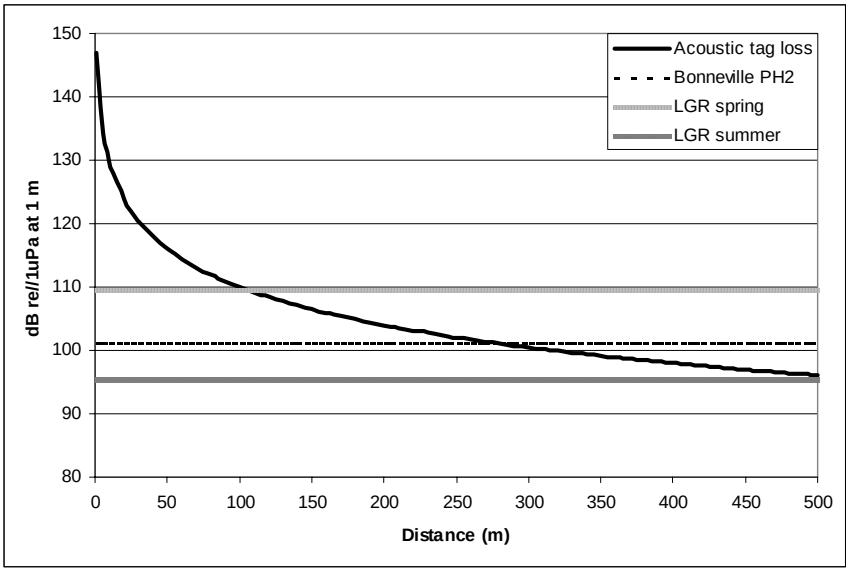

Figure 21. Estimated loss in signal strength of a 307 kHz, 147 dB acoustic tag calculated due to spherical spreading with increasing distance from a receiver relative to sound measurements at 307 kHz collected at Bonneville Dam powerhouse 2 and Lower Granite Dam in spring and summer. To account for the signal-to-noise ratio necessary to exceed the detection threshold of the receiver system, 3 dB was added to the 307 kHz signal.

To determine the actual detection range of the tag, the contribution of signal loss from acoustic energy scattering also needs to be considered. Energy is scattered by particles in the water, fish, water boundaries, and air bubbles (Urick 1983). The variables that cause the scattering of energy vary between location. In the case of the tailrace generation, the variables that cause the scattering of energy vary by level. These variables make it difficult to determine the effect scattering has on the detection range of the signal without taking actual measurements. We used field data collected at Bonneville Dam powerhouse 2 to estimate the range of tag detection relative to signal-to-noise ratio. The power of the signal was estimated by summing the power of the acoustic signal (from 306 kHz to 308 kHz) and estimating the noise level by summing the 3 kHz frequency range on each side of the acoustic signal. Results of calculated signal-to-noise ratios by distance from the hydrophone and relative to gain added to the incoming signal show that the tag should be detected to greater than 61 m with 0, 20, or 40 dB of gain (Figure 22).

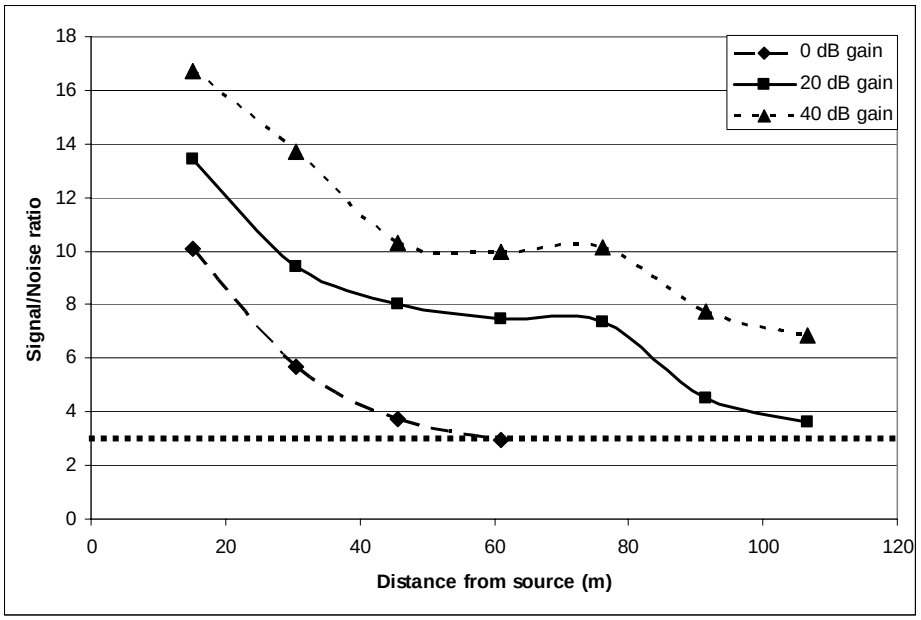

Figure 22. Calculated signal to noise ratio of a 307 kHz acoustic tag measured over a range of distances from the hydrophone at Bonneville Dam powerhouse 2. The signal was passed through an amplifier with 0, 20, and 40 dB gain. A 3 dB detection threshold was used as the minimum signal to noise ratio that could be detected by the receiver.

These results show it is possible to detect acoustic tags in the tailrace of dams though the distance of detection will depend on the individual dam and the dam's operation levels during testing. There are several ways to improve the range of detectability of the acoustic tags in the tailrace. One way is to increase the output signal of the acoustic tag, although there are trade-offs to this method. To increase signal output, either the tag size will need to be increased or the life of the tag shortened. A second way to increase tag detectability is to use a directional hydrophone. The distance the tag can be detected will be increased, but the angle of coverage will be reduced increasing chances of missing a tag signal. Another way to increase detectability is to improve the efficiency of the ceramic element in the hydrophone. The current hydrophones used in the Columbia and Snake River Basins are broadband hydrophones. An element specifically designed from use in the 307-kHz range would improve signal detectability.

5.2.2 Acoustic Tracking Baseline Arrays

This section considers the placement and design of acoustic tracking baselines in the draft tubes and powerhouse tailrace of two lower Columbia River dams. Using information gained from analysis of the detectability of acoustic tags in the presence of noise generated by turbines combined with experience tracking fish through a turbine intake at McNary Dam, tracking baselines were designed for the draft tubes and powerhouse tailrace for Bonneville Dam powerhouse 1 and McNary Dam.

Bonneville Dam Draft Tube Tracking Array – The draft tubes of powerhouse 1 at Bonneville Dam are unique in that they have both vertical and horizontal flow splitter walls. The splitter walls divide the draft tube into four sections. The resulting sections are too small and "tube like" to be attractive for detailed tracking of acoustic transmitters passing through them. Neither the line-of-sight nor the time-of-arrival methods are considered feasible for tracking a micro-transmitter passing through the upstream sections of these draft tubes. However, it would be feasible to monitor the outlets of the four sections and detect micro-transmitters exiting each section and to track the transmitters as they passed the remaining distance through the draft tube.

It may be feasible to look downstream from the stop log slot using the line-of-sight acoustic tracking system. (This assumption is probably reasonable given experience at McNary Dam and the results of background noise measurements at the draft tube exits of both McNary and Bonneville Dams.) The transducers would have to be installed on a frame and lowered into the slot. All four receivers would be positioned in the center vertically on the frame and aimed downstream. One receiver would be positioned near the top of the frame, one near the bottom, and two in the middle of the frame in line with the downstream end of the splitter wall. This configuration will provide coverage of a large volume of the draft tube for the downstream 1.8 to 3.0 m of the draft tube. In addition, this configuration will provide coverage into the tailrace, but will only provide limited coverage—up to about 6.1 m—inside the draft tube. Model data from the 1/25-scale model for McNary Dam shows that flows from 4.6 to 6.1 mps can be expected in this section of the draft tube. At these water velocities, an acoustic tag would be within the detection volume within the draft tube for 1 s at best requiring a high ping rate to collect position data. Tags with a ping rate of 15 pps were used to track fish through the turbine intake a McNary Dam in 2000 (Carlson et al. 2002; studies conducted by PNNL for Walla Walla District USACE).

The time-of-arrival acoustic tracking array provides a much larger sampling volume than the line-of-sight array when deployed in the lower end of the draft tube, providing coverage for most of the area in the draft tube downstream of the stop log slot. This array can also be extended into the tailrace and provide added coverage of fish movement and behavior through the boil, direction of movement, and residence time as the fish moves downstream. Four hydrophones attached to each of the four corners of a frame lowered into the stop log slot and six hydrophones mounted at the outside corners of the downstream corners of the draft tube would provide three-dimensional coverage inside the draft tube (Figure 23). Using the FishTrack3D^{TM} error estimation program, the geometric dilution of precision of a tracking array was estimated. Error analysis showed position estimates to be within 0.3 or 0.6 m within the tracking array and closer to 0.9 m at the edges and outside of the boundary of the tracking array (Figure 24). Actual error in location estimation will probably be greater than those estimated with FishTrack3D^{TM} because of the noisy environment of the draft tube, compared to the quiet environment in which FishTrack3D^{TM} was modeled and tested (Faber et al. 2002).

Properly positioned hydrophones in the immediate tailrace below the turbine unit of interest could provide three-dimensional coverage with good accuracy (Figure 25). Because of the bathymetry in the tailrace of Bonneville Dam powerhouse 1, placement of hydrophones will result in unique

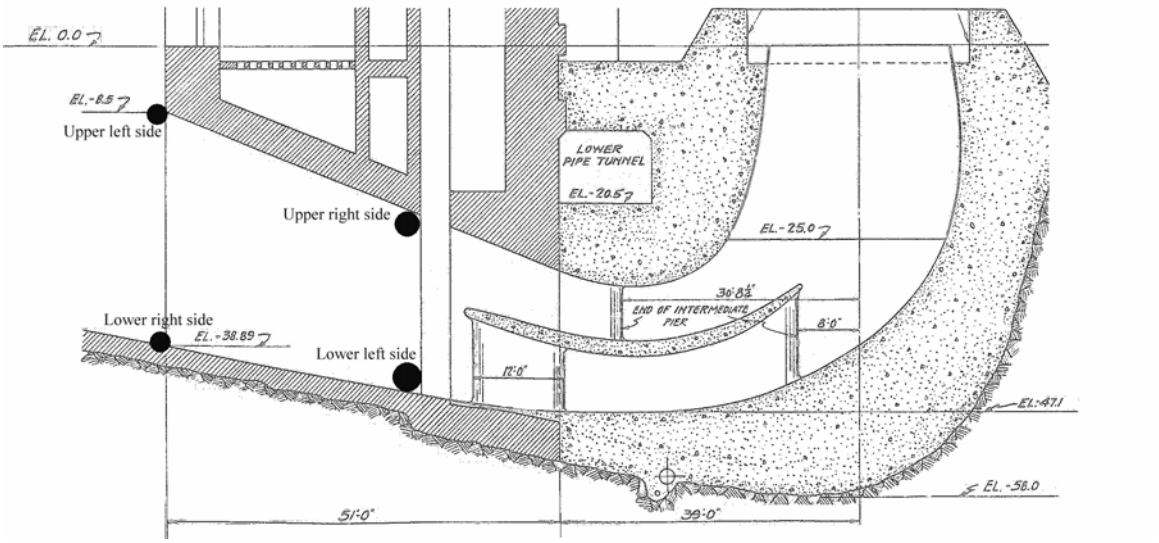

Figure 23. Side view of possible hydrophone locations on a frame in the stop log slot in the draft tube and on the pier nose in the tailrace at Bonneville Dam powerhouse 1.

challenges. The tailrace becomes shallow quickly downstream of the dam. These extreme changes in elevation will make anchoring hydrophone mounts difficult but possible with the right mounts and assistance of divers.

McNary Dam Draft Tube – The draft tubes at McNary Dam, unlike powerhouse 1 at Bonneville Dam, are divided in half by one vertical splitter wall. With this draft tube configuration, it is possible to view into the upstream section of the draft tube using the line-of-sight acoustic system. For the line-of-sight array, there are two possible array designs, depending on which section of the draft tube is of greatest interest. The designs could be used for either the A or C side of the draft tube. Because flows are greatest in the C side, according to the Waterways Experiment Station 1/25-scale model, drawings are for the C side of the draft tube.

One of the array designs uses the stop log slot for inserting a frame with the receivers attached and aimed upstream. The receiver array aimed upstream from the slot toward the turbine covers a large area directly below the turbine to about 7.6 m downstream of the back wall (Figure 26). The other possible array configuration involves mounting the array at the downstream end of the draft tube looking back into the draft tube. This configuration would cover the largest volume of the draft tube and cover a length of about 24.4 m though it would not be able to detect tags in the area directly below the runner (Figure 27).

A time-of-arrival array of the same design discussed for the draft tube at Bonneville Dam could be deployed in the lower section of the draft tube at McNary Dam and in the immediate tailrace. The tailrace at McNary Dam is well suited for a time-of-arrival acoustic tracking array. The bottom slopes much more gradually than at Bonneville Dam powerhouse 1, and the area directly downstream of the powerhouse is fairly level.

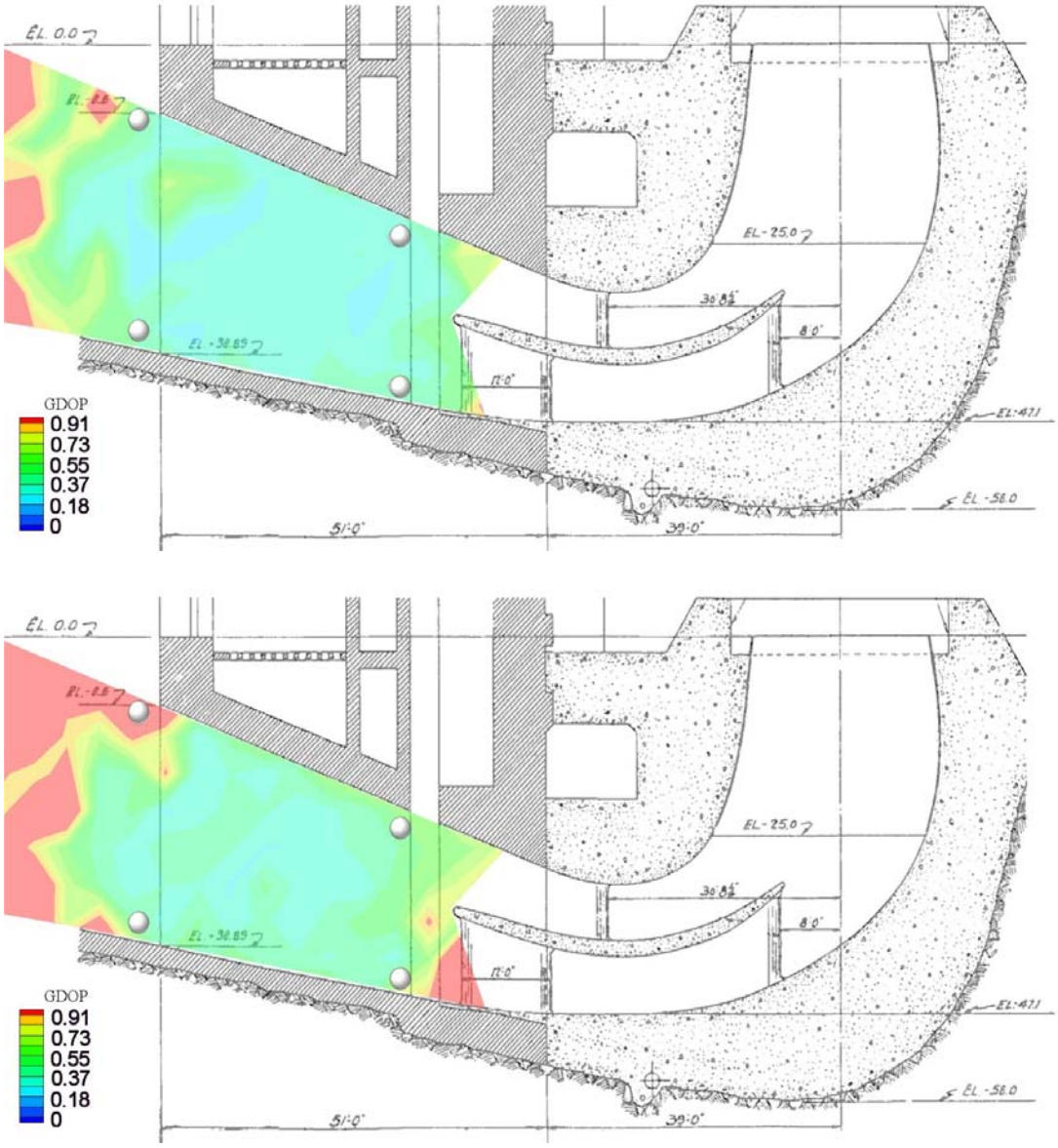

Figure 24. Estimated error (m) in predicted location of acoustic tags for the time-of-arrival tracking array for (a) center and (b) near the edge of a draft tube at Bonneville Dam powerhouse 1 using FishTrack3D^{TM} to estimate geometric dilution of precision.

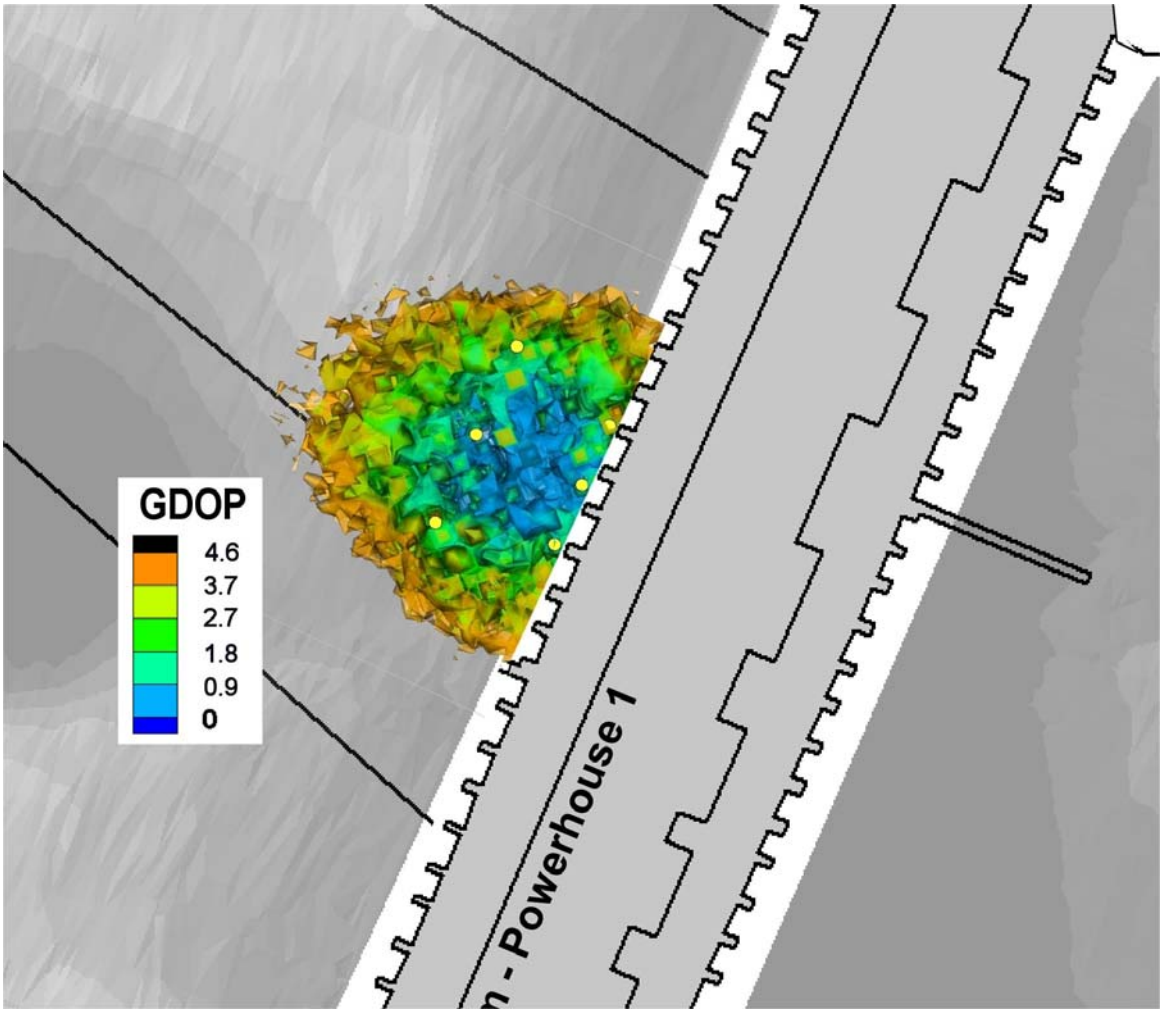

Figure 25. Estimated error (m) in predicted location of acoustic tags for the time-of-arrival tracking array in the immediate tailrace of Bonneville Dam powerhouse 1 using FishTrack3D™ to estimate geometric dilution of precision.

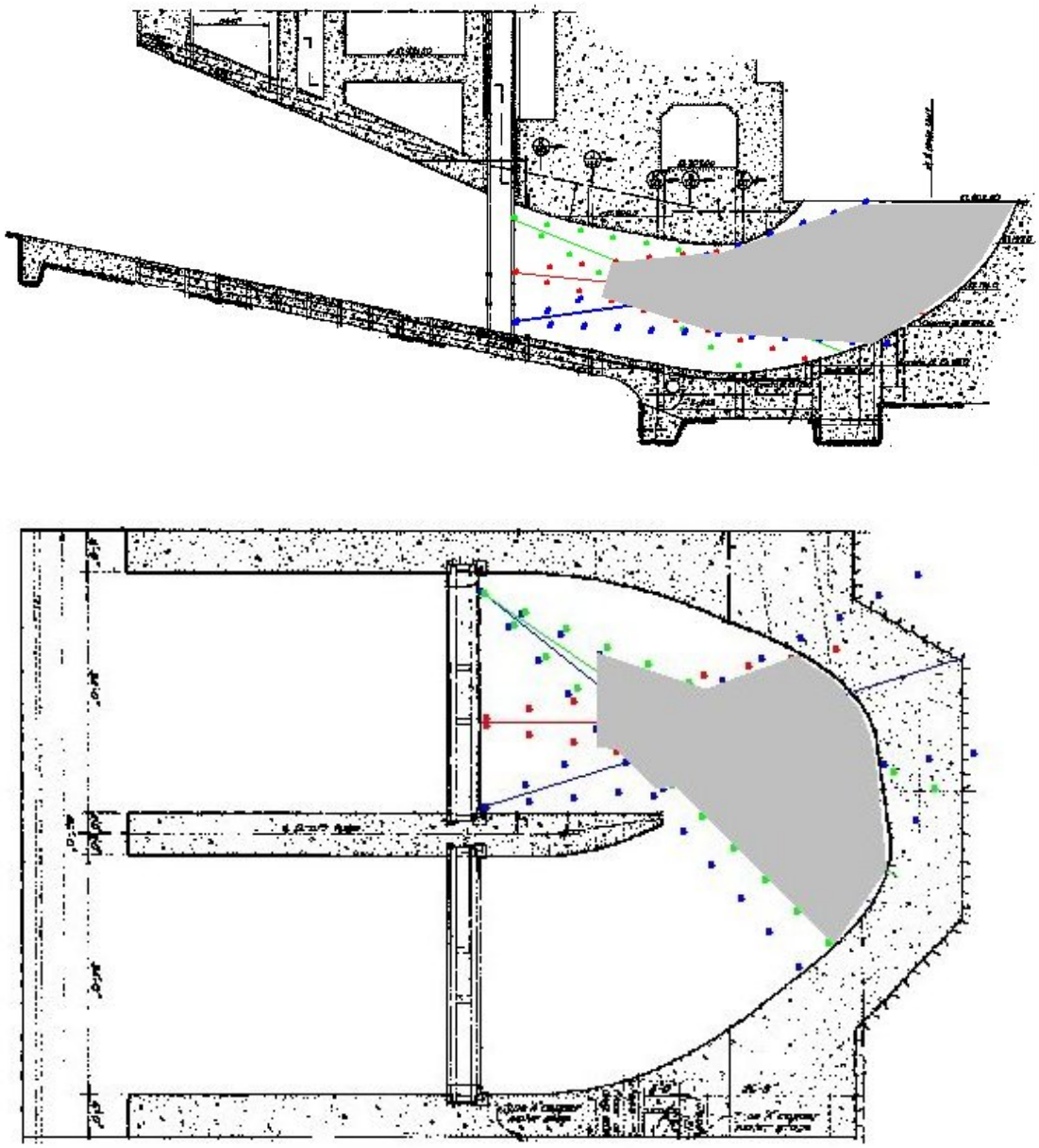

Figure 26. Receiver positions and sampling volume for (a) side and (b) plan view of area covered by line-of-sight array aimed upstream from the stop log slot in draft tube at McNary Dam.

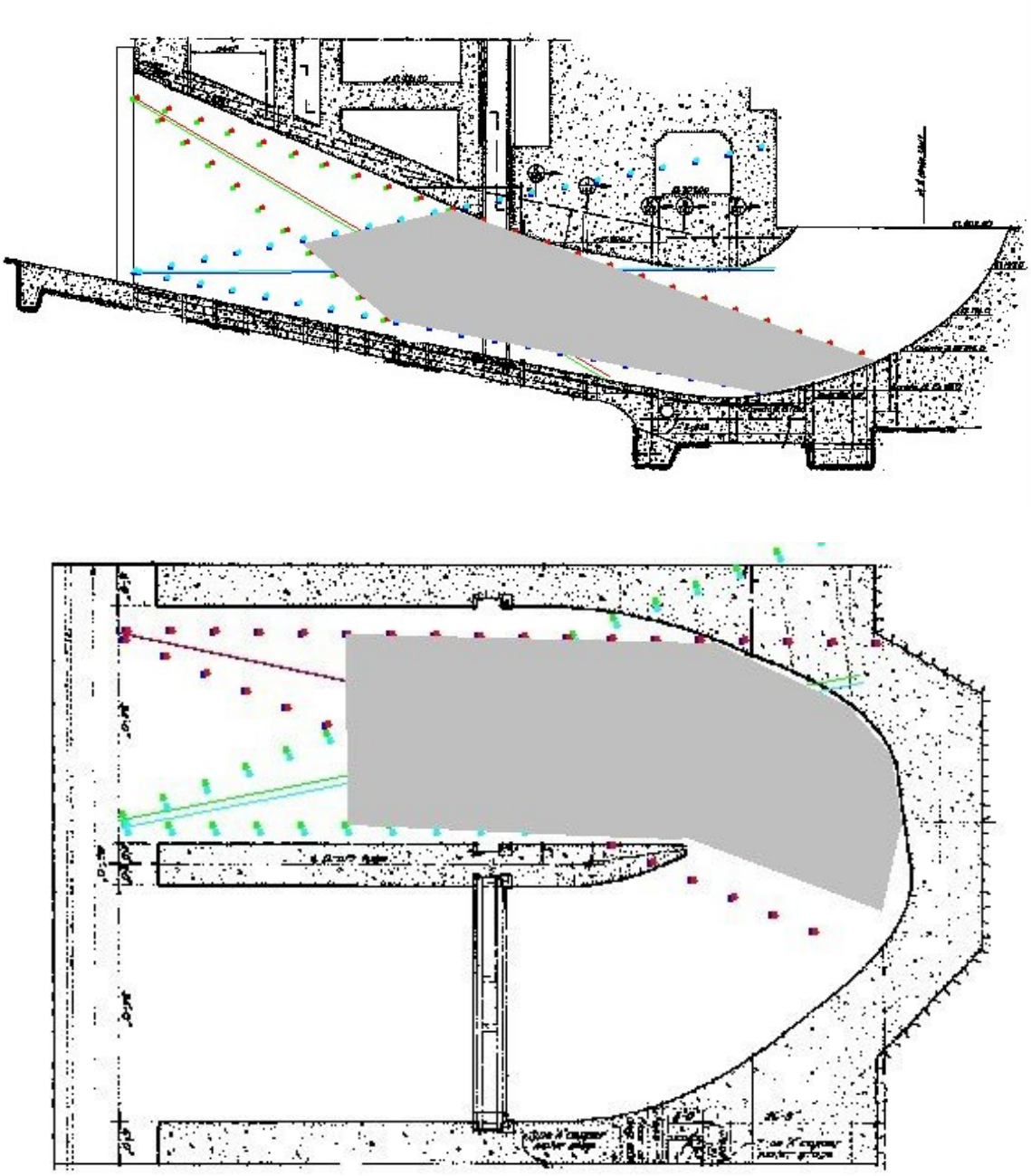

Figure 27. Receiver positions and sampling volume for (a) side and (b) plan view of area covered by line-of-sight array aimed upstream from the lower end of the draft tube at McNary Dam.

5.2.3 Acoustic Tag and Drogue Design

Frequencies currently used for acoustic tags in the Columbia River Basin, 307 kHz and 420 kHz, should be suitable for use in the turbine draft tube region of dams, though increased sound pressure levels were measured at 410 and 430 kHz in the tailrace of Lower Granite Dam. To increase the flexibility of the tags, a standard frequency should be used for both acoustic tracking arrays to reduce the variety of tags necessary and allow for tracking of tags through both array types during simultaneous testing, increasing the tracking range of individual tags.

There are compromises between tag size, duty cycle, operation life, and source level when designing an acoustic tag. Any increase in duty cycle, operation life, or source level will increase energy consumption. An increase in energy consumption requires more or larger batteries; in turn, the tag must be made bigger or the other two elements must be made smaller. Tag size is limited by the size of the fish; a tag weighing no more than 5% of the fish body weight is recommended, to reduce the effect of tag weight on fish behavior (Adams et al. 1998). For subyearling (~8 g) and yearlings (~25 g), the tag should weigh no more than 0.4 g and 1.25 g, respectively. For steelhead kelt (~ 2000 g), the tag can weigh more. The size and shape of the tag will also depend on if the tag is surgically or gastrically implanted.

The operating life span of the tag needs to be long enough for the tag to be activated, tested to ensure tag is active, released through the turbine unit, and acoustic data collected. In a 1999 study by PNNL for the Walla Walla USACE at McNary Dam, the tags used had an operating life of about 20 min; in a 2000 study at the same dam, the tag operating life was 120 min. In this study, tags were gastrically inserted into the fish before release, and time was required for the fish to recover before release. Thus 20 min was not long enough and allowed for no error. We suggest a tag life of at least 30 min if an active tag will be gastrically inserted in the fish or possibly using an acoustic signal or magnetically activating the tag to allow more time for the fish to recover, or allow for surgical implantation in the fish.

The acoustic tag must have a source level that is sufficient to allow detection by the receiving array within the desired range. Inside the draft tube of a dam, the desired range can be nearly 30.5 m. The greatest average sound pressure measurements collected in a dam tailrace were collected at Lower Granite Dam in the spring at 125 dB. Back calculating using 125 dB as the background sound pressure level, taking into account only spherical spreading loss, the tag output 30.5 m from a receiver would need to be 156 dB to match the background noise. To be detected by the receiver, the tag would need to have a source level of at least 159 dB if the receiver had a 3 dB receiver sensitivity. This output is possible. Acoustic tags used at McNary Dam in 2000 (study by PNNL for Walla Walla District USACE) had a source level of 160 dB with a ping rate of 15 pps but weighed 1.86 g. With advances in the technology, tag sizes can, and have been, reduced, but there will still be trade-offs between the size of the tag possible and the ping rate to obtain the necessary source level.

In the high flow environment of the draft tube, ping rates of at least 30 pps are desirable to obtain spatial resolution of less than 0.3 m. This resolution is adequate for estimating tag trajectory and

describing large variations in trajectory caused by strike or hydraulic changes. However, this resolution could not be used to measure the force of an actual strike or acceleration caused by a hydraulic event.

The constraints on tag size and shape are reduced for drogues because the tag does not have to be tightly packaged for insertion into the fish and because the drogue will have similar mass to the fish, not 5% the mass of the fish. With drogues, a larger battery can be used, providing the energy necessary for a greater ping rate and/or source level. The drogues will be of similar design as those described for the LED drogues (Figure 7).

5.2.4 Summary

Field tests conducted in the powerhouse tailraces of Lower Granite Dam and Bonneville Dam powerhouse 2 showed that standard 307-kHz acoustic tags are detected in this environment out to ranges of 61 m to over 110 m from a hydrophone mounted at the exit of a draft tube. This range will differ between dams and operating conditions and will need to be assessed during study planning. These differences in sound pressure intensity and frequency between dams is consistent with difference at low frequencies found by Anderson et al. (1989) in the forebays of Lower Granite Dam, McNary Dam, and Bonneville Dam powerhouses 1 and 2.

Because of high water velocities in the draft tube and the immediate tailrace of the dam, acoustic tags with a higher ping rate than currently used will be necessary. This may reduce the amount that the signal strength of the tag can be increased. Standard ping rates for fish tracking in the Columbia River Basin are in the range of 2 pps (Faber et al. 2001). Ping rates of 15 pps at 420 kHz with an average tag life of 120 min were used to track fish through the turbine intake a McNary Dam in 2000 (Carlson et al. 2002). Water velocities in the draft tubes at McNary Dam can vary from less than 0.7 mps near boundaries to over 7.3 mps from data collected in the 1/25-scale physical model at the Waterways Experiment Station. At water velocities of 7.3 mps and a tag ping rate of 15 pps, the spatial resolution of the tag will be 0.5 m. The ping rate necessary will depend on the region of interest and the spatial resolution of the data required.

The draft tube and immediate tailrace at McNary Dam can be covered using line-of-sight and time-of-arrival tracking arrays. However, the same degree of coverage is not feasible at Bonneville Dam powerhouse 1 because of the configuration of the draft tube splitter walls. Though tracking with line-of-sight and time-of-arrival methods is possible, developing a tag with a high enough source level and ping rate and small enough size that does not affect fish behavior is important. Adams et al. (1998) suggest not implanting tags greater than about 5% of the fish body weight into smolts.

The current version of the line-of-sight tracking array tracks tags at a frequency of 420 kHz. The 420-kHz tag used in turbine intake tests at McNary Dam had a greater source level than the 307-kHz tag. However, sound level measurements at the draft tube exits and immediate tailrace at Bonneville Dam powerhouse 2 and Lower Granite Dam show increased background noise levels at between 410 and 430 kHz. The line-of-sight system can be modified to track 307-kHz tags. This could also improve coverage if both line-of-sight and time-of-arrival systems were

deployed where tagged fish were tracked using the line-of-sight system as they moved from below the turbine runner through the draft tube, and the time-of-arrival system was used to track the fish as they passed through the lower end of the draft tube and into the tailrace.

In a turbine intake at McNary Dam, fish and drogues with micro-transmitters were successfully tracked through the intake using a line-of-sight array. However, tracking tagged fish or drogues from the stay vanes to the runner blades with line-of-sight or time-of-arrival arrays is not feasible; the reason is that the spatial resolution is only 0.6 m with the current ping rate of 15 pps and water velocities of 9.1 mps. Another problem of trying to track an active acoustic micro-transmitter through a scroll case is multi-path. With the ping rate necessary to provide useful spatial resolution in the confined scroll case, it may be difficult to separate a direct signal from multi-path. The direct signal may also be corrupted by multi-path.

Producing an acoustic tag for kelt of adequate size, source level, and ping rate is possible considering the size of the fish. Producing a tag near 5% of the weight of subyearling and yearling smolt will be more difficult especially with the size constraints of the tag, especially for subyearlings. Compromises between source level, ping rate, tag life, and size will be necessary to produce a tag suitable for tracking salmon smolt through the turbine draft tubes. Building a similar tag for deployment in a drogue has far fewer constraints because of fewer packaging constraints.

5.3 Ultrasonic Imaging Sonar

In the test flume, DIDSON images were range restricted to the first 5 m from the face of the acoustic camera. Figure 28 shows a DIDSON image of an LED drogue. All images collected in the flume were recorded at 1.8 and 2.0 MHz at flows of 1.5, 3.0, or 4.6 mps. Review of DIDSON images acquired at 1.8 and 2.0 MHz showed that the DIDSON image display was much clearer when collected at the 2.0-MHz setting. Based on this finding, we focused efforts into data collection at 2.0 MHz.

Before the drogue was released, the injection system's ball valves were opened to introduce air into the water and cloud the DIDSON video image. The density of the bubble cloud produced was notably different between the 1.5, 3.0, and 4.6 mps flows. Analysis of images revealed that even with the bubble cloud present, the injected drogues could be observed at flows of 1.5 mps and 3.0 mps; however, no drogues were observed at 4.6 mps flows in the bubble clouds. The amount of air entrained in the water at 4.6 mps was extreme and probably exceeds levels of entrained air experienced in a draft tube. Also, air bubbles were larger than those experienced in the turbine environment.

In a simple test to determine if turbidity affected detection ability in a turbid environment, 10-micron glass beads were released into the flume. Though the glass beads were detected with the DIDSON, the drogues released into the flume could be identified in the "turbid" environment.

Using the DIDSON, we found it possible to identify some fish by species using physical characteristics such as body shape, fin shape, and fish size (Figure 29). The northern pikeminnow

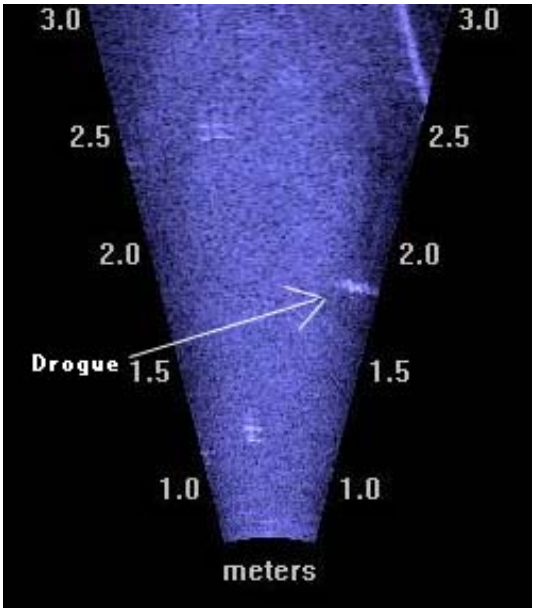

Figure 28. DIDSON image, recorded at 2.0 MHz, of a drogue released into the flume at an inducted flow rate of 3.0 mps.

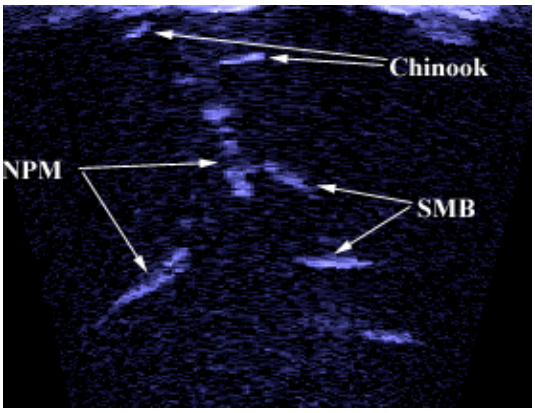

Figure 29. DIDSON image of northern pikeminnow (NPM), smallmouth bass (SMB), and Chinook salmon smolt collected in a tank.

was easiest to distinguish due to the size and shape of its pectoral fins (Figure 30). Steelhead and Chinook salmon were often differentiated by size, but in some cases, it was possible to differentiate smallmouth bass from steelhead and the Chinook salmon by physical characteristics. We were not able to distinguish between steelhead and Chinook salmon of similar size and were not able to differentiate between a 120-mm smallmouth bass and steelhead or Chinook salmon.

The DIDSON measurement tool was used to estimate the lengths of imaged fish with known lengths between 137 and 502 mm. Using the tool, we were able to estimate actual fish length to within 2 cm in all cases; the resolution of the actual measuring tool is 1 cm.

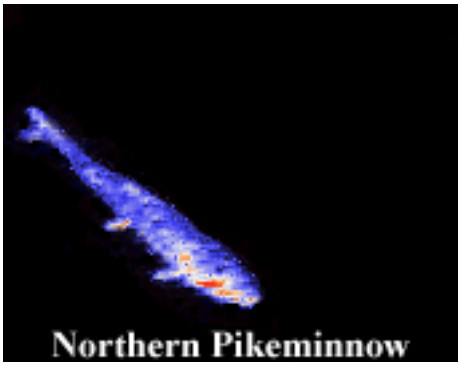

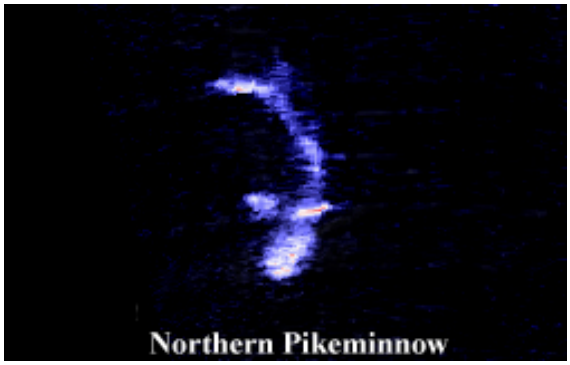

Figure 30. DIDSON images of northern pikeminnow collected in a tank. Cursory evaluation points to the fins as being a key component of identifying northern pikeminnow.

Because of the sampling rate of the DIDSON, it is not the best tool for observing fish or drogue behavior in a turbine intake or in the draft tubes. The normal sampling rate of the DIDSON is about 8 to 10 frames/s. With flows at the stay vanes and wicket gates approaching 9.1 mps, the spatial resolution would be only 0.9 m providing little data on trajectory and no data that could provide fish behavior information though it may be useful for a distribution estimation of run-of-the-river fish as they approach and pass into the scroll case (Figure 31). The same is true in the draft tubes with flows up to about 7.3 mps. The DIDSON is a useful tool for researchers to view fish in dark or turbid waters, and it does not require tagging the fish and possibly altering their behavior.

Increasing the frame rate of the DIDSON to greater than 9.1 mps would provide adequate spatial resolution to crudely evaluate the behavior of fish and their trajectories in high flow environments. At present, it is an ideal tool for observing fish movement and documenting behavior in low flow environments where standard video is not possible.

Test results show that the DIDSON can detect objects through bubble clouds and turbid water quite well and could be deployed in a draft tube environment though the spatial resolution from the frame rate of the DIDSON would not provide good behavior patterns or strike probability at the high flows in the turbine intake and draft tube environments. To cover the region upstream of the stop log slot at Bonneville Dam, the DIDSON could be deployed on a frame in the stop log slot looking upstream. The DIDSON positioned on the frame, with 10.5-degree beams vertical and 29-degree beams horizontal looking through one of the four sections in the splitter, could detect objects about 9.1 m upstream before the 10.5-degree beams made contact with the cement.

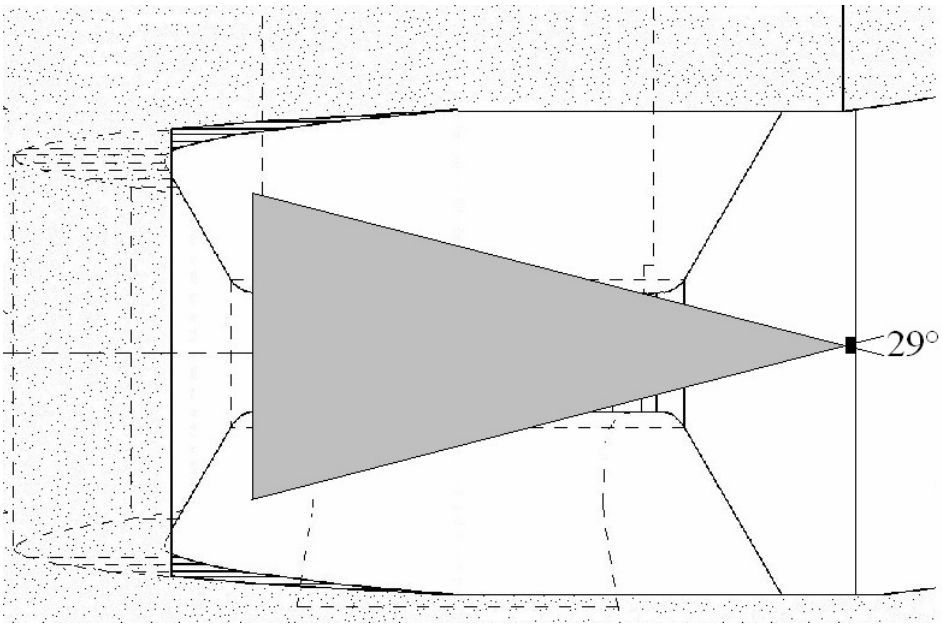

Figure 31. Position of DIDSON attached to downstream edge of turbine intake splitter wall with 29-degree beam array oriented vertically for evaluation of vertical distribution of run-of-the-river fish as they approach and enter the scroll case.

The image rate of the DIDSON is about 10 frames/s providing a maximum of about 15 frames of data, as the object of interest passes through the splitter opening. This could provide information on trajectory, and a snapshot of orientation, of the fish or object through this section of the draft tube but would provide no fine-scale movement within the splitter region. An acoustic tag emitting sound at the same frequency as the DIDSON could be used to enhance the resolution and increase ease of object identification as the tagged object passes through the ensonified beam of the DIDSON. Detected pings from the tag will show up as a bright line in the direction of the tagged object (Ed Belcher, personal communication).

6.0 Conclusions and Recommendations

All of the technologies considered in this study have good and bad points for particular measurement applications. High-speed digital imaging provides the best spatial resolution but has the shortest range of detection, with the range dependent on water conditions. High-speed digital imaging can achieve both high spatial and temporal resolution for tracking drogues or fish through the field of view of a camera array. However, as the rate at which images are acquired increases, the amount of light required for good image quality also increases. This means that the intensity of light emitted by a LET source must be increased in proportion to the video camera frame rate to retain larger fields of view. The cost of increase in light for drogues would not be significant because a doubling of light could be accomplished by doubling the number of high-intensity LEDs in the drogue's light array. On the other hand, the problem would be significantly more difficult for fish where adding LEDs to the array attached to the fish could increase its mass and volume to the point where it would become too large for the fish to carry.

Both of the ultrasonic tracking technologies, line-of-sight and time-of-arrival, provide good range of detection but have low spatial resolution as a result of the ping rate of tags currently available, though ping rate can possibly be doubled to almost 30 pps. Constraints on ping rate include power available due to constraints on the battery and tag size. An additional problem in the turbine environment is the amount of structure. Multi-path of the signal can be a problem in determining initial signal vs. multi-path. Signal multi-path needs to decay before the next ping. Because of these constraints in the draft tube region, a ping rate of 25 to 30 pps is the limit unless pings are individually coded, which adds to difficulty in processing the data. The ultrasonic tracking technologies have long-range detection and can detect micro-transmitters for the entire length of the draft tube and turbine intake. The line-of-sight array can be deployed with four receivers in a plane and cover a large volume of a draft tube with a configuration like McNary Dam, but not Bonneville Dam powerhouse 1. The time-of-arrival array requires the deployment of at least four hydrophones in three dimensions to provide three-dimensional coverage, and the accuracy of a micro-transmitter position within the array depends greatly on the geometry of the array.

The DIDSON acoustic imaging sonar was found to be a versatile tool, providing near video quality images in water where the range of optical cameras was restricted by turbidity or low light conditions. From the images we were able to identify fish orientation and make out features of fish that could help in species identification. In the high-velocity conditions of the turbine intake and the region of the draft tube near the scroll case, however, the frame rate of the DIDSON was too slow to provide the spatial resolution necessary to describe fish behavior or observe fish or drogues strikes on structures. However, the DIDSON sonar may have application estimating distribution of run-of-the-river fish as they approach the scroll case. In the splitter region of the draft tube at Bonneville Dam, the DIDSON could also be used for tracking trajectory of drogues or fish through a section of splitter that would not be possible with the acoustic tracking arrays. Images collected in this region could provide snapshots in time of fish passing through the splitter to determine fish orientation and describe if fish are able to orient with the flow or tumble out of control in these conditions.

Based on our experience with fish passage through turbines, additional observations are needed of regions within the turbine environment. These additional observations will allow researchers to study the response of drogues and fish to flow field dynamics and their interaction with turbine structures. These areas include the following: (1) leading edges of stay vanes and wicket gates, (2) turbine runner, (3) draft tube elbow, and (4) leading edges of draft tube splitter piers. Each of the technologies described is applicable to evaluating certain sections of the turbine environment and answering different questions.

Different applications and the technology best suited for answering the questions starting from the scroll case and working down stream are as follows.

1. Evaluate the interaction of drogues and fish with the leading edges of wicket gates and stay vanes to determine the percentage of fish and drogues that come in contact with the structure and the severity of the strike. High-speed digital cameras are the only tools that would provide great enough spatial resolution to capture the trajectory of a drogue or fish approaching the stay vane and wicket gate and capture a strike.

2. Estimate the vertical distribution of fish at passage through turbine wicket gates. Either high-speed digital cameras and the DIDSON, or both, can be used to evaluate vertical distribution at wicket gates. The high-speed digital cameras would provide the best spatial resolution but require tagging of fish with LETs and injecting the fish into the intake at known locations. Fish images collected with the DIDSON would provide a good estimate of vertical distribution if proven by other means, such as high-speed digital cameras, that vertical distribution doesn't change within several feet of the wicket gate to where they pass through the wicket gate. If there is a large change in vertical distribution near the wicket gates, then estimates of vertical distribution will be within a couple feet. With information on change in vertical distribution at the wicket gates provided by digital cameras, the DIDSON could provide distributions for run-of-the-river fish and could provide information at entrances to several wicket gates.

3. Estimate location of fish entry into the turbine runner and proximity to the runner blade at entry. High-speed digital cameras are the only technologies evaluated that could be used to track fish or drogues through the region above the turbine runner and through the runner because of the high water velocities. Fish and drogues would need to be equipped with LETs and released at specific locations to ensure detection by the cameras.

4. Trajectory of fish and drogues below the runner and through the turbine draft tube elbow. Similar to the turbine runner, to obtain good spatial resolution high-speed digital cameras are needed. The LETs would have to be released from a specific location above the runner to ensure the LET passed through in a certain region to ensure detection by the cameras. To ensure the cameras are close enough to detect the LETs, several cameras would need to be mounted to the wall of the draft tube and aimed up at the runner. The line-of-sight acoustic tracking array could be deployed from a frame in the stop log slot to detect micro-transmitters attached to fish and drogues as they pass from the underside of the runner and track their trajectories to approximately 6.1 m upstream of the receiver array (including the

draft tube elbow at McNary Dam). The acoustic array would provide a greater trajectory length than the cameras but at a lower spatial resolution.

5. Trajectory changes relative to flow and chance of fish or drogues striking at the upstream edge of the draft tube. The high-speed digital camera is the only technology with a high sample rate that would provide enough resolution to detect changes in fish or drogue trajectory and strikes on the upstream edge of the splitter wall. The DIDSON and line-of-sight acoustic tracking array could estimate trajectory of fish or drogues as they approached and passed by the splitter wall. However, the technologies would not detect changes in trajectory because of strike or turbulence beyond that it may have occurred. Further, the chance of detecting a strike on the splitter wall is poor.

6. Trajectory of fish through the horizontal splitters at Bonneville Dam powerhouse 1. In this situation, high-speed digital cameras are the best choice to evaluate how changes in hydraulic conditions affect trajectory. The DIDSON could also be deployed in this region and would have a range of about 11.6 m if deployed properly. However, it would only be able to collect about 15 images if the fish or drogue was in the ensonified area the entire time.

7. Interaction of fish with the draft tube stop log slot. One of the acoustic tracking arrays detects fish and drogues as they pass the stop log slot and identifies if they became entrained in the stop log slot. However, the acoustic arrays do not provide sufficient resolution to identify fine-scale changes in trajectory as a result of hydraulic changes. The high-speed digital cameras aimed across the slot provide finer scale trajectory changes as a result of hydraulic conditions. Two cameras—one either side of the intake—would need to be aimed across to cover the entire width of the intake at one section of elevation, or multiple cameras on one side could provide coverage of almost two-thirds of the intake width and a greater range of the water column.

8. Tracking fish through the turbine boil. The time-of-arrival acoustic tracking array provides the largest area of coverage for tracking fish and drogues through the turbine boil down-stream of the draft tube exit. This tracking array could be extended into the draft tube intake to track trajectories from within the draft tube into the tailrace. Currently, the maximum ping rate of acoustic tags used with this system is 4 pps but could be increased substantially because the necessary tag life is on the order of hours instead of the standard 2 weeks.

A number of factors including but not limited to spatial resolution, length of trajectory, and environmental conditions need to be considered depending on what the question is to be answered. Table 4 lists the advantages, disadvantages, and attributes of the technologies evaluated.

Spatial resolution can be improved for both acoustic tracking arrays by increasing the ping rate of the tag. The power of the tag will also need to be increased due to the probability of greater noise in the draft tube than was measured in the tailrace regions of the dams. Increasing the ping rate and power output of the tag for the time-of-arrival array is possible as the life of the tag does not

Table 4. Sampling attributes for line-of-sight, time-of-arrival, and DIDSON acoustic systems, and high-speed digital cameras.

Sampling attribute	Line-of-sight	Time-of-arrival	DIDSON	High-speed cameras
Resolution	Low	Low	Low	High
Invasive to fish	Yes	Yes	No	Yes
Affected by structure	Yes	Yes	No	No
Affected by bubbles	Yes	Yes	No	Yes
Affected by turbidity	No	No	No	Yes
Range	Long	Long	Long	Short
Fish orientation	No	No	Yes	Yes
Species ID	No	Yes	Possible	Possible

need to be as long as was originally designed. The acoustic tag used with the line-of-sight tracking array was designed to last 30 min.

The greatest drawback with the DIDSON is the slow sample rate, reducing its utility in high flow areas. Application of the DIDSON for use at regions within the turbine intake and draft tube would be increased tremendously by increasing the sample rate to at least 60 samples per second or more if possible. Conversely to the DIDSON, a short viewing range is the weakness of the high-speed digital cameras. Brightness and number of LEDs could be increased; however, this would possibly increase the number of batteries required, increasing the size of the tag. Another possible solution is finding cameras with greater light sensitivity than the Redlake cameras used in our testing.

Along with trade-offs between sample rate and range of detection, deployment of imaging equipment in the draft tube region of the dam will be difficult. As a result of high flow and turbulence, protecting instruments and cables will require extensive planning and review.

7.0 Literature Cited

Adams, NS, DW Rondorf, SD Evans, JE Kelly, and RW Perry. 1998. "Effects of Surgically and Gastrically Implanted Radio Transmitters on Swimming Performance and Predator Avoidance of Juvenile Chinook Salmon (*Oncorhynchus tshawytscha*)." *Canadian Journal of Fisheries and Aquatic Science* 55(4):781-787.

Anderson, JJ, EF Blake, RT Miyamoto, and SO McConnell. 1989. *Measurement of Low Frequency Sound at Bonneville, McNary and Lower Granite Dams-1988*. Report prepared for U.S. Army Corps of Engineers by Fisheries Research Institute, University of Washington School of Fisheries, Seattle, Washington.

Carlson, TJ and MA Weiland. 2001. *Light-Emitting Tag Testing in Conjunction with Testing of the Minimum Gap Runner Turbine Design at Bonneville Dam Powerhouse 1*. Report prepared for the U.S. Army Corp of Engineers, Portland District, Portland, Oregon by Pacific Northwest National Laboratory, Richland, Washington.

Carlson, TJ, MA Weiland, VK Sutton, AR Wirtz, M Macaulay and JR Skalski. 2002. *Ultrasonic 3-D Tracking of Fish and Drogues Passing through a Kaplan Turbine Intake at McNary Dam, 1999 & 2000*. Report prepared for the U.S. Army Corps of Engineers, Walla Walla District, Walla Walla, Washington by Pacific Northwest National Laboratory, Richland, Washington.

Faber, DM, TJ Carlson, KM Cash, and SA Zimmerman. 2002. *Design of Acoustic 3-D Tracking Arrays for Fish Behavior Studies*. Report prepared for the U.S. Army Corp of Engineers, Portland District, Portland, Oregon by Pacific Northwest National Laboratory, Richland, Washington.

Faber, DM, MA Weiland, RA Moursund, TJ Carlson, N Adams and D Rondorf. 2001. *Evaluation of the Fish Passage Effectiveness of the Bonneville I Prototype Surface Collector using Three-Dimensional Ultrasonic Fish Tracking*. Report prepared for the U.S. Army Corp of Engineers, Portland District, Portland, Oregon by Pacific Northwest National Laboratory, Richland, Washington.

Jähne, B and H HauBecker. 2000. *Computer Vision and Applications: A Guide for Students and Practioneers.* Academic Press, Burlington, Massachusetts. 679 pp.

Johnson, R. 2001. *Splitbeam Evaluation of Near-Field Fish Behavior at Bonneville Dam First Powerhouse, Unit 8*. Report prepared for the U.S. Army Corps of Engineers, Portland District, Portland, Oregon by Pacific Northwest National Laboratory, Richland, Washington.

Lindgren, M. 2000. "Release System Development." In *Proceedings of the Turbine Passage Survival Workshop,* ed. T.J. Carlson. Report prepared for the U.S. Army Corps of Engineers, Portland District, Portland, Oregon by Pacific Northwest National Laboratory, Richland, Washington.

Moursund, RA, KD Ham, RS Titzler, RP Mueller, GE Johnson, J Hedgepeth and JR Skalski. 2002. *Hydroacoustic Evaluation of Fish Passage at The Dalles Dam in 2001*. Report prepared for the U.S. Army Corp of Engineers, Portland District, Portland, Oregon by Battelle, Columbus, Ohio.

Neitzel, DA, MC Richmond, DD Dauble, RP Mueller, RA Moursund, CS Abernethy, GR Guensch and GF Cada. 2000. *Laboratory Studies on the Effects of Shear on Fish*. DOE/ID-10822, U.S. Department of Energy, Idaho Operations Office, Idaho Falls, Idaho, 55 pp.

Urick, RJ. 1983. *Principles of Underwater Sound*. McGraw-Hill, New York, 423 pp.

Appendix A

Appendix A

Description and characteristics of available ultrabright light-emitting diodes. Lines shaded are the light-emitting diodes tested.

Size (mm)	Color	Wavelength	Angle	mcd	Company	Part Number
5	Blue	466	10	6000	Marktech	MT7163-UBL
5	Blue	466	20	1400	AND	AND410HB
5	Blue	470	15	3000	TheLed	T1 3/4-15B
5	Blue green	505	45	7100	MCD	MCDPE520S
5	Blue green	505	15	5300	MCD	MCDPE500S
5	Blue green	505	15	3800	TheLed	T1-3/4-20BL-GRN
5	Blue green	505	30	2300	MCD	MCDPE510S
5	Green	505	12	2200	AND	AND412HG
5	Green	525	15	10000	TheLed	T1 3/4-15G
5	Green	525	15	8000	MCD	MCDPG500S
5	Green	525	30	4300	MCD	MCDPG510S
5	Green	525	45	2200	MCD	MCDPG520S
5	Green	540	10	7000	Marktech	MT7153-TUG
5	Green	540	20	5000	AND	AND520HG
5	Green	540	20	5000	AND	AND520HG
5	Green	567	20	780	AND	AND240GCP
5	Green	567	8	700	AND	AND190GCP
5	Green	571	8	3500	Marktech	TLGE183P
5	Green	574	8	2500	AND	AND183HGP
5	Yellow	585	30	2000	TheLed	T1 3/4-30YEL
5	Yellow	587	8	8000	Marktech	TLYH180P
5	Yellow	587	17	3500	Marktech	S4E38XX
5	Yellow	590	8	8000	TheLed	T1 3/4-8YL
5	Yellow	590	8	4000	AND	AND180HYP
5	Yellow	590	16	3200	AND	ANDS4E38XX16
5	Yellow	590	20	3000	AND	ANDS4E38XX20
5	Yellow	590	6	2500	AND	AND180AYP
5	Yellow	590	20	2500	AND	AND157HYP
5	Yellow	590	20	800	AND	AND156EYP
5	Orange	605	8	7000	Marktech	TLOH180P
5	Orange	605	22	2000	Marktech	TLOH157P
5	Orange	605	30	1900	TheLed	T1 34/30ORG
5	Orange	612	8	10000	TheLed	T1 3/4-8OR
5	Orange	612	8	7000	AND	AND180HAP
5	Orange	612	20	2000	AND	AND157HAP
5	Red	613	8	8000	Marktech	TLSH180P
5	Red	613	22	2300	Marktech	TLSH157P
5	Orange	620	30	800	AND	AND156AOP
5	Red	623	8	6000	AND	AND180HSP
5	Red	623	25	1200	AND	AND157HSP
5	Red	625	30	2000	TheLed	T1 3/4-30RD
5	Red	630	4	15000	Marktech	TLRH190P

Size (mm)	Color	Wavelength	Angle	mcd	Company	Part Number
5	Red	636	8	8000	TheLed	T1 3/4-8RD
5	Red	644	8	6000	AND	AND180HRP
5	Red	644	20	1800	AND	AND157HRP
5	Red	660	12	3600	AND	AND180CRP
5	Red	660	16	2000	AND	AND130CR
5	Red	660	22	2000	AND	AND120CRP
5	Red	660	22	2000	AND	AND120CR
5	Red	660	25	1280	AND	AND155CRP
5	Red	660	35	1100	AND	AND120BR
5	White	-	15	7200	MCD	MCDPW500S
5	White	-	20	5600	TheLed	T1 3/4-20W
5	White	-	30	5400	MCD	MCDPW510S
5	White	-	45	4200	MCD	MCDPW520S
5	White	-	15	3500	AND	AND620HW
5	White	-	20	1700	AND	AND520HW
5	White	-	50	1560	TheLed	T1 3/4-50W
7.62	Blue	460	65	400	MCD	MCDL-945PBC
7.62	Green	555	65	400	MCD	MCDL-945PGC
7.62	Yellow	590	65	8750	MCD	MCDL-945MYC
7.62	Yellow	592	65	2500	MCD	MCDL-945UYC
7.62	Orange	620	65	2500	MCD	MCDL-945VEC
7.62	Orange	620	65	800	MCD	MCDL-945UEC
7.62	Red	630	65	10500	MCD	MCDL-945MEC
7.62	Red	640	65	1100	MCD	MCDL-945URC
7.62	White	-	65	500	MCD	MCDL-945PWC
10	Green	574	8	2000	AND	AND190HGP
10	Yellow	587	4	2300	Marktech	TLYH190P
10	Yellow	590	6	6300	AND	AND190HYP
10	Orange	605	4	20000	Marktech	TLOH190P
10	Orange	612	6	6300	AND	AND190HAP
10	Orange	620	4	18000	AND	AND190WOP
10	Orange	620	4	12000	AND	AND190AOP
10	Red	644	8	10000	AND	AND191CRP
10	Red	660	8	11000	AND	AND190CRP

Appendix B

Appendix B

Horizontal (X-Z plane) and vertical (Y-Z plane) plots of the modeled location of an object in three different camera arrays (straight-planar, rectangular, planar, and three-dimensional) for camera pairs 1 and 2, 1 and 3, and 1 and 4.

Straight-Planar Array Cameras 1 and 2

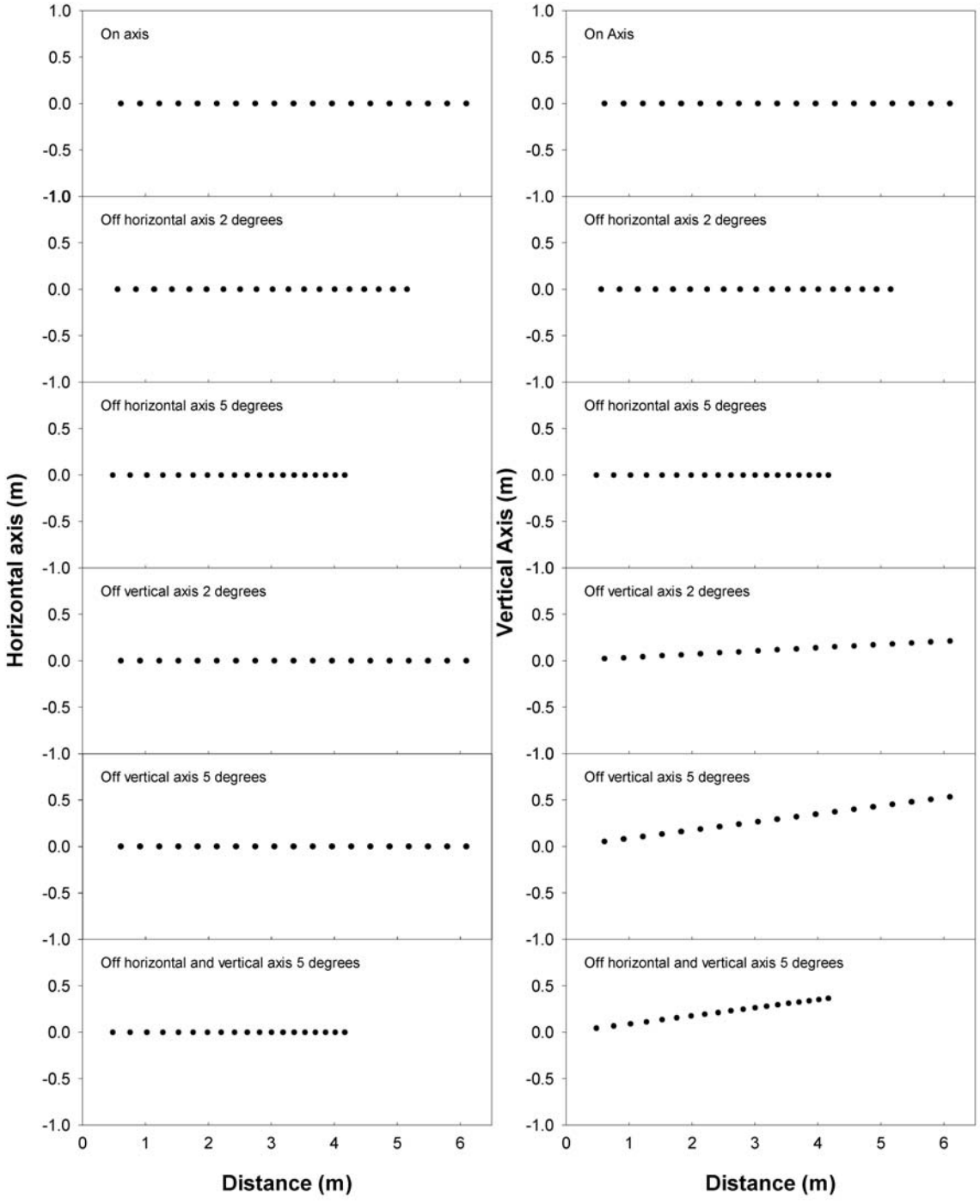

Straight-Planar Array Cameras 1 and 3

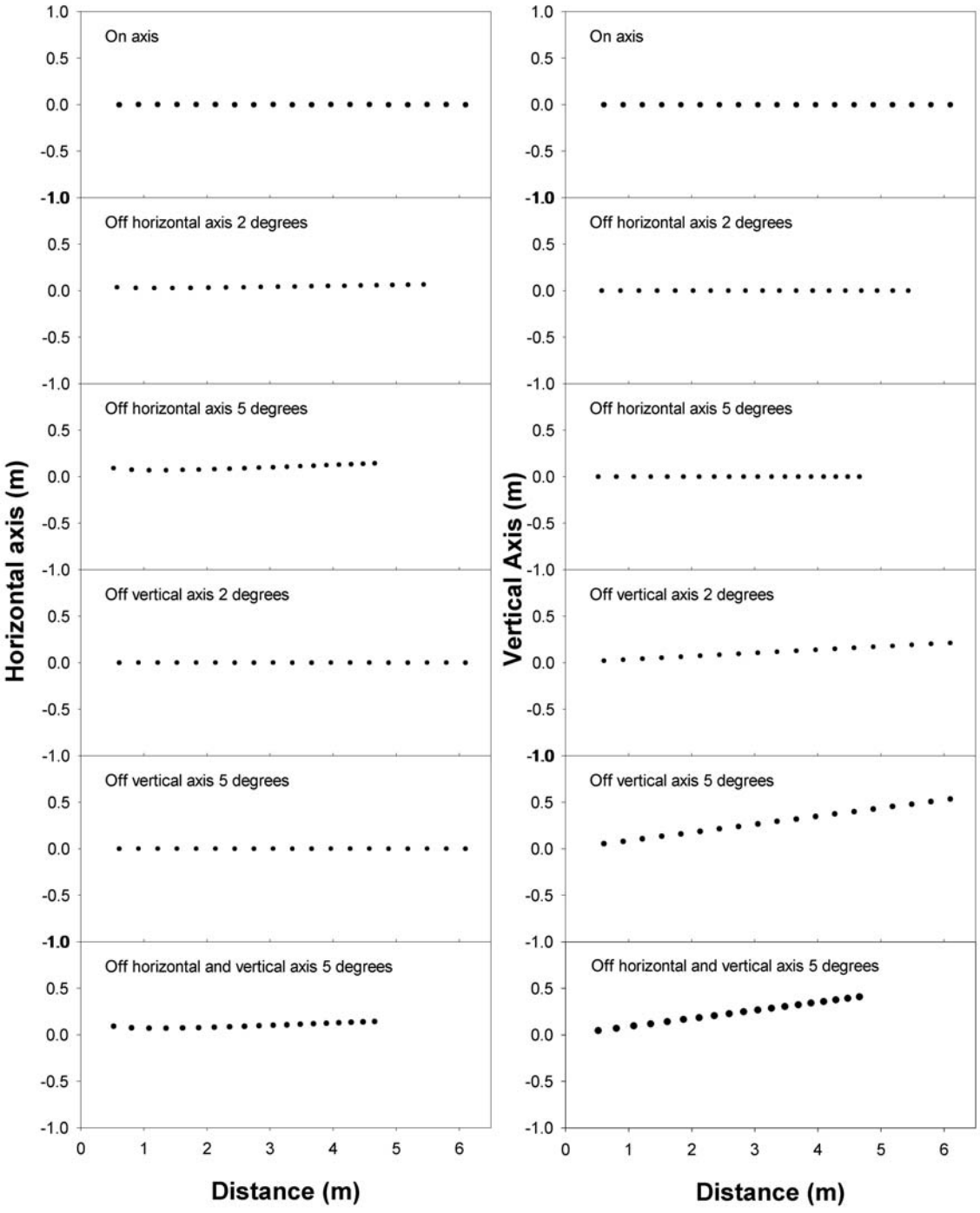

Straight-Planar Array Cameras 1 and 4

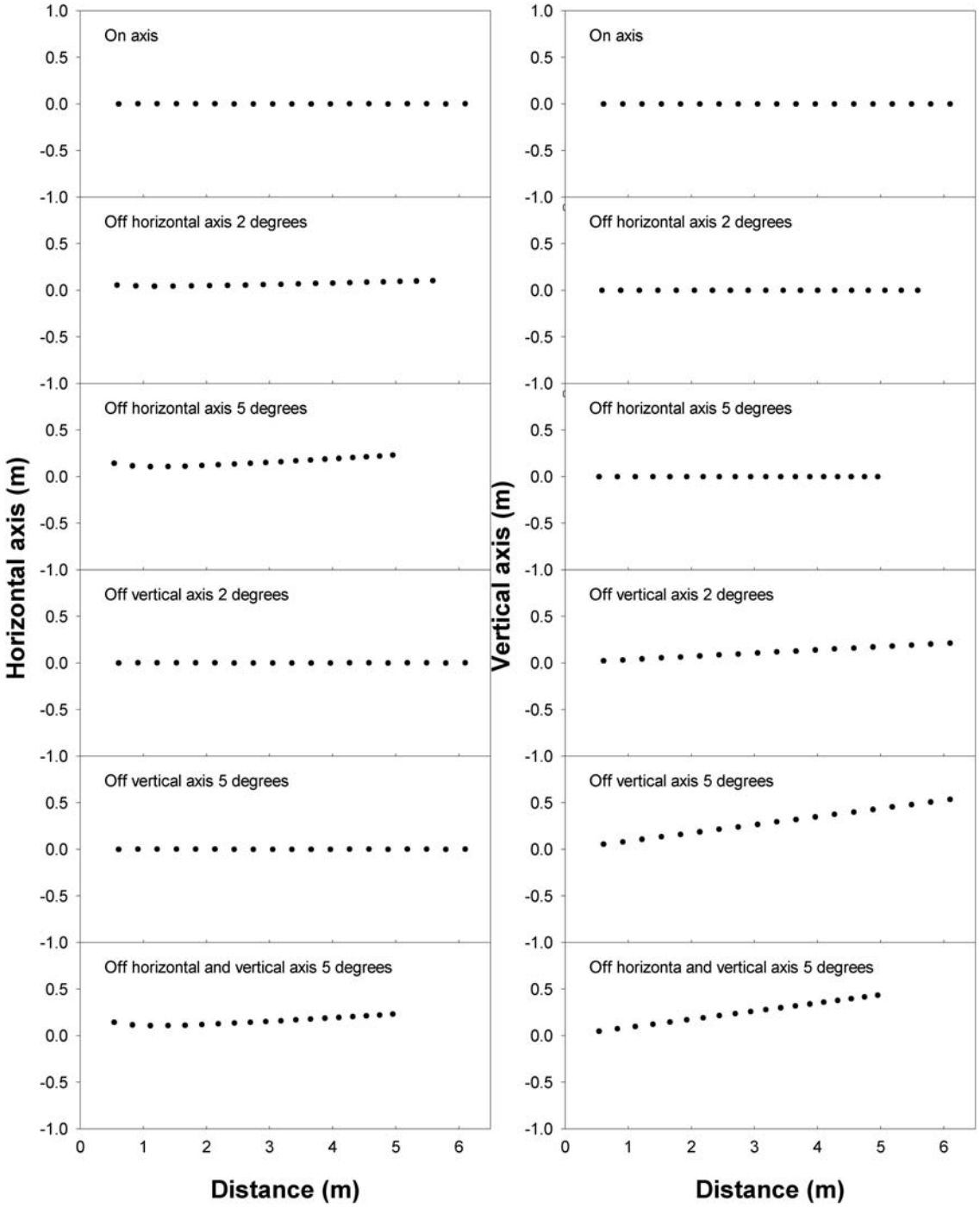

Rectangular-Planar Array Cameras 1 and 2

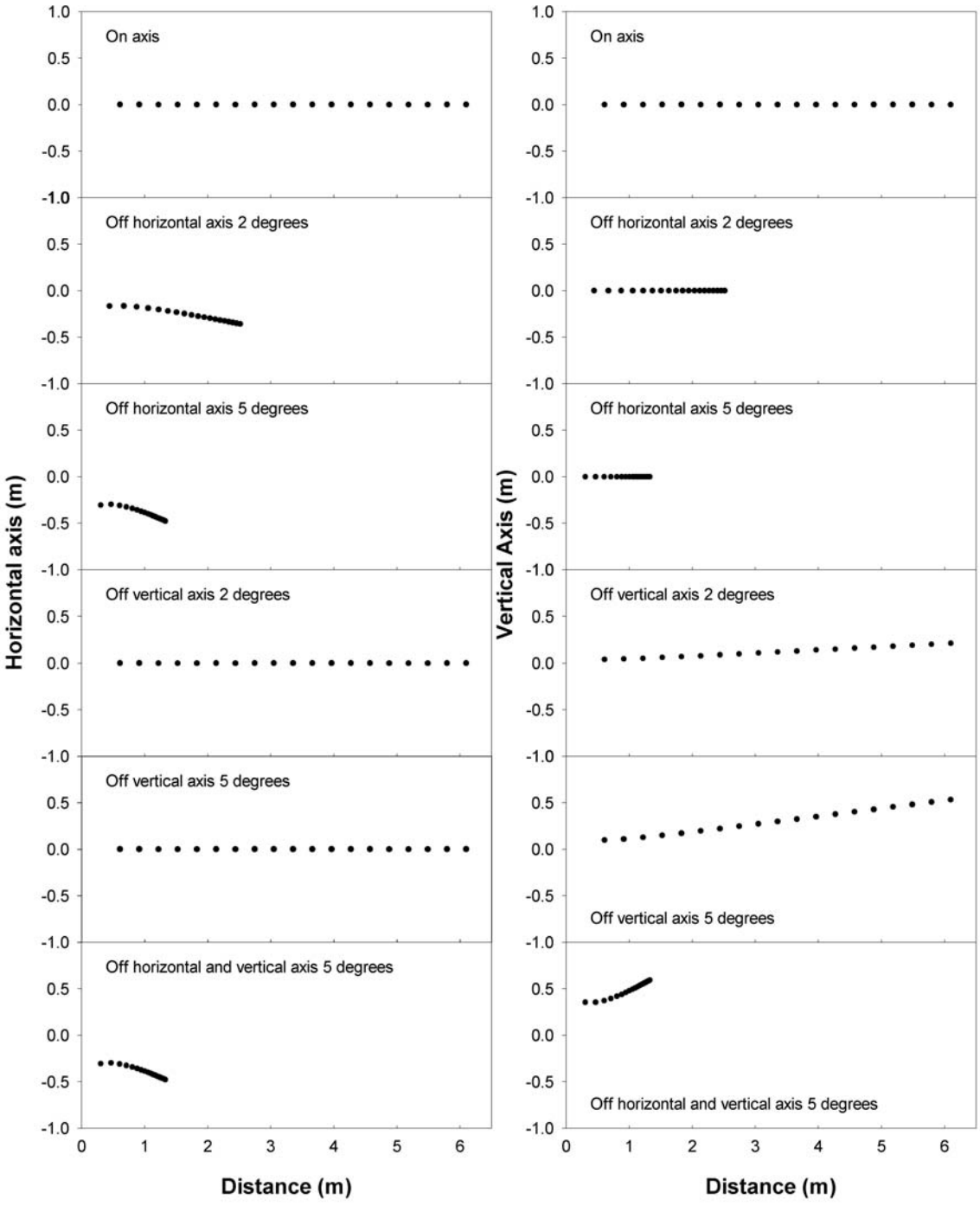

Rectangular-Planar Array Cameras 1 and 3

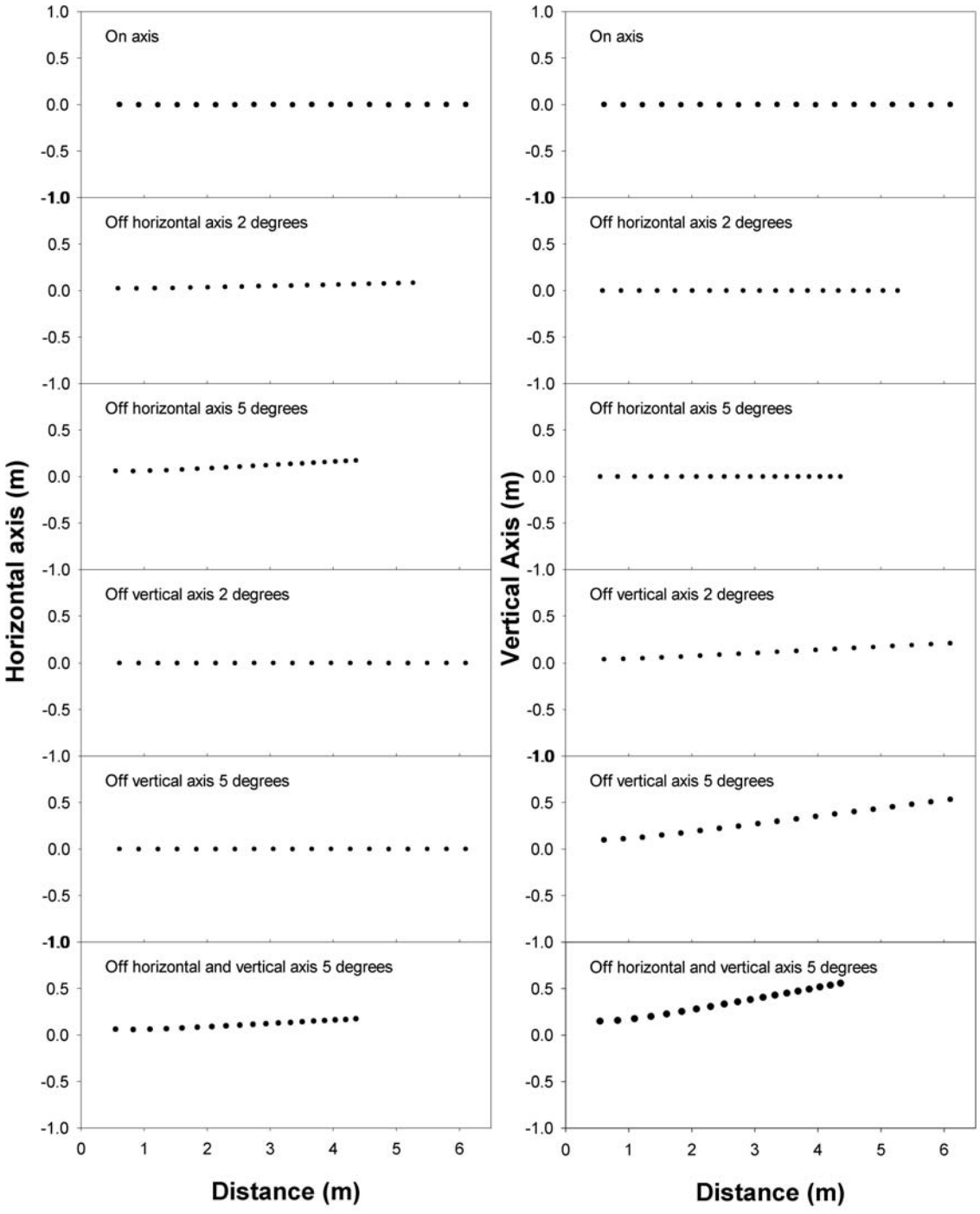

Rectangular-Planar Array Cameras 1 and 4

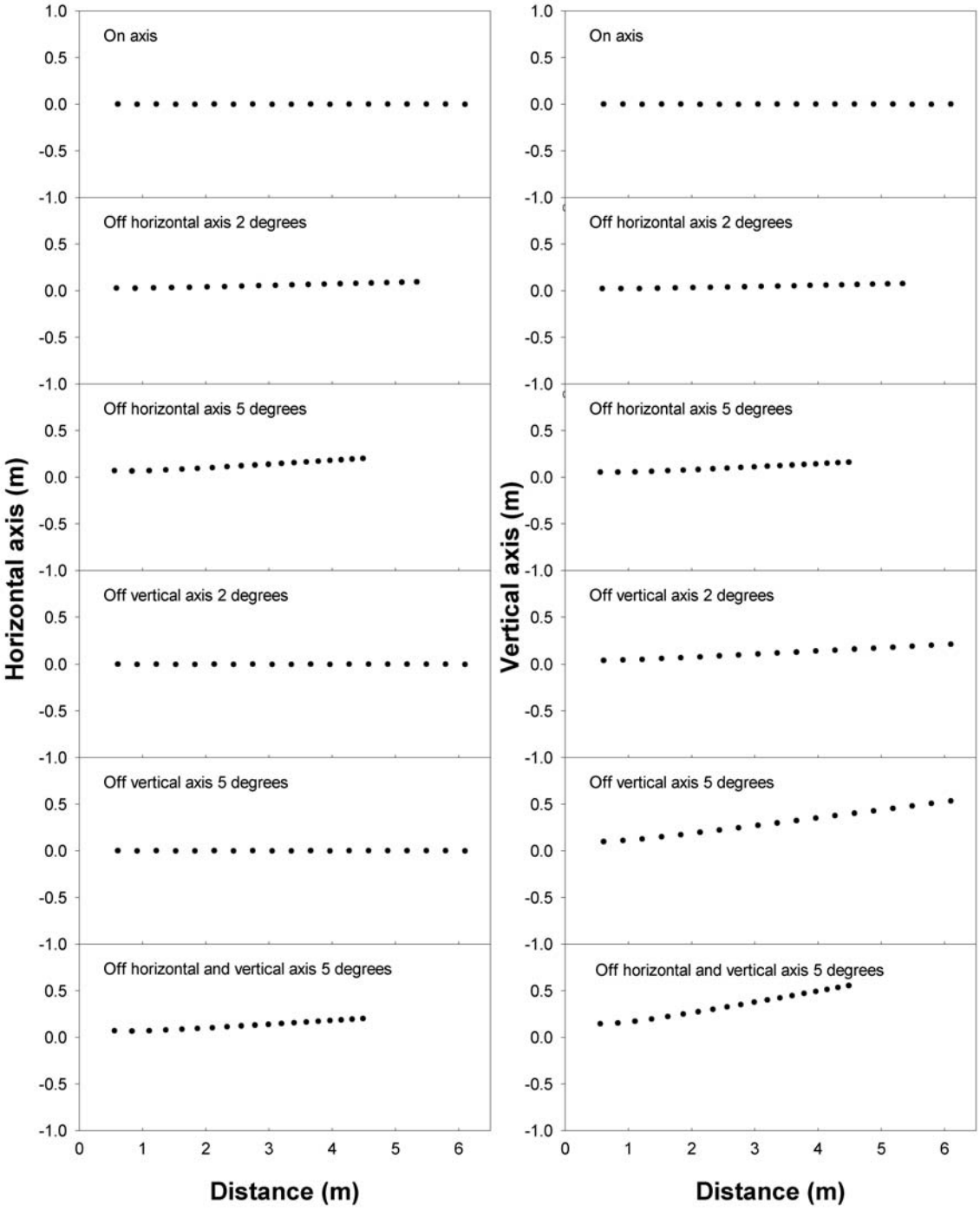

Three-Dimensional Array Cameras 1 and 2

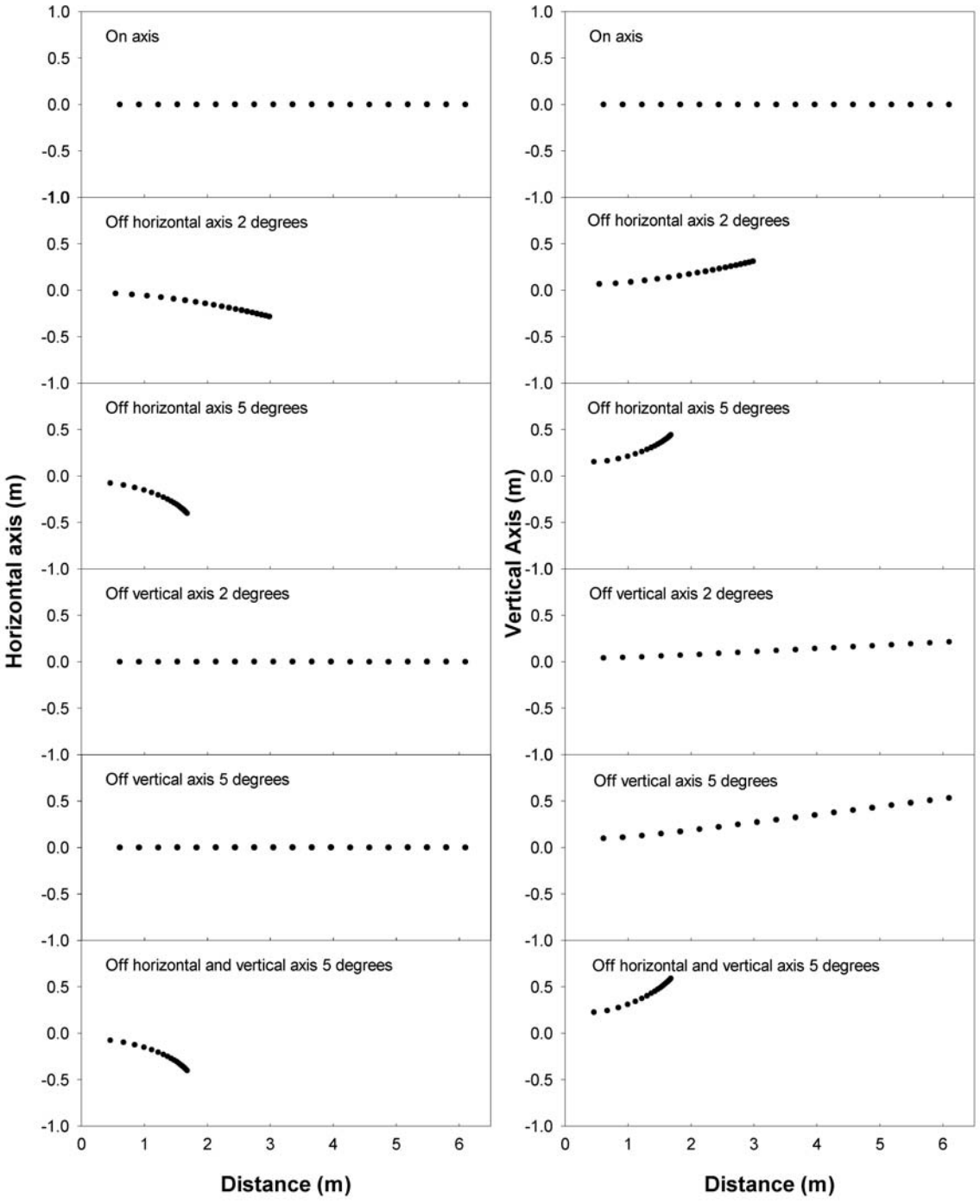

Three-Dimensional Array Cameras 1 and 3

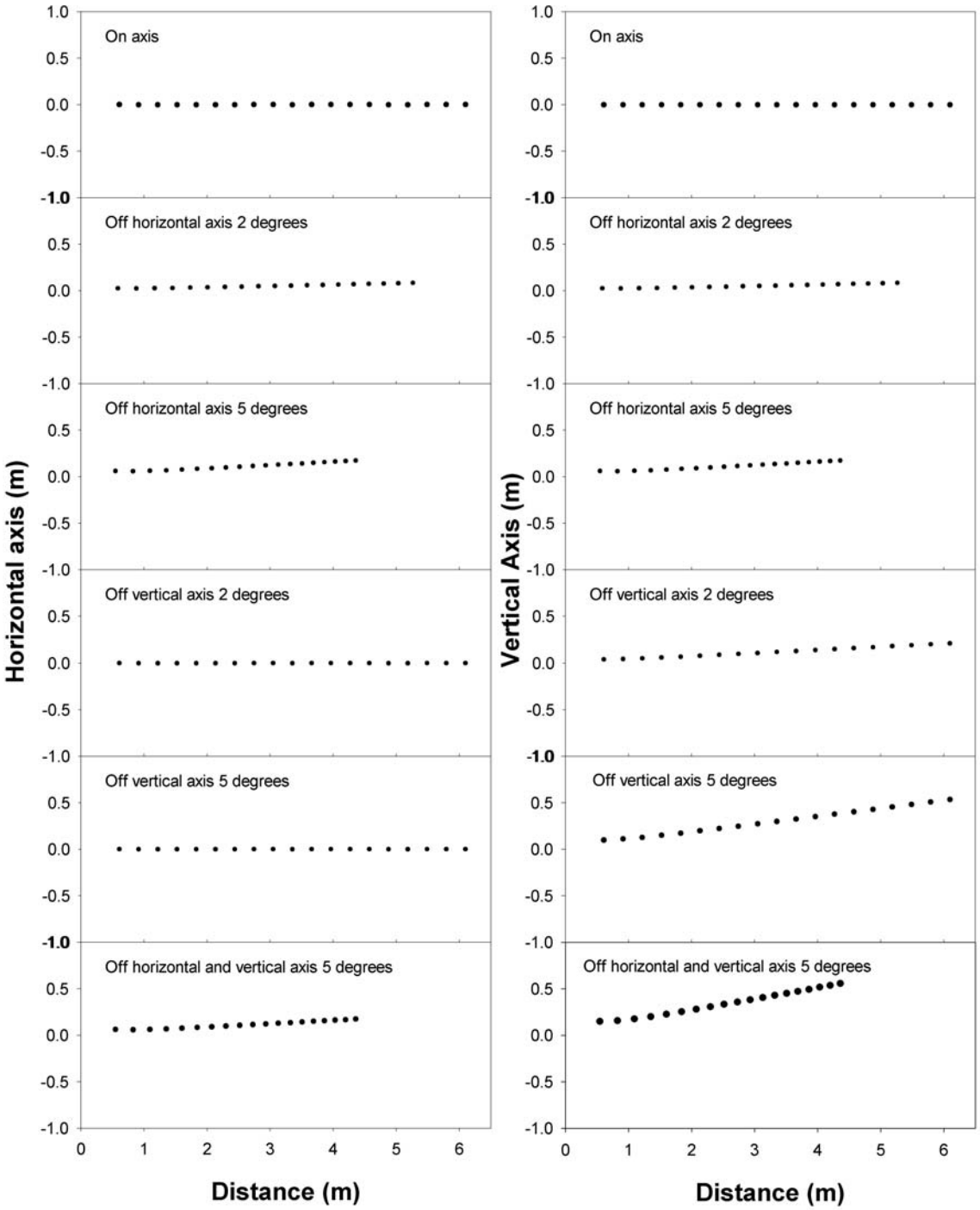

Three-Dimensional Array Cameras 1 and 4

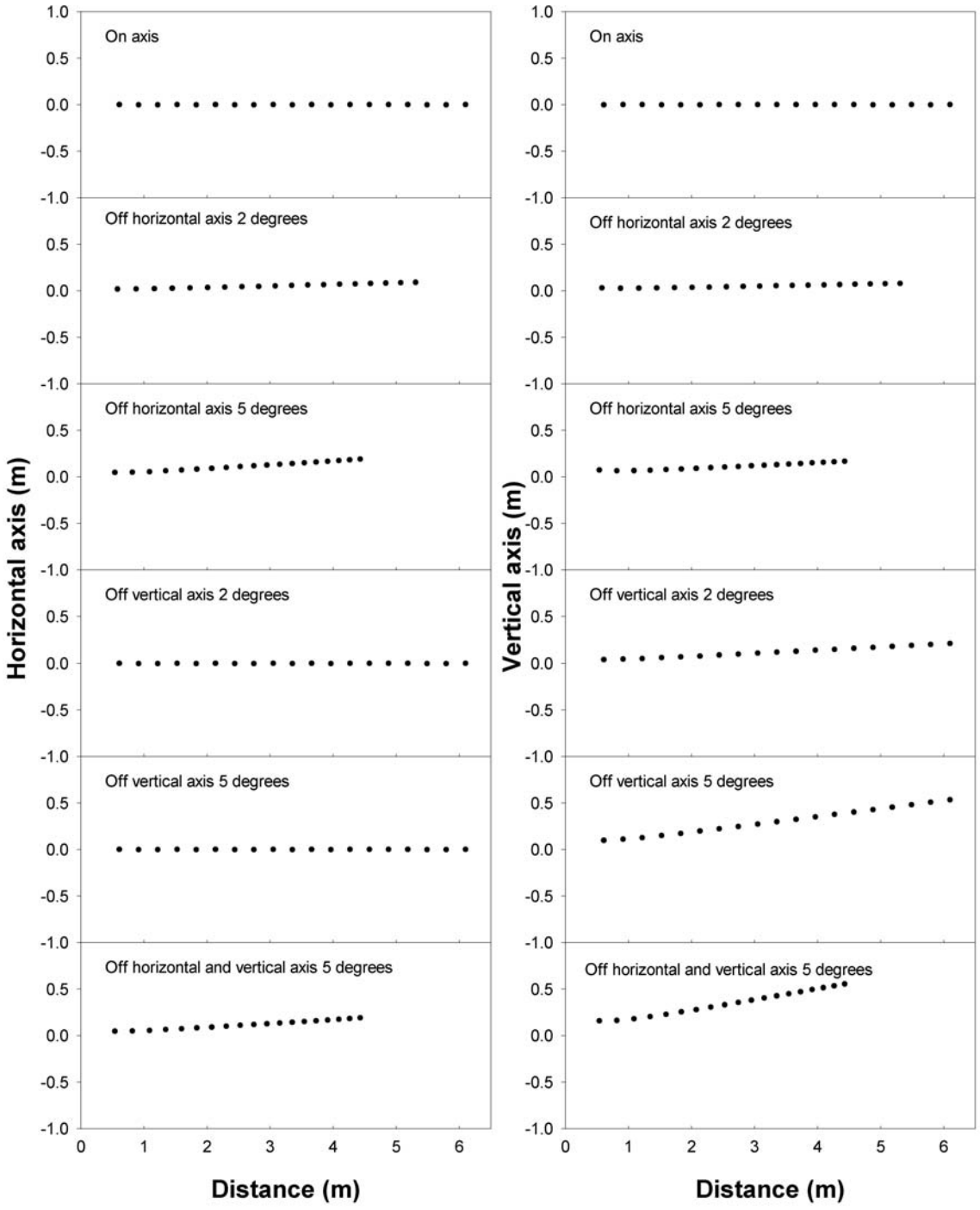

Appendix C

Appendix C

Bias (m) in horizontal (X-Z plane) and vertical (Y-Z plane) trajectories of the modeled location of an object in three different camera arrays (straight-planar, rectangular, planar, and three-dimensional) for camera pairs 1 and 2, 1 and 3, and 1 and 4.

Camera 1 and 2

On Axis											
True Location			Straight planar			Rectangular planar			3D		
X	Y	Z	X	Y	Z	X	Y	Z	X	Y	Z
0	0	0.61	0.00	0.00	0.00	0.00	0.00	0.00	0.00	0.00	0.00
0	0	0.91	0.00	0.00	0.00	0.00	0.00	0.00	0.00	0.00	0.00
0	0	1.22	0.00	0.00	0.00	0.00	0.00	0.00	0.00	0.00	0.00
0	0	1.52	0.00	0.00	0.00	0.00	0.00	0.00	0.00	0.00	0.00
0	0	1.83	0.00	0.00	0.00	0.00	0.00	0.00	0.00	0.00	0.00
0	0	2.13	0.00	0.00	0.00	0.00	0.00	0.00	0.00	0.00	0.00
0	0	2.44	0.00	0.00	0.00	0.00	0.00	0.00	0.00	0.00	0.00
0	0	2.74	0.00	0.00	0.00	0.00	0.00	0.00	0.00	0.00	0.00
0	0	3.05	0.00	0.00	0.00	0.00	0.00	0.00	0.00	0.00	0.00
0	0	3.35	0.00	0.00	0.00	0.00	0.00	0.00	0.00	0.00	0.00
0	0	3.66	0.00	0.00	0.00	0.00	0.00	0.00	0.00	0.00	0.00
0	0	3.96	0.00	0.00	0.00	0.00	0.00	0.00	0.00	0.00	0.00
0	0	4.27	0.00	0.00	0.00	0.00	0.00	0.00	0.00	0.00	0.00
0	0	4.57	0.00	0.00	0.00	0.00	0.00	0.00	0.00	0.00	0.00
0	0	4.88	0.00	0.00	0.00	0.00	0.00	0.00	0.00	0.00	0.00
0	0	5.18	0.00	0.00	0.00	0.00	0.00	0.00	0.00	0.00	0.00
0	0	5.49	0.00	0.00	0.00	0.00	0.00	0.00	0.00	0.00	0.00
0	0	5.79	0.00	0.00	0.00	0.00	0.00	0.00	0.00	0.00	0.00
0	0	6.10	0.00	0.00	0.00	0.00	0.00	0.00	0.00	0.00	0.00
Off Horizontal Axis 2 Degrees											
True Location			Straight planar			Rectangular planar			3D		
X	Y	Z	X	Y	Z	X	Y	Z	X	Y	Z
0	0	0.61	0.00	0.00	0.05	0.16	0.00	0.16	0.03	0.07	0.07
0	0	0.91	0.00	0.00	0.06	0.16	0.00	0.24	0.05	0.08	0.11
0	0	1.22	0.00	0.00	0.08	0.17	0.00	0.35	0.06	0.09	0.18
0	0	1.52	0.00	0.00	0.10	0.19	0.00	0.47	0.08	0.10	0.26
0	0	1.83	0.00	0.00	0.13	0.20	0.00	0.61	0.09	0.12	0.37
0	0	2.13	0.00	0.00	0.16	0.22	0.00	0.77	0.11	0.14	0.49
0	0	2.44	0.00	0.00	0.20	0.23	0.00	0.93	0.12	0.16	0.62
0	0	2.74	0.00	0.00	0.24	0.25	0.00	1.11	0.14	0.17	0.78
0	0	3.05	0.00	0.00	0.28	0.26	0.00	1.30	0.16	0.19	0.94
0	0	3.35	0.00	0.00	0.33	0.27	0.00	1.51	0.17	0.20	1.12
0	0	3.66	0.00	0.00	0.38	0.29	0.00	1.71	0.19	0.22	1.31
0	0	3.96	0.00	0.00	0.44	0.30	0.00	1.93	0.20	0.23	1.51
0	0	4.27	0.00	0.00	0.50	0.31	0.00	2.15	0.22	0.25	1.72
0	0	4.57	0.00	0.00	0.57	0.32	0.00	2.38	0.23	0.26	1.94
0	0	4.88	0.00	0.00	0.63	0.33	0.00	2.61	0.24	0.27	2.16
0	0	5.18	0.00	0.00	0.71	0.34	0.00	2.85	0.25	0.28	2.39
0	0	5.49	0.00	0.00	0.78	0.34	0.00	3.09	0.26	0.29	2.63
0	0	5.79	0.00	0.00	0.86	0.35	0.00	3.33	0.27	0.30	2.87
0	0	6.10	0.00	0.00	0.94	0.36	0.00	3.58	0.28	0.31	3.12

Off Horizontal Axis 5 Degrees											
Location			Straight planar			Rectangular planar			3D		
X	Y	Z	X	Y	Z	X	Y	Z	X	Y	Z
0	0	0.61	0.00	0.00	0.13	0.30	0.00	0.30	0.08	0.15	0.15
0	0	0.91	0.00	0.00	0.16	0.30	0.00	0.45	0.10	0.16	0.25
0	0	1.22	0.00	0.00	0.20	0.31	0.00	0.62	0.12	0.19	0.37
0	0	1.52	0.00	0.00	0.25	0.33	0.00	0.81	0.15	0.21	0.53
0	0	1.83	0.00	0.00	0.31	0.34	0.00	1.03	0.18	0.24	0.71
0	0	2.13	0.00	0.00	0.37	0.36	0.00	1.25	0.20	0.26	0.92
0	0	2.44	0.00	0.00	0.45	0.37	0.00	1.49	0.23	0.28	1.14
0	0	2.74	0.00	0.00	0.54	0.39	0.00	1.74	0.25	0.30	1.37
0	0	3.05	0.00	0.00	0.63	0.40	0.00	2.00	0.27	0.33	1.62
0	0	3.35	0.00	0.00	0.74	0.41	0.00	2.26	0.29	0.34	1.88
0	0	3.66	0.00	0.00	0.84	0.42	0.00	2.53	0.31	0.36	2.15
0	0	3.96	0.00	0.00	0.96	0.43	0.00	2.80	0.32	0.37	2.42
0	0	4.27	0.00	0.00	1.08	0.44	0.00	3.07	0.34	0.38	2.69
0	0	4.57	0.00	0.00	1.21	0.45	0.00	3.35	0.35	0.40	2.97
0	0	4.88	0.00	0.00	1.34	0.45	0.00	3.63	0.36	0.41	3.26
0	0	5.18	0.00	0.00	1.48	0.46	0.00	3.91	0.37	0.42	3.54
0	0	5.49	0.00	0.00	1.63	0.47	0.00	4.19	0.38	0.43	3.83
0	0	5.79	0.00	0.00	1.78	0.47	0.00	4.48	0.39	0.43	4.13
0	0	6.10	0.00	0.00	1.93	0.48	0.00	4.77	0.40	0.44	4.42
Off Vertical Axis 2 Degrees											
Location			Straight planar			Rectangular planar			3D		
X	Y	Z	X	Y	Z	X	Y	Z	X	Y	Z
0	0	0.61	0.00	0.02	0.00	0.00	0.04	0.00	0.00	0.04	0.00
0	0	0.91	0.00	0.03	0.00	0.00	0.05	0.00	0.00	0.05	0.00
0	0	1.22	0.00	0.04	0.00	0.00	0.05	0.00	0.00	0.05	0.00
0	0	1.52	0.00	0.05	0.00	0.00	0.06	0.00	0.00	0.06	0.00
0	0	1.83	0.00	0.06	0.00	0.00	0.07	0.00	0.00	0.07	0.00
0	0	2.13	0.00	0.07	0.00	0.00	0.08	0.00	0.00	0.08	0.00
0	0	2.44	0.00	0.09	0.00	0.00	0.09	0.00	0.00	0.09	0.00
0	0	2.74	0.00	0.09	0.00	0.00	0.10	0.00	0.00	0.10	0.00
0	0	3.05	0.00	0.11	0.00	0.00	0.11	0.00	0.00	0.11	0.00
0	0	3.35	0.00	0.12	0.00	0.00	0.12	0.00	0.00	0.12	0.00
0	0	3.66	0.00	0.13	0.00	0.00	0.13	0.00	0.00	0.13	0.00
0	0	3.96	0.00	0.14	0.00	0.00	0.14	0.00	0.00	0.14	0.00
0	0	4.27	0.00	0.15	0.00	0.00	0.15	0.00	0.00	0.15	0.00
0	0	4.57	0.00	0.16	0.00	0.00	0.16	0.00	0.00	0.16	0.00
0	0	4.88	0.00	0.17	0.00	0.00	0.17	0.00	0.00	0.17	0.00
0	0	5.18	0.00	0.18	0.00	0.00	0.18	0.00	0.00	0.18	0.00
0	0	5.49	0.00	0.19	0.00	0.00	0.19	0.00	0.00	0.19	0.00
0	0	5.79	0.00	0.20	0.00	0.00	0.20	0.00	0.00	0.20	0.00
0	0	6.10	0.00	0.21	0.00	0.00	0.21	0.00	0.00	0.21	0.00

Off Vertical Axis 5 Degrees											
Location			Straight planar			Rectangular planar			3D		
X	Y	Z	X	Y	Z	X	Y	Z	X	Y	Z
0	0	0.61	0.00	0.05	0.00	0.00	0.10	0.00	0.00	0.10	0.00
0	0	0.91	0.00	0.08	0.00	0.00	0.11	0.00	0.00	0.11	0.00
0	0	1.22	0.00	0.11	0.00	0.00	0.13	0.00	0.00	0.13	0.00
0	0	1.52	0.00	0.13	0.00	0.00	0.15	0.00	0.00	0.15	0.00
0	0	1.83	0.00	0.16	0.00	0.00	0.17	0.00	0.00	0.17	0.00
0	0	2.13	0.00	0.19	0.00	0.00	0.20	0.00	0.00	0.20	0.00
0	0	2.44	0.00	0.21	0.00	0.00	0.22	0.00	0.00	0.22	0.00
0	0	2.74	0.00	0.24	0.00	0.00	0.25	0.00	0.00	0.25	0.00
0	0	3.05	0.00	0.27	0.00	0.00	0.27	0.00	0.00	0.27	0.00
0	0	3.35	0.00	0.29	0.00	0.00	0.30	0.00	0.00	0.30	0.00
0	0	3.66	0.00	0.32	0.00	0.00	0.32	0.00	0.00	0.32	0.00
0	0	3.96	0.00	0.35	0.00	0.00	0.35	0.00	0.00	0.35	0.00
0	0	4.27	0.00	0.37	0.00	0.00	0.37	0.00	0.00	0.37	0.00
0	0	4.57	0.00	0.40	0.00	0.00	0.40	0.00	0.00	0.40	0.00
0	0	4.88	0.00	0.43	0.00	0.00	0.43	0.00	0.00	0.43	0.00
0	0	5.18	0.00	0.45	0.00	0.00	0.45	0.00	0.00	0.45	0.00
0	0	5.49	0.00	0.48	0.00	0.00	0.48	0.00	0.00	0.48	0.00
0	0	5.79	0.00	0.51	0.00	0.00	0.51	0.00	0.00	0.51	0.00
0	0	6.10	0.00	0.53	0.00	0.00	0.53	0.00	0.00	0.53	0.00
Off Horizontal and Vertical Axis 5 Degrees											
Location			Straight planar			Rectangular planar			3D		
X	Y	Z	X	Y	Z	X	Y	Z	X	Y	Z
0	0	0.61	0.00	0.04	0.13	0.30	0.35	0.30	0.08	0.23	0.15
0	0	0.91	0.00	0.07	0.16	0.30	0.35	0.45	0.10	0.24	0.25
0	0	1.22	0.00	0.09	0.20	0.31	0.37	0.62	0.12	0.27	0.37
0	0	1.52	0.00	0.11	0.25	0.33	0.40	0.81	0.15	0.31	0.53
0	0	1.83	0.00	0.13	0.31	0.34	0.42	1.03	0.18	0.34	0.71
0	0	2.13	0.00	0.15	0.37	0.36	0.44	1.25	0.20	0.37	0.92
0	0	2.44	0.00	0.17	0.45	0.37	0.46	1.49	0.23	0.40	1.14
0	0	2.74	0.00	0.19	0.54	0.39	0.48	1.74	0.25	0.43	1.37
0	0	3.05	0.00	0.21	0.63	0.40	0.49	2.00	0.27	0.45	1.62
0	0	3.35	0.00	0.23	0.74	0.41	0.51	2.26	0.29	0.47	1.88
0	0	3.66	0.00	0.25	0.84	0.42	0.52	2.53	0.31	0.49	2.15
0	0	3.96	0.00	0.26	0.96	0.43	0.53	2.80	0.32	0.51	2.42
0	0	4.27	0.00	0.28	1.08	0.44	0.55	3.07	0.34	0.52	2.69
0	0	4.57	0.00	0.29	1.21	0.45	0.55	3.35	0.35	0.54	2.97
0	0	4.88	0.00	0.31	1.34	0.45	0.56	3.63	0.36	0.55	3.26
0	0	5.18	0.00	0.32	1.48	0.46	0.57	3.91	0.37	0.56	3.54
0	0	5.49	0.00	0.34	1.63	0.47	0.58	4.19	0.38	0.57	3.83
0	0	5.79	0.00	0.35	1.78	0.47	0.59	4.48	0.39	0.58	4.13
0	0	6.10	0.00	0.37	1.93	0.48	0.59	4.77	0.40	0.59	4.42

Camera 1 and 3

On Axis											
True Location			Straight planar			Rectangular planar			3D		
X	Y	Z	X	Y	Z	X	Y	Z	X	Y	Z
0	0	0.61	0.00	0.00	0.00	0.00	0.00	0.00	0.00	0.00	0.00
0	0	0.91	0.00	0.00	0.00	0.00	0.00	0.00	0.00	0.00	0.00
0	0	1.22	0.00	0.00	0.00	0.00	0.00	0.00	0.00	0.00	0.00
0	0	1.52	0.00	0.00	0.00	0.00	0.00	0.00	0.00	0.00	0.00
0	0	1.83	0.00	0.00	0.00	0.00	0.00	0.00	0.00	0.00	0.00
0	0	2.13	0.00	0.00	0.00	0.00	0.00	0.00	0.00	0.00	0.00
0	0	2.44	0.00	0.00	0.00	0.00	0.00	0.00	0.00	0.00	0.00
0	0	2.74	0.00	0.00	0.00	0.00	0.00	0.00	0.00	0.00	0.00
0	0	3.05	0.00	0.00	0.00	0.00	0.00	0.00	0.00	0.00	0.00
0	0	3.35	0.00	0.00	0.00	0.00	0.00	0.00	0.00	0.00	0.00
0	0	3.66	0.00	0.00	0.00	0.00	0.00	0.00	0.00	0.00	0.00
0	0	3.96	0.00	0.00	0.00	0.00	0.00	0.00	0.00	0.00	0.00
0	0	4.27	0.00	0.00	0.00	0.00	0.00	0.00	0.00	0.00	0.00
0	0	4.57	0.00	0.00	0.00	0.00	0.00	0.00	0.00	0.00	0.00
0	0	4.88	0.00	0.00	0.00	0.00	0.00	0.00	0.00	0.00	0.00
0	0	5.18	0.00	0.00	0.00	0.00	0.00	0.00	0.00	0.00	0.00
0	0	5.49	0.00	0.00	0.00	0.00	0.00	0.00	0.00	0.00	0.00
0	0	5.79	0.00	0.00	0.00	0.00	0.00	0.00	0.00	0.00	0.00
0	0	6.10	0.00	0.00	0.00	0.00	0.00	0.00	0.00	0.00	0.00
Off Horizontal Axis 2 Degrees											
True Location			Straight planar			Rectangular planar			3D		
X	Y	Z	X	Y	Z	X	Y	Z	X	Y	Z
0	0	0.61	0.04	0.00	0.04	0.02	0.00	0.02	0.02	0.02	0.02
0	0	0.91	0.03	0.00	0.05	0.02	0.00	0.04	0.02	0.02	0.04
0	0	1.22	0.03	0.00	0.05	0.02	0.00	0.05	0.02	0.02	0.05
0	0	1.52	0.03	0.00	0.07	0.03	0.00	0.07	0.03	0.03	0.07
0	0	1.83	0.03	0.00	0.09	0.03	0.00	0.10	0.03	0.03	0.10
0	0	2.13	0.03	0.00	0.11	0.04	0.00	0.12	0.04	0.04	0.12
0	0	2.44	0.03	0.00	0.14	0.04	0.00	0.16	0.04	0.04	0.16
0	0	2.74	0.04	0.00	0.16	0.04	0.00	0.20	0.04	0.04	0.20
0	0	3.05	0.04	0.00	0.20	0.05	0.00	0.23	0.05	0.05	0.23
0	0	3.35	0.04	0.00	0.23	0.05	0.00	0.28	0.05	0.05	0.28
0	0	3.66	0.05	0.00	0.27	0.05	0.00	0.33	0.05	0.05	0.33
0	0	3.96	0.05	0.00	0.30	0.06	0.00	0.38	0.06	0.06	0.38
0	0	4.27	0.05	0.00	0.35	0.06	0.00	0.43	0.06	0.06	0.43
0	0	4.57	0.05	0.00	0.39	0.06	0.00	0.49	0.06	0.06	0.49
0	0	4.88	0.05	0.00	0.44	0.07	0.00	0.55	0.07	0.07	0.55
0	0	5.18	0.06	0.00	0.49	0.07	0.00	0.62	0.07	0.07	0.62
0	0	5.49	0.06	0.00	0.55	0.08	0.00	0.69	0.08	0.08	0.69
0	0	5.79	0.06	0.00	0.60	0.08	0.00	0.76	0.08	0.08	0.76
0	0	6.10	0.07	0.00	0.66	0.08	0.00	0.83	0.08	0.08	0.83

Off Horizontal Axis 5 Degrees											
Location			Straight planar			Rectangular planar			3D		
X	Y	Z	X	Y	Z	X	Y	Z	X	Y	Z
0	0	0.61	0.09	0.00	0.09	0.06	0.00	0.06	0.06	0.06	0.06
0	0	0.91	0.07	0.00	0.11	0.06	0.00	0.09	0.06	0.06	0.09
0	0	1.22	0.07	0.00	0.14	0.06	0.00	0.12	0.06	0.06	0.12
0	0	1.52	0.07	0.00	0.17	0.07	0.00	0.17	0.07	0.07	0.17
0	0	1.83	0.07	0.00	0.22	0.08	0.00	0.23	0.08	0.08	0.23
0	0	2.13	0.08	0.00	0.27	0.08	0.00	0.29	0.08	0.08	0.29
0	0	2.44	0.08	0.00	0.32	0.09	0.00	0.36	0.09	0.09	0.36
0	0	2.74	0.09	0.00	0.38	0.10	0.00	0.45	0.10	0.10	0.45
0	0	3.05	0.09	0.00	0.45	0.11	0.00	0.53	0.11	0.11	0.53
0	0	3.35	0.10	0.00	0.53	0.11	0.00	0.62	0.11	0.11	0.62
0	0	3.66	0.10	0.00	0.61	0.12	0.00	0.73	0.12	0.12	0.73
0	0	3.96	0.11	0.00	0.69	0.13	0.00	0.84	0.13	0.13	0.84
0	0	4.27	0.11	0.00	0.79	0.13	0.00	0.95	0.13	0.13	0.95
0	0	4.57	0.12	0.00	0.88	0.14	0.00	1.07	0.14	0.14	1.07
0	0	4.88	0.12	0.00	0.99	0.15	0.00	1.19	0.15	0.15	1.19
0	0	5.18	0.13	0.00	1.09	0.16	0.00	1.32	0.16	0.16	1.32
0	0	5.49	0.13	0.00	1.20	0.16	0.00	1.46	0.16	0.16	1.46
0	0	5.79	0.14	0.00	1.32	0.17	0.00	1.59	0.17	0.17	1.59
0	0	6.10	0.14	0.00	1.44	0.17	0.00	1.74	0.17	0.17	1.74
Off Vertical Axis 2 Degrees											
Location			Straight planar			Rectangular planar			3D		
X	Y	Z	X	Y	Z	X	Y	Z	X	Y	Z
0	0	0.61	0.00	0.02	0.00	0.00	0.04	0.00	0.00	0.04	0.00
0	0	0.91	0.00	0.03	0.00	0.00	0.05	0.00	0.00	0.05	0.00
0	0	1.22	0.00	0.04	0.00	0.00	0.05	0.00	0.00	0.05	0.00
0	0	1.52	0.00	0.05	0.00	0.00	0.06	0.00	0.00	0.06	0.00
0	0	1.83	0.00	0.06	0.00	0.00	0.07	0.00	0.00	0.07	0.00
0	0	2.13	0.00	0.07	0.00	0.00	0.08	0.00	0.00	0.08	0.00
0	0	2.44	0.00	0.09	0.00	0.00	0.09	0.00	0.00	0.09	0.00
0	0	2.74	0.00	0.09	0.00	0.00	0.10	0.00	0.00	0.10	0.00
0	0	3.05	0.00	0.11	0.00	0.00	0.11	0.00	0.00	0.11	0.00
0	0	3.35	0.00	0.12	0.00	0.00	0.12	0.00	0.00	0.12	0.00
0	0	3.66	0.00	0.13	0.00	0.00	0.13	0.00	0.00	0.13	0.00
0	0	3.96	0.00	0.14	0.00	0.00	0.14	0.00	0.00	0.14	0.00
0	0	4.27	0.00	0.15	0.00	0.00	0.15	0.00	0.00	0.15	0.00
0	0	4.57	0.00	0.16	0.00	0.00	0.16	0.00	0.00	0.16	0.00
0	0	4.88	0.00	0.17	0.00	0.00	0.17	0.00	0.00	0.17	0.00
0	0	5.18	0.00	0.18	0.00	0.00	0.18	0.00	0.00	0.18	0.00
0	0	5.49	0.00	0.19	0.00	0.00	0.19	0.00	0.00	0.19	0.00
0	0	5.79	0.00	0.20	0.00	0.00	0.20	0.00	0.00	0.20	0.00
0	0	6.10	0.00	0.21	0.00	0.00	0.21	0.00	0.00	0.21	0.00

Off Vertical Axis 5 Degrees											
Location			Straight planar			Rectangular planar			3D		
X	Y	Z	X	Y	Z	X	Y	Z	X	Y	Z
0	0	0.61	0.00	0.05	0.00	0.00	0.10	0.00	0.00	0.10	0.00
0	0	0.91	0.00	0.08	0.00	0.00	0.11	0.00	0.00	0.11	0.00
0	0	1.22	0.00	0.11	0.00	0.00	0.13	0.00	0.00	0.13	0.00
0	0	1.52	0.00	0.13	0.00	0.00	0.15	0.00	0.00	0.15	0.00
0	0	1.83	0.00	0.16	0.00	0.00	0.17	0.00	0.00	0.17	0.00
0	0	2.13	0.00	0.19	0.00	0.00	0.20	0.00	0.00	0.20	0.00
0	0	2.44	0.00	0.21	0.00	0.00	0.22	0.00	0.00	0.22	0.00
0	0	2.74	0.00	0.24	0.00	0.00	0.25	0.00	0.00	0.25	0.00
0	0	3.05	0.00	0.27	0.00	0.00	0.27	0.00	0.00	0.27	0.00
0	0	3.35	0.00	0.29	0.00	0.00	0.30	0.00	0.00	0.30	0.00
0	0	3.66	0.00	0.32	0.00	0.00	0.32	0.00	0.00	0.32	0.00
0	0	3.96	0.00	0.35	0.00	0.00	0.35	0.00	0.00	0.35	0.00
0	0	4.27	0.00	0.37	0.00	0.00	0.37	0.00	0.00	0.37	0.00
0	0	4.57	0.00	0.40	0.00	0.00	0.40	0.00	0.00	0.40	0.00
0	0	4.88	0.00	0.43	0.00	0.00	0.43	0.00	0.00	0.43	0.00
0	0	5.18	0.00	0.45	0.00	0.00	0.45	0.00	0.00	0.45	0.00
0	0	5.49	0.00	0.48	0.00	0.00	0.48	0.00	0.00	0.48	0.00
0	0	5.79	0.00	0.51	0.00	0.00	0.51	0.00	0.00	0.51	0.00
0	0	6.10	0.00	0.53	0.00	0.00	0.53	0.00	0.00	0.53	0.00
Off Horizontal and Vertical Axis 5 Degrees											
Location			Straight planar			Rectangular planar			3D		
X	Y	Z	X	Y	Z	X	Y	Z	X	Y	Z
0	0	0.61	0.09	0.05	0.09	0.06	0.15	0.06	0.06	0.15	0.06
0	0	0.91	0.07	0.07	0.11	0.06	0.16	0.09	0.06	0.16	0.09
0	0	1.22	0.07	0.09	0.14	0.06	0.18	0.12	0.06	0.18	0.12
0	0	1.52	0.07	0.12	0.17	0.07	0.20	0.17	0.07	0.20	0.17
0	0	1.83	0.07	0.14	0.22	0.08	0.23	0.23	0.08	0.23	0.23
0	0	2.13	0.08	0.16	0.27	0.08	0.25	0.29	0.08	0.25	0.29
0	0	2.44	0.08	0.19	0.32	0.09	0.28	0.36	0.09	0.28	0.36
0	0	2.74	0.09	0.21	0.38	0.10	0.30	0.45	0.10	0.30	0.45
0	0	3.05	0.09	0.23	0.45	0.11	0.33	0.53	0.11	0.33	0.53
0	0	3.35	0.10	0.25	0.53	0.11	0.36	0.62	0.11	0.36	0.62
0	0	3.66	0.10	0.27	0.61	0.12	0.38	0.73	0.12	0.38	0.73
0	0	3.96	0.11	0.29	0.69	0.13	0.41	0.84	0.13	0.41	0.84
0	0	4.27	0.11	0.30	0.79	0.13	0.43	0.95	0.13	0.43	0.95
0	0	4.57	0.12	0.32	0.88	0.14	0.45	1.07	0.14	0.45	1.07
0	0	4.88	0.12	0.34	0.99	0.15	0.47	1.19	0.15	0.47	1.19
0	0	5.18	0.13	0.36	1.09	0.16	0.49	1.32	0.16	0.49	1.32
0	0	5.49	0.13	0.37	1.20	0.16	0.52	1.46	0.16	0.52	1.46
0	0	5.79	0.14	0.39	1.32	0.17	0.54	1.59	0.17	0.54	1.59
0	0	6.10	0.14	0.41	1.44	0.17	0.55	1.74	0.17	0.55	1.74

Camera 1 and 4

On Axis											
True Location			Straight planar			Rectangular planar			3D		
X	Y	Z	X	Y	Z	X	Y	Z	X	Y	Z
0	0	0.61	0.00	0.00	0.00	0.00	0.00	0.00	0.00	0.00	0.00
0	0	0.91	0.00	0.00	0.00	0.00	0.00	0.00	0.00	0.00	0.00
0	0	1.22	0.00	0.00	0.00	0.00	0.00	0.00	0.00	0.00	0.00
0	0	1.52	0.00	0.00	0.00	0.00	0.00	0.00	0.00	0.00	0.00
0	0	1.83	0.00	0.00	0.00	0.00	0.00	0.00	0.00	0.00	0.00
0	0	2.13	0.00	0.00	0.00	0.00	0.00	0.00	0.00	0.00	0.00
0	0	2.44	0.00	0.00	0.00	0.00	0.00	0.00	0.00	0.00	0.00
0	0	2.74	0.00	0.00	0.00	0.00	0.00	0.00	0.00	0.00	0.00
0	0	3.05	0.00	0.00	0.00	0.00	0.00	0.00	0.00	0.00	0.00
0	0	3.35	0.00	0.00	0.00	0.00	0.00	0.00	0.00	0.00	0.00
0	0	3.66	0.00	0.00	0.00	0.00	0.00	0.00	0.00	0.00	0.00
0	0	3.96	0.00	0.00	0.00	0.00	0.00	0.00	0.00	0.00	0.00
0	0	4.27	0.00	0.00	0.00	0.00	0.00	0.00	0.00	0.00	0.00
0	0	4.57	0.00	0.00	0.00	0.00	0.00	0.00	0.00	0.00	0.00
0	0	4.88	0.00	0.00	0.00	0.00	0.00	0.00	0.00	0.00	0.00
0	0	5.18	0.00	0.00	0.00	0.00	0.00	0.00	0.00	0.00	0.00
0	0	5.49	0.00	0.00	0.00	0.00	0.00	0.00	0.00	0.00	0.00
0	0	5.79	0.00	0.00	0.00	0.00	0.00	0.00	0.00	0.00	0.00
0	0	6.10	0.00	0.00	0.00	0.00	0.00	0.00	0.00	0.00	0.00
Off Horizontal Axis 2 Degrees											
True Location			Straight planar			Rectangular planar			3D		
X	Y	Z	X	Y	Z	X	Y	Z	X	Y	Z
0	0	0.61	0.05	0.00	0.03	0.03	0.02	0.02	0.02	0.03	0.03
0	0	0.91	0.05	0.00	0.03	0.03	0.02	0.03	0.02	0.03	0.04
0	0	1.22	0.04	0.00	0.04	0.03	0.02	0.05	0.02	0.03	0.05
0	0	1.52	0.04	0.00	0.05	0.03	0.03	0.06	0.03	0.03	0.08
0	0	1.83	0.05	0.00	0.07	0.04	0.03	0.09	0.03	0.03	0.10
0	0	2.13	0.05	0.00	0.09	0.04	0.03	0.11	0.03	0.04	0.12
0	0	2.44	0.05	0.00	0.10	0.05	0.04	0.14	0.04	0.04	0.16
0	0	2.74	0.05	0.00	0.12	0.05	0.04	0.18	0.04	0.04	0.19
0	0	3.05	0.06	0.00	0.15	0.05	0.04	0.21	0.05	0.05	0.23
0	0	3.35	0.06	0.00	0.17	0.06	0.05	0.25	0.05	0.05	0.27
0	0	3.66	0.07	0.00	0.20	0.06	0.05	0.30	0.06	0.05	0.32
0	0	3.96	0.07	0.00	0.23	0.07	0.05	0.34	0.06	0.05	0.37
0	0	4.27	0.08	0.00	0.27	0.07	0.05	0.39	0.06	0.06	0.42
0	0	4.57	0.08	0.00	0.30	0.07	0.06	0.45	0.07	0.06	0.47
0	0	4.88	0.09	0.00	0.34	0.08	0.06	0.50	0.07	0.07	0.53
0	0	5.18	0.09	0.00	0.38	0.08	0.07	0.56	0.08	0.07	0.59
0	0	5.49	0.09	0.00	0.42	0.09	0.07	0.62	0.08	0.07	0.66
0	0	5.79	0.10	0.00	0.46	0.09	0.07	0.69	0.09	0.08	0.72
0	0	6.10	0.10	0.00	0.51	0.09	0.08	0.76	0.09	0.08	0.79

Off Horizontal Axis 5 Degrees											
Location			Straight planar			Rectangular planar			3D		
X	Y	Z	X	Y	Z	X	Y	Z	X	Y	Z
0	0	0.61	0.14	0.00	0.07	0.07	0.05	0.05	0.05	0.07	0.07
0	0	0.91	0.11	0.00	0.09	0.07	0.05	0.08	0.05	0.06	0.10
0	0	1.22	0.11	0.00	0.11	0.07	0.06	0.11	0.05	0.07	0.13
0	0	1.52	0.11	0.00	0.13	0.08	0.06	0.16	0.06	0.07	0.18
0	0	1.83	0.11	0.00	0.17	0.09	0.07	0.21	0.07	0.08	0.23
0	0	2.13	0.12	0.00	0.21	0.09	0.08	0.27	0.08	0.09	0.30
0	0	2.44	0.12	0.00	0.25	0.10	0.08	0.33	0.09	0.09	0.36
0	0	2.74	0.13	0.00	0.30	0.11	0.09	0.41	0.10	0.10	0.44
0	0	3.05	0.14	0.00	0.35	0.12	0.10	0.49	0.11	0.10	0.52
0	0	3.35	0.15	0.00	0.41	0.13	0.10	0.57	0.12	0.11	0.61
0	0	3.66	0.16	0.00	0.48	0.14	0.11	0.67	0.13	0.12	0.71
0	0	3.96	0.17	0.00	0.55	0.15	0.12	0.77	0.13	0.12	0.81
0	0	4.27	0.18	0.00	0.62	0.16	0.12	0.87	0.14	0.13	0.92
0	0	4.57	0.19	0.00	0.70	0.16	0.13	0.98	0.15	0.14	1.03
0	0	4.88	0.20	0.00	0.78	0.17	0.14	1.10	0.16	0.14	1.15
0	0	5.18	0.20	0.00	0.87	0.18	0.14	1.22	0.17	0.15	1.27
0	0	5.49	0.21	0.00	0.95	0.19	0.15	1.34	0.17	0.16	1.40
0	0	5.79	0.22	0.00	1.05	0.20	0.16	1.48	0.18	0.16	1.53
0	0	6.10	0.23	0.00	1.15	0.20	0.16	1.61	0.19	0.17	1.67
Off Vertical Axis 2 Degrees											
Location			Straight planar			Rectangular planar			3D		
X	Y	Z	X	Y	Z	X	Y	Z	X	Y	Z
0	0	0.61	0.00	0.02	0.00	0.00	0.04	0.00	0.00	0.04	0.00
0	0	0.91	0.00	0.03	0.00	0.00	0.05	0.00	0.00	0.05	0.00
0	0	1.22	0.00	0.04	0.00	0.00	0.05	0.00	0.00	0.05	0.00
0	0	1.52	0.00	0.05	0.00	0.00	0.06	0.00	0.00	0.06	0.00
0	0	1.83	0.00	0.06	0.00	0.00	0.07	0.00	0.00	0.07	0.00
0	0	2.13	0.00	0.07	0.00	0.00	0.08	0.00	0.00	0.08	0.00
0	0	2.44	0.00	0.09	0.00	0.00	0.09	0.00	0.00	0.09	0.00
0	0	2.74	0.00	0.09	0.00	0.00	0.10	0.00	0.00	0.10	0.00
0	0	3.05	0.00	0.11	0.00	0.00	0.11	0.00	0.00	0.11	0.00
0	0	3.35	0.00	0.12	0.00	0.00	0.12	0.00	0.00	0.12	0.00
0	0	3.66	0.00	0.13	0.00	0.00	0.13	0.00	0.00	0.13	0.00
0	0	3.96	0.00	0.14	0.00	0.00	0.14	0.00	0.00	0.14	0.00
0	0	4.27	0.00	0.15	0.00	0.00	0.15	0.00	0.00	0.15	0.00
0	0	4.57	0.00	0.16	0.00	0.00	0.16	0.00	0.00	0.16	0.00
0	0	4.88	0.00	0.17	0.00	0.00	0.17	0.00	0.00	0.17	0.00
0	0	5.18	0.00	0.18	0.00	0.00	0.18	0.00	0.00	0.18	0.00
0	0	5.49	0.00	0.19	0.00	0.00	0.19	0.00	0.00	0.19	0.00
0	0	5.79	0.00	0.20	0.00	0.00	0.20	0.00	0.00	0.20	0.00
0	0	6.10	0.00	0.21	0.00	0.00	0.21	0.00	0.00	0.21	0.00

Off Vertical Axis 5 Degrees											
Location			Straight planar			Rectangular planar			3D		
X	Y	Z	X	Y	Z	X	Y	Z	X	Y	Z
0	0	0.61	0.00	0.05	0.00	0.00	0.10	0.00	0.00	0.10	0.00
0	0	0.91	0.00	0.08	0.00	0.00	0.11	0.00	0.00	0.11	0.00
0	0	1.22	0.00	0.11	0.00	0.00	0.13	0.00	0.00	0.13	0.00
0	0	1.52	0.00	0.13	0.00	0.00	0.15	0.00	0.00	0.15	0.00
0	0	1.83	0.00	0.16	0.00	0.00	0.17	0.00	0.00	0.17	0.00
0	0	2.13	0.00	0.19	0.00	0.00	0.20	0.00	0.00	0.20	0.00
0	0	2.44	0.00	0.21	0.00	0.00	0.22	0.00	0.00	0.22	0.00
0	0	2.74	0.00	0.24	0.00	0.00	0.25	0.00	0.00	0.25	0.00
0	0	3.05	0.00	0.27	0.00	0.00	0.27	0.00	0.00	0.27	0.00
0	0	3.35	0.00	0.29	0.00	0.00	0.30	0.00	0.00	0.30	0.00
0	0	3.66	0.00	0.32	0.00	0.00	0.32	0.00	0.00	0.32	0.00
0	0	3.96	0.00	0.35	0.00	0.00	0.35	0.00	0.00	0.35	0.00
0	0	4.27	0.00	0.37	0.00	0.00	0.37	0.00	0.00	0.37	0.00
0	0	4.57	0.00	0.40	0.00	0.00	0.40	0.00	0.00	0.40	0.00
0	0	4.88	0.00	0.43	0.00	0.00	0.43	0.00	0.00	0.43	0.00
0	0	5.18	0.00	0.45	0.00	0.00	0.45	0.00	0.00	0.45	0.00
0	0	5.49	0.00	0.48	0.00	0.00	0.48	0.00	0.00	0.48	0.00
0	0	5.79	0.00	0.51	0.00	0.00	0.51	0.00	0.00	0.51	0.00
0	0	6.10	0.00	0.53	0.00	0.00	0.53	0.00	0.00	0.53	0.00
Off Horizontal and Vertical Axis 5 Degrees											
Location			Straight planar			Rectangular planar			3D		
X	Y	Z	X	Y	Z	X	Y	Z	X	Y	Z
0	0	0.61	0.14	0.05	0.07	0.07	0.15	0.05	0.05	0.16	0.07
0	0	0.91	0.11	0.07	0.09	0.07	0.15	0.08	0.05	0.16	0.10
0	0	1.22	0.11	0.10	0.11	0.07	0.17	0.11	0.05	0.18	0.13
0	0	1.52	0.11	0.12	0.13	0.08	0.20	0.16	0.06	0.20	0.18
0	0	1.83	0.11	0.15	0.17	0.09	0.22	0.21	0.07	0.23	0.23
0	0	2.13	0.12	0.17	0.21	0.09	0.25	0.27	0.08	0.25	0.30
0	0	2.44	0.12	0.19	0.25	0.10	0.27	0.33	0.09	0.28	0.36
0	0	2.74	0.13	0.21	0.30	0.11	0.30	0.41	0.10	0.30	0.44
0	0	3.05	0.14	0.23	0.35	0.12	0.33	0.49	0.11	0.33	0.52
0	0	3.35	0.15	0.26	0.41	0.13	0.35	0.57	0.12	0.36	0.61
0	0	3.66	0.16	0.28	0.48	0.14	0.37	0.67	0.13	0.38	0.71
0	0	3.96	0.17	0.30	0.55	0.15	0.40	0.77	0.13	0.40	0.81
0	0	4.27	0.18	0.32	0.62	0.16	0.42	0.87	0.14	0.43	0.92
0	0	4.57	0.19	0.34	0.70	0.16	0.45	0.98	0.15	0.45	1.03
0	0	4.88	0.20	0.36	0.78	0.17	0.47	1.10	0.16	0.47	1.15
0	0	5.18	0.20	0.38	0.87	0.18	0.49	1.22	0.17	0.49	1.27
0	0	5.49	0.21	0.40	0.95	0.19	0.51	1.34	0.17	0.52	1.40
0	0	5.79	0.22	0.41	1.05	0.20	0.53	1.48	0.18	0.53	1.53
0	0	6.10	0.23	0.43	1.15	0.20	0.55	1.61	0.19	0.55	1.67